Numerical simulation of surface ship hull beam whipping response due to submitted to underwater explosion

Ssu-Chieh Tsai

Master Thesis

presented in partial fulfillment
of the requirements for the double degree:
“Advanced Master in Naval Architecture” conferred by University of Liege
"Master of Sciences in Applied Mechanics, specialization in Hydrodynamics, Energetics and Propulsion” conferred by Ecole Centrale de Nantes

developed at ICAM
in the framework of the

“EMSHIP”
Erasmus Mundus Master Course
in “Integrated Advanced Ship Design”

Supervisor: Prof. Hervé Le Sourne, L'Institut Catholique d'Arts et Métiers

Reviewer: Prof. Antoine Ducoin, Ecole Centrale de Nantes

Nantes, February 2017

This page is intentionally left blank.

DECLARATION OF AUTHORSHIP

I declare that this thesis and the work presented in it are my own and has been generated by me as the result of my own original research.

Where I have consulted the published work of others, this is always clearly attributed.

Where I have quoted from the work of others, the source is always given. With the exception of such quotations, this thesis is entirely my own work.

I have acknowledged all main sources of help.

Where the thesis is based on work done by myself jointly with others, I have made clear exactly what was done by others and what I have contributed myself.

This thesis contains no material that has been submitted previously, in whole or in part, for the award of any other academic degree or diploma.

I cede copyright of the thesis in favour of the University of ICAM.

Date: 15/01/2017 Signature

This page is intentionally left blank.

ABSTRACT

Numerical simulation of surface ship hull beam whipping response due to submitted to underwater explosion

By **Ssu-Chieh Tsai**

This study presents a method to evaluate the whipping response of a surface ship subjected to an underwater explosion. Within the analysis, the effects from both first shock wave and secondary bubble oscillation are considered. The analytical model "Doubly Asymptotic Approximation" (DAA) is applied to obtain the acoustic pressure. The main purpose of this study is to clarify the influence of the secondary bubble pulsation on the ship structure whipping response.

Once the method is widely described, it is implemented in two distinct numerical finite element software packages: an explicit code developed for LS-DYNA as well as an implicit code executed in ANSYS. First of all, DAA model is applied to a clamped plate and a semi-cylinder structure which is simulated as a simplified ship model in LS-DYNA so as to observe the structural behavior with respect to the nonlinear pressure, such as effective plastic strain and vertical deformation. Afterwards, the code is modified and applied to the same cylinder model in ANSYS by following an identic procedure; thus, the results obtained from both codes can be compared.

Finally, the presented method is applied to a frigate surface ship FEM model with a coarse mesh, provided by STX Europe. This model will be employed as the reference ship for carrying out the structural response calculation.

This page is intentionally left blank.

CONTENTS

LIST OF FIGURES

LIST OF TABLES

1. INTRODUCTION

1.1. Motivation

It is unavoidable that surface ships might be attacked by weapons during the operation period; moreover, underwater explosion (UNDEX) will have significant wave shock and bubble oscillation on the bottom of the navy vessel which will have the most severe impact on ship structure. Thus, it is important to successfully develop a structure able to withstand shock response at the primary design stage.

The first study of UNDEX on the navy ship was reported by Abbot (Abbot, 1881); afterward, the related tests and researches were studied before World War I. During WWI and WWII, intensive and significant efforts had been made on developing and optimizing surface ship structural design. Keil (Keil, 1961) studied ship response and hull damages due to the various phase of UNDEX with the consideration of shock wave and bubble pulsation; it was proved that it is possible to carry out explosion tests against ships.

Figure 1.1 : Underwater explosion to a surface ship

In addition, theoretical methods were observed after the 1900s: Convers (Herring, 1941) proved that not only the shock wave but also the gas bubble had an obvious effect on ship hull structures; US submarine report (BRAND, 1945) pointed out the relationship between the progression of bubble migration and the exponential decay of pressure with as time passed by. Joseph and Ignace (Kelle & Kolodner, 1956) developed the theory of damped oscillations with the interaction of gas bubble effect due to the underwater explosion; they were able to

predict the diminishing period of damped oscillations as well as the explosive damage.

It is well known that the high pressure from first shock wave has a direct severe influence on ship structure; nevertheless, even the pressure of the bubble oscillation is much smaller than the first shock wave, the entire ship hull beam can enter in resonance with the bubble oscillations, what is called whipping phenomenon. Canada DTIC (Vernon, 1986) pointed out the importance of considering bubble pulsation dynamic when predicting by theoretical equations the whipping response of a ship hull submitted to underwater blast loads.

Slamming impact and underwater explosion lead to strong impact pressure loads occurring in a short period. The transient vibration of a ship body submitted to this king of instantaneous pressure load is called the whipping response. (Tuitman, 2010)

Mauricio Garcia Navarro (Navarro, 2015) modeled the structural response of a flat plate loaded by a linear incident pressure due to first shock wave by the underwater explosion. Despite the incident pressure of bubble oscillation has less influence compared to first shock wave regarding the ship hull local damage, the entire ship may enter in resonance with the first and secondary bubble oscillations and this phenomenon may cause significant structural damage on ship hull as well as on embarked materials. Thus, the first and secondary bubble pulsation excitations become an important issue to discuss when studying the response of a ship submitted to an underwater explosion.

This study can be considered as an extension of the work of Mauricio Garcia Navarro, focusing on the two first oscillations of the gas bubble.

Several empirical and analytical methods will be validated, and the most proper method to calculate the changing radius, velocity, and acceleration of bubble migration will be determined to obtain the incident pressure due to bubble oscillation.

Furthermore, with the cooperation of STX Europe, the calculated pressure loads will be applied on a reference surface ship finite element model. The resulting structural response, as well as the ship hull damage, will be assessed, the main objective for STX being to improve the ship structure resistance as well as the behavior of embarked mounting systems. It is also expected that the analysis method and results could be applied to the related developing research in the future.

1.2. Objective

In order to carry out the ship whipping response loaded by the pressure fields coming from an underwater explosion, this study will have two main objectives. The first one is to figure out the appropriate theoretical or analytical methodology to obtain the time evolution of the acoustic pressure load distribution, considering not only the first shock wave but also the bubble pulsations during its first two oscillations. The second objective is to perform a finite element transient analysis to ship structure, considering the pressure load distribution calculated analytically and distributed over the entire ship hull. The corresponding work thus has been divided into several steps:

- Review analytical and empirical methodologies in order to find out and validate the incident pressure for nonlinear bubble oscillations phase.
- Program using MATLAB different analytical and empirical approaches to calculating the incident pressure.
- By comparing the results obtained from the different approaches, determine the most appropriate method. Moreover, in order to acquire the incident pressure time evolution during the entire explosion, combine the first shock wave pressure field with the bubble oscillations one.
- Considering the fluid-structure interaction, calculate the final pressure load to be applied to the ship hull finite elements exposed to the underwater explosion.
- Verify the pressure field calculation and the entire methodology by analyzing, using LS-DYNA, two simple models: a plate representing a ship hull section and a half-cylinder representing an entire ship hull.
- With the cooperation of STX Europe, adapt the program from MATLAB code to ANSYS language which can be utilized in STX.
- Considering a given charge and a given standoff distance, calculate and apply the resulting pressure distribution on two ANSYS finite element models: the half-cylinder previously studded with LS-DYNA and an entire surface ship hull coarsely meshed and provided by STX. Analyze the structural responses using ANSYS and compare the results related to the half-cylinder with Ls-DYNA results obtained previously.

1.3. Flow Chart

In this study, the different steps of initial investigation, code programming up to finite element simulations are highlighted in Figure 1.2. There are three main stages in this research: programming and calculating the incident pressure according to the chosen approach; applying the calculated pressure loads on LS-DYNA and ANSYS finite element models and analyze the response of an embarked material using the Dynamic Design Analysis Method (the so-called DDAM approach).

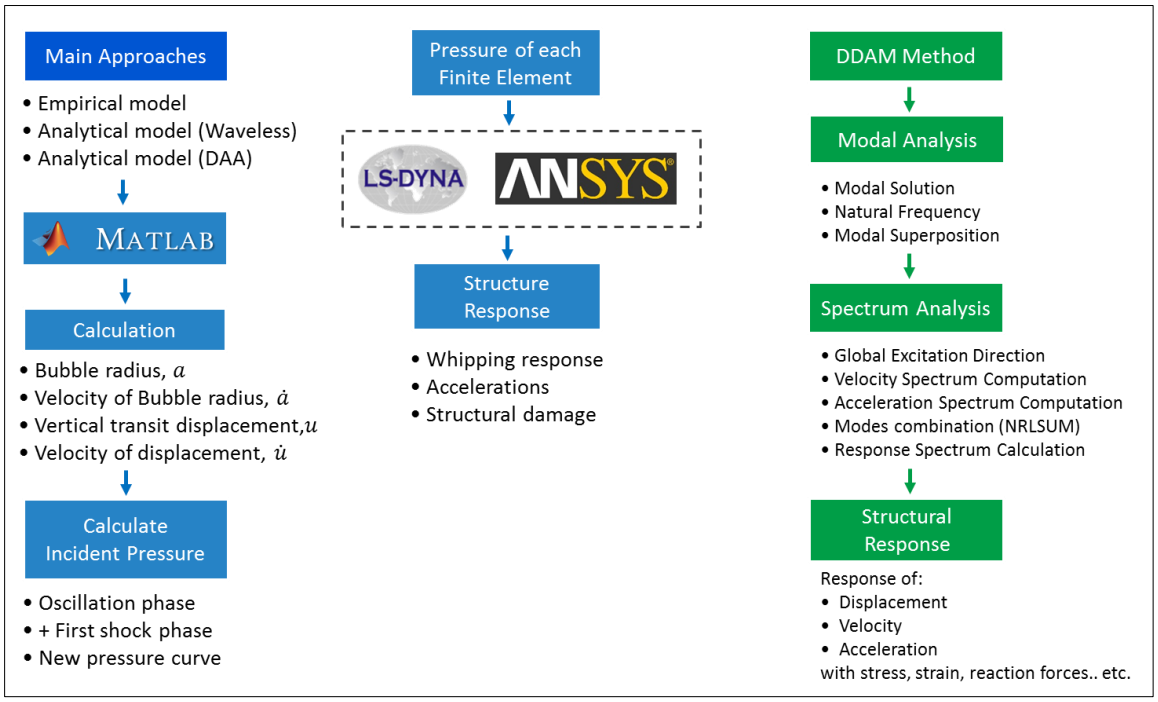

Figure 1.2 : Proceure of study

As shown in Figure 1.2, the first step consisted in reviewing the different methodologies and theories. The main purpose was to determine the best approach to calculating the incident pressure generated by the oscillations of the gas bubble produced by the underwater explosion. It was first requested to calculate the evolution of the bubble radius, the bubble vertical transient displacement and the velocity of the bubble wall during the migration process.

2. LITERATURE REVIEW OF UNDERWATER EXPLOSION

It is important to figure out accurately the pressure which loads the ship hull during the bubble migration process before starting any finite element analysis. In this chapter, the underwater explosion and resulting bubble pulsation and migration phenomena will be presented first; Then, the approach commonly used to calculate the pressure due to the shock wave phase will be detailed. In the third part of this section, the bubble oscillation phase will be investigated, and the different existing methods to calculate the resulting pressure field will be reviewed.

2.1. Bubble phenomenon

During the bubble migration process, in order to have balance with hydrostatic pressure, it is obvious that the bubble volume increases while the internal pressure is decreased, this alternative motion can be assumed as a mass-spring system as well. The bubble oscillation and migration process is illustrated in Figure 2.1, as proposed by (Snay, 1956). This figure clearly shows that the pressure level evolution is closely related to the bubble oscillation phenomenon. First of all, when the charge explodes, a high and compressed gas pressure arise in the small bubble. At the same time, the so-called first shock wave, which related pressure can be represented by a nonlinear exponential decay, happens in an extremely short time period. Afterward, the bubble volume starts to expand up to a maximum and, balancing with the hydrostatic water pressure, begins to decrease. Each time the bubble reaches its minimum, a pressure wave is generated and, of course, received by the hull of the ship exposed to the underwater explosion. The level of energy decreasing during the bubble oscillation phase, only the first and second bubble pulses are commonly considered in a UNDEX ship response analysis.

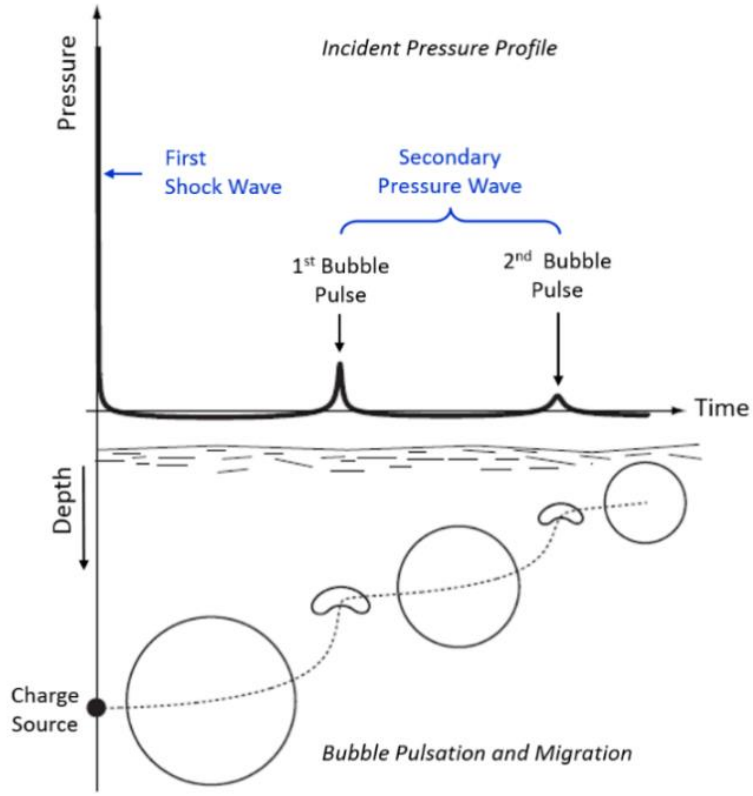

Figure 2.1: The evaluation of incident pressure and bubble migration process (Snay, 1956)

With the progression of studies, the shock response of non-contact UNDEX became an important issue not only for the naval ship but also for the merchant vessel and the different phenomena associated to an UNDEX was discussed: impact of the shock wave, cavitation near the ship hull, hull beam whipping, etc. Thomas (Vernon, 1986) used spherical explosion bubble theory to predict the whipping response of a surface ship submitted to bubble pulsations; he pointed out that the bubble pulse frequency and ship hull bending natural frequency can coincide, leading to a severe loading scenario. On the other hand, practical measurement methodologies and simulation methods have been developed over the past 20 years. Figure 2.2 describes with more detail the relationship between bubble oscillations and the incident pressure evolution (BRAND, 1945); this figure shows clearly that a pressure peak occurs each time the bubble radius reaches its minimum.

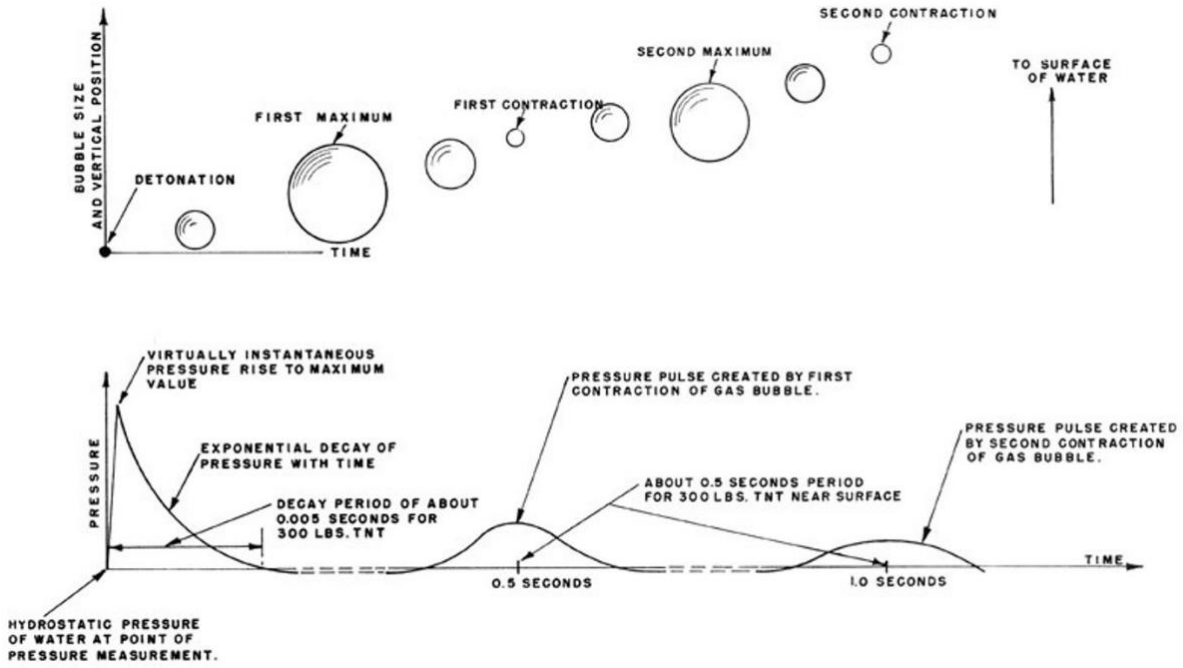

Figure 2.2: The relationship between oscillation of migration bubble and related pressure propagation caused by underwater explosion. (Resource from: Submarine report No.58 (BRAND, 1945)

Costanzo (Costanzo, 2010) also discussed the phenomena encountered in an underwater explosion and presented some numerical simulations as well as experimental trials.

Figure 2.3 plots the surface effects due to UNDEX; whereas Figure 2.4 present the comparison of observed actual surface phenomena as well as the simulation from Hydrocode calculation of progressing gas bubble due to the first shock wave.

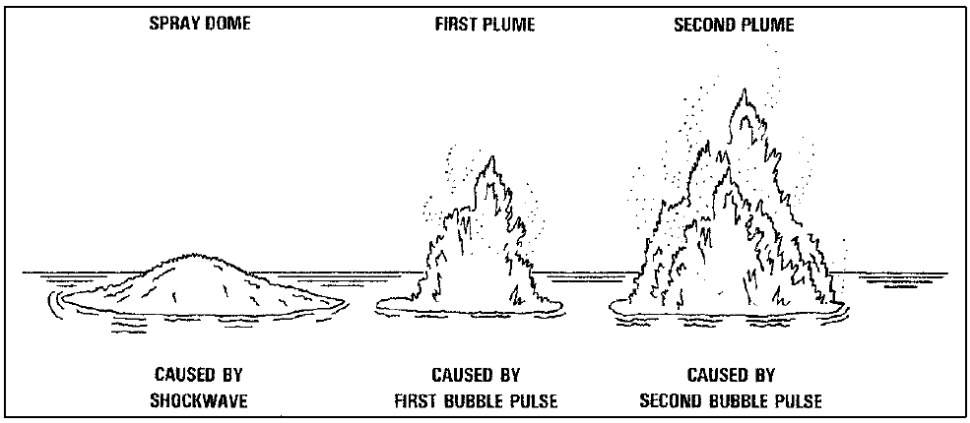

Figure 2.3: Surface Phenomena for underwater explosion (Source from: (Costanzo, 2010))

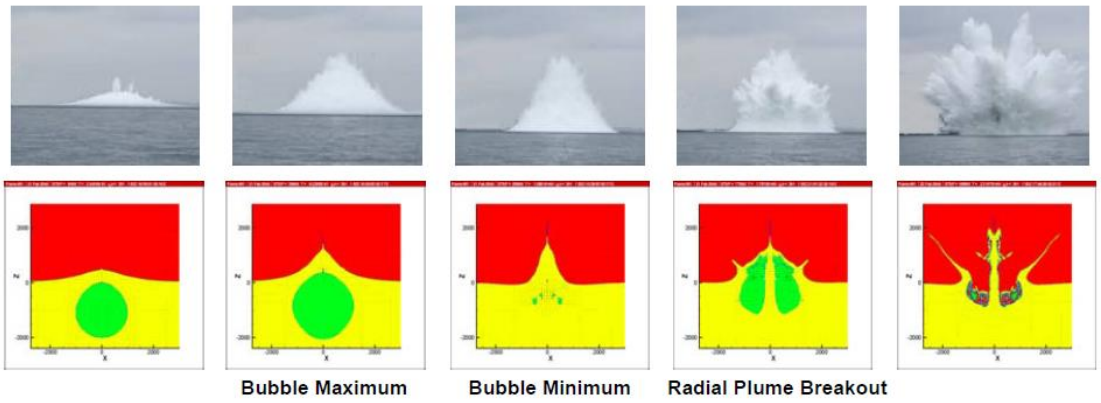

Figure 2.4: UNDEX Plume Above-Surface Effects (Costanzo, 2010)

The sea free surface has an influence on the propagation of the shock wave which reflects on it. Hollyer (Hollyer, 1959) highlighted the fact that the free surface acts as a reflecting boundary regarding the spatial propagation of the shock wave. Figure 2.5 illustrates the reflection of the shock wave from an explosion occurring at point A and a pressure measured at point T. The water will be vapored while the pressure is decreased down to the vapor pressure, causing a cutoff effect on the pressure wave. Figure 2.6 shows the surface cutoff phenomenon and the summation of direct and reflect shock waves at point T.

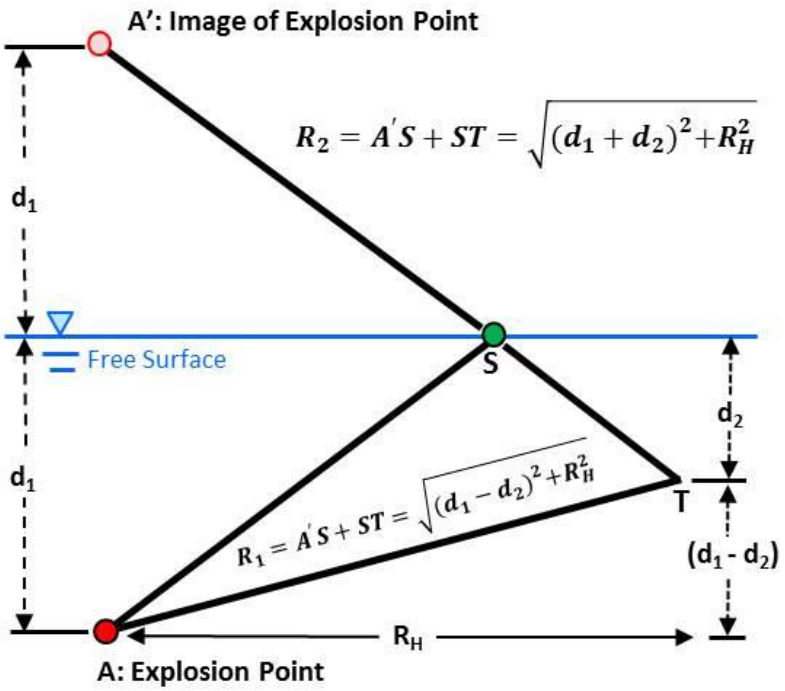

Figure 2.5: The geometry of surface reflection of shock wave

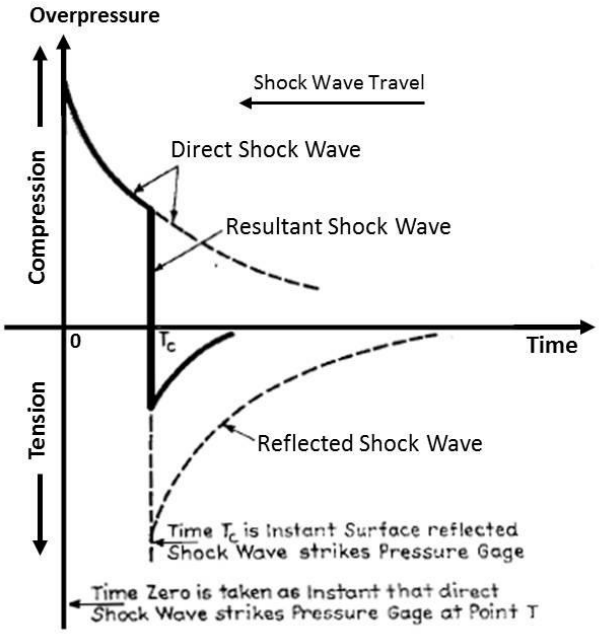

Figure 2.6: Surface cutoff phenomenon with summation of direct and reflected shock waves

2.2. Shock Wave Phase

Reid (Reid, 1996) developed the mathematical formulation (Eq. 2.2) to calculate the shock wave pressure in a free field, based on empirical coefficients which depend on the type of explosive. In Eq.2-1, it is observed that the explosive type has a big influence on the peak value:

$$P_0 = K_1 \left(\frac{W^{\frac{1}{3}}}{R} \right)^{A1} \qquad 2\text{-}1$$

$$P_m = P_0 e^{-\frac{t}{\theta}} \qquad 2\text{-}2$$

Where

P_0: Peak pressure in MPa

P_m: Pressure with an exponential decay in free field

W: The charge mass in kg

R: The distance from charge to standoff point

K_1 and A1: Equivalent coefficients depends on charge type (

Table 2-1)

Hence, with Eqs. 2-1 and 2-2, the complete pressure for shock wave phase can be rewritten as:

$$P_m = K_1 \left(\frac{W^{\frac{1}{3}}}{R} \right)^{A1} e^{-\frac{t}{\theta}} \qquad 2\text{-}3$$

In addition, the constant of the exponential decay θ can be obtained from Eq.2-4, where K2 and A2 are equivalent coefficients also related to the type of the charge (

Table 2-1):

$$\theta = K_2 W^{\frac{1}{3}} \left(\frac{W^{\frac{1}{3}}}{R} \right)^{A2} \qquad 2\text{-}4$$

Table 2-1: Equivalent coefficients for different materials (Reid, 1996)

	Coefficient	HBX-1	TNT	PENT	NUCLEAR
Shock –wave	K1	53.51	52.12	56.21	1.06E+04
Pressure	A1	1.144	1.18	1.194	1.13
Decay	K2	0.092	0.092	0.086	3.627
Time-Constant	A2	-0.247	-0.185	-0.257	-0.22
Impulse	K3	7.263	6.52	6.518	4.50E+07
	A3	0.856	0.98	0.903	0.91
Energy Flux	K4	106.8	94.34	103.11	1.15E+07
Density	A4	2.039	2.155	2.9	2.04
Bubble Period	K5	2.302	2.064	2.098	249.1
Bubble Radius	K6	3.775	3.383	3.439	400.5

It is worth noting that the shock wave duration is very small, around few milliseconds and too short to generate buoyance effect (Hunter & Geers, 2002). The duration of the application of the shock wave to the ship hull is also too short to generate fluid-structure interaction.

In 2002, Geers and Hunter developed the formula for precise description of far-field shock wave pressure; it can be rearranged by placing a_c instead of W with similitude relation: (Geers & Hunter, 2002)

$$P(R,t) = P_c[a_c/R]^{1+A} f([a_c/R]^B v_c t/a_c) \qquad 2\text{-}5$$

Where:

- R: the distance from center of charge to the standoff point

- a_c: initial charge radius(m), $a_c = \left(\frac{3V_c}{4\pi}\right)^{\frac{1}{3}}$
- P_c and v_c: constants related with the charge material for shock-wave similitude equations, the recommended values are listed in Table 2-2, the units of P_c and v_c are GPa and km/s respectively. (Cole, 1948)
- A and B: the constants associated with the explosive material are listed in Table 2-2.

Also, time decay $f(\tau)$ be written as:

$$f(\tau) = e^{-\tau}, \qquad when\ \tau \leq 1 \qquad 2\text{-}6$$

$$f(\tau) = 0.8251e^{-1.338\tau} + 0.1749e^{-0.1805\tau}, \qquad when\ \tau \leq 7 \qquad 2\text{-}7$$

Table 2-2: Material constants for shock-wave similitude equations (Cole, 1948)

Material	Source	P_c	v_c	A	B
TNT (1.52 g/cc)	Coles *et al.* (1946)	1.42	0.992	0.13	0.18
TNT (1.60 g/cc)	Farley and Snay (1978)	1.45	1.24	0.13	0.23
TNT (1.60 g/cc)	Price (1979)	1.67	1.01	0.18	0.185
Pentolite (1.71 g/cc) (50/50 PETN/TNT)	Thiel (1961)	1.65	1.22	0.14	0.23
Pentolite (1.71 g/cc) (unknown comp.)	Price (1979)	1.92	1.29	0.194	0.257
HBX-1 (1.72 g/cc) (40/38/17/5 RDX/TNT/A1/D-2 Wax)	Swisdak (1978)	1.71	1.47	0.15	0.29
HBX-1 (1.72 g/cc) (unknown comp.)	Price (1979)	1.58	1.17	0.144	0.247

The impulse function $I(t)$ of blast can then be calculated by integrating the pressure over the time:

$$I(t) = \int_0^t P(t)dt \qquad 2\text{-}8$$

The area below the pressure curve represents the energy provided by the shock wave to the ship hull and can be defined as:

$$E(t) = \frac{1}{\rho c}\int_0^t P(t)^2 dt \qquad 2\text{-}9$$

- ***Shock Factor***

Reid (Reid, 1996) pointed out that when θ is large enough, the keel shock factor (KSF) can be equivalent to the hull shock factor (HSF). According to experiments and theory, KSF can be assumed proportional to the vertical velocity of the ship considered as a rigid body. The shock factors can be described as follows:

$$\mathrm{KSF} = \frac{\mathrm{W^n}}{\mathrm{D}} \qquad 2\text{-}10$$

$$\mathrm{HSF} = \frac{\mathrm{W^n}}{\mathrm{D}} \cdot \frac{1+\sin\theta}{2} \qquad 2\text{-}11$$

Where

- W: the mass of explosive in TNT equivalence (kg)
- D: the standoff distance from target (m)
- *n* : varies slight different value from underwater experiments
- θ : shock wave angle between a horizontal line and distance from the measured point

In ISSC (2006) it is observed that the maximum shock factor (SF) can be evaluated by equation 2-12 while Figure 2.7 illustrates the calculation of the shock factor from the shock wave angle and standoff distance.

$$\mathrm{SF} = \frac{\sqrt{W}}{\mathrm{D}} \qquad 2\text{-}12$$

$$\mathrm{HSF} = \frac{\mathrm{W^{1/2}}}{\mathrm{D}} \cdot \frac{1+\sin\theta}{2} \qquad 2\text{-}13$$

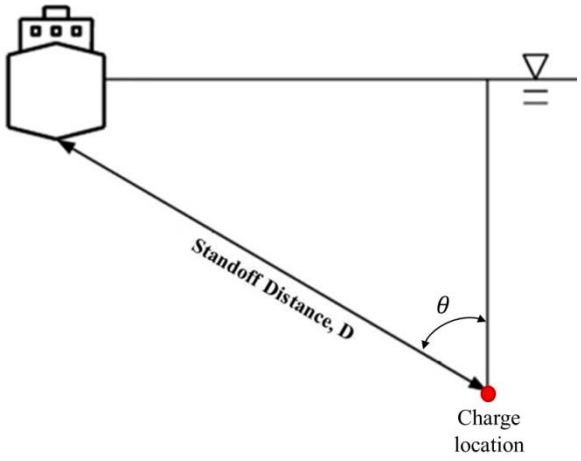

Figure 2.7: Schematic diagram of shock factor angle and standoff distance

2.3. Secondary Bubble Pressure Pulse (Bubble Oscillation Phase)

In this section, different approaches proposed by various authors will be discussed and compared so as to determine the pressure waves coming from the explosive gas bubble pulsations. The main goal is to figure out the differences on the hypotheses which were considered by the authors and the proposed formulations.

First of all, DeRuntz (DeRuntz, 1989) explained some theoretical formulations of Underwater Shock Analysis code (USA code), and the numerical solver NASTRAN was used to perform a simulation with finite-element models. In this article, several computations of submerged structure models were implemented for the application of shock wave analysis, such as spherical shell, infinite cylindrical shell and concentric fluid-coupled shells.

Furthermore, Hunter and Geers (Hunter & Geers, 2003) used the propagation of pressure in acoustic fields and the corresponding particle velocities, generated by an underwater explosion, especially for the oscillation phenomenon of gas bubble.

More recently, Webster (Webster, 2007) proposed an expression based on empirical data to estimate the bubble pulse pressure time history. He indicated that this expression could be applied at early design stage. For the purpose of obtaining the pressure-time history which includes the first shock wave, the first bubble pulse as well as the second bubble pulse, he showed that the propagation of bubble radius plays an important role in this calculation. Therefore, K5 and K6 stands for constants depending on the charge material are required to obtain the maximum radius and time period. In 2010, Defense R&D Canada investigated how to calculate the radius of bubble migration by analytical equations and Riley (Riley, 2010) provided the constants value K5 and K6 of TNT charge for three cycles during bubble migration in the study.

2.3.1. Analytical methods

Many analytical formulations have been developed to estimate the incident pressure on a surface hull generated by first and second bubble pulses.

The main objective of Geers and Hunter's work was the derivation of a methodology to obtain both the incident acoustic pressure and the gas bubble velocity (Hunter & Geers, 2003). To obtain realistic pressure and velocity fields, it is important to consider initial conditions of bubble migration, such as the initial radius of the bubble and its migration vertical displacement as well as the initial internal pressure inside the gas bubble. Thus, Geers (Hunter & Geers, 2002) developed two types of analytical models to obtain the bubble radius *a* and its vertical migration displacement *u*: the so-called waveless and DAA models, which are discussed in the following paragraphs.

- ***Waveless model***

Waveless is the first simplified analytical method (Hunter & Geers, 2002),which means wave effects are considered in the liquid but not in the gas bubble. The waveless equations of motion of the gas bubble, which take into account both the bubble dilatation and its migration, are presented below:

$$a\ddot{a} + \frac{3}{2}\dot{a}^2 - \frac{1}{4}\dot{u}^2 - gu = \rho_l^{-1}\left[P_g - (P_{atm} + \rho_l g d_i)\right] \quad 2\text{- }14$$

$$a\ddot{u} + 3\dot{a}\dot{u} - 2g = 0 \quad 2\text{- }15$$

Where

a: Bubble radius (m)

u: Vertical migration displacement (m)

g: Gravity 9.81 (m/s^2)

d_i: Initial charge depth (m)

ρ_l: Density of liquid, (1025 kg/m^3 for sea water density);

P_{atm}: Atmosphere pressure ($P_{atm} = 101325\ Pa$)

P_g : Pressure inside gas bubble, $P_g = K_c \left(\frac{V_c}{V}\right)^{\gamma}$

K_c : Adiabatic charge constant for explosive materials (Pa)

V_c: Charge volume, $V_c = m_c/\rho_{TNT}\ (m^3)$

V: Volume of bubble, $V = (4/3)\pi a^3$ in m^3

γ: Constant ratio of specific heats for the gas, $\gamma = 1.30$

m_c: Charge mass (kg)

ρ_C: Charge density, ($\rho_C = \rho_{TNT} = 1630\ kg/m^3$)

Damping is not considered in the above equations, which means: $\rho_g = \dot{\rho}_g = \zeta = \dot{\zeta} = 0$.

Where:

ρ_g: The conservation of mass yield for mass density in gas bubble, $\rho_g = \rho_c(V_c/V)$

ζ : Specific-acoustic-impedance ratio, $\zeta = \frac{\rho_g c_g}{\rho_l c_l}$

c_g: Sound speed inside gas bubble, $c_g = c_c(V_c/V)^{\frac{1}{2}(\gamma-1)}$

c_c: Sound speed in charge, $c_c = \sqrt{\gamma K_c/\rho_c}$

c_l: Sound speed in the liquid, $c_l = 1415\ m/s$

Regarding the initial conditions at initial time t_I, it can be assumed as: $a(t_I) = a_I$, $\dot{a}(t_I) = \dot{a}_I$, $u(t_I) = 0$ and $\dot{u}(t_I) = 0$, thus, above equations can be organized as:

$$a\ddot{a} + \frac{3}{2}\dot{a}^2 - \frac{1}{4}\dot{u}^2 - gu = \rho_l^{-1}\left[P_g - (P_{atm} + \rho_l g d_i)\right] \quad \text{2- 16}$$

$$\rightarrow \ddot{a} + \frac{3\dot{a}^2}{2a} - \frac{\dot{u}^2}{4a} - \frac{gu}{a} = \frac{1}{\rho_l a}\left[P_g - (P_{atm} + \rho_l g d_i)\right]$$

$$\rightarrow \ddot{a} = \frac{1}{\rho_l a}\left[P_g - (P_{atm} + \rho_l g d_i)\right] - \frac{3\dot{a}^2}{2a} + \frac{\dot{u}^2}{4a} + \frac{gu}{a}$$

$$\rightarrow \ddot{a} = \frac{1}{\rho_l a}\left[K_c\left(\frac{V_c}{V}\right)^{\gamma} - (P_{atm} + \rho_l g d_i)\right] - \frac{3\dot{a}^2}{2a} + \frac{\dot{u}^2}{4a} + \frac{gu}{a}$$

$$a\ddot{u} + 3\dot{a}\dot{u} - 2g = 0 \quad \text{2- 17}$$

$$\rightarrow \ddot{u} + \frac{3\dot{a}\dot{u}}{a} - \frac{2g}{a} = 0$$

$$\rightarrow \ddot{u} = \frac{2g}{a} - \frac{3\dot{a}\dot{u}}{a}$$

It is important to obtain the initial radius of charge and bubble (a_c and a_I) which between phases and volume from a joint analysis with both shock wave and bubble pulses. Therefore, with Eqs.2- 5 and 2-7, the initial radius of charge a_c can be obtained and considered as the initial conditions for next secondary bubble pulsation phase.

However, Hunter and Geers (Hunter & Geers, 2002) also pointed out the comparison with empirical method shown in Figure 2.8 for the constants of Table 2-2, in two figures, it indicates the relations between initial conditions parameters when $t_I/T_c = 3,4,5,6,7$ according to Eqs. 2-21 and 2-23 (where t_I is determined from the initial conditions of subsequent bubble-response oscillation phase), which referred from three sets of TNT charge constants (Cole, 1948). In order to obtain the initial bubble radius of shock wave phase, initial bubble radius a_I and initial radius of charge can be obtained based on the assuming ratio of t_I/T_c .

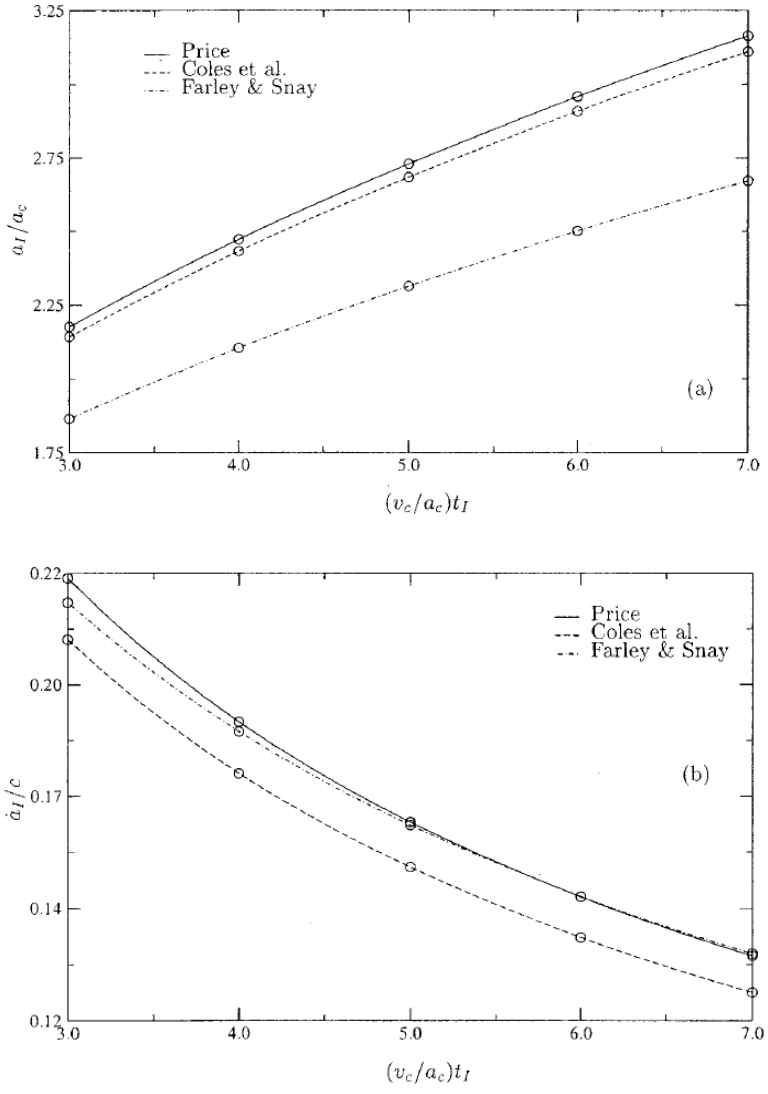

Figure 2.8: Initial displacement and velocity as functions of the initial time selected for the oscillation phase, and as determined from three sets of charge constants. (Hunter & Geers, 2002)

Furthermore, with the consideration of far-field pressure, the motion of the bubble surface during the shock-wave phase should be in consideration of as the initial condition for the following nonlinear bubble propagation. Hence, the relation between acceleration of charge volume and the charge radius can be described as Eq.2-18, 2-19, 2-20 and 2-21 represent the integration of volume acceleration equation with $\dot{V}(0) = 0$ and $V(0) = (4/3)\,\pi a_c^3$ when the charge period $T_c = a_c/v_c$ (Hunter & Geers, 2002):

$$\ddot{V}(t) = \frac{4\pi a_c}{\rho_l} P_c[0.8251exp(-1.338t/T_c) + 0.1749exp(-0.1805t/T_c)] \quad 2\text{-}18$$

$$\dot{V}(t) = \frac{4\pi a_c}{\rho_l} P_c[1.5857 - 0.6167exp(-1.338t/T_c) - 0.9690exp(-0.1805t/T_c)] \quad 2\text{-}19$$

$$V(t) = \frac{4}{3}\pi a_c^3 + \frac{4\pi a_c}{\rho_l} P_c \left[1.5857t - 5.8293 + 0.4609exp\left(-\frac{1.338t}{T_c}\right) + 5.3684exp(-0.1805t/T_c)\right] \quad 2\text{-}20$$

$$a(t) = [3V(t)/4\pi]^{1/3} \quad 2\text{-}21$$

$$\dot{a}(t) = \dot{V}(t)/4\pi a^2(t) \quad 2\text{-}22$$

- ***DAA Model***

The second wave model has been implemented by Geers and Hunter (Hunter & Geers, 2003) into the so-called doubly asymptotic approximation (DAA) approach, where the wave effects between the liquid and gas bubble are taken into account. As the sound speed in water is considered, the influence of damping is also taken into account. The resulting five non-linear equations proposed by Geers and Hunter write as:

$$\dot{a} = \frac{-1}{a}\emptyset_{l0} - \frac{1}{c_l}\left(\dot{\emptyset}_{l0} - \dot{a}^2 - \frac{1}{3}\dot{u}^2 - \frac{2\dot{u}}{3a}\emptyset_{l1}\right) \quad 2\text{-}23$$

$$\dot{u} = \frac{-2}{a}\emptyset_{l1} - \frac{1}{c_l}\left(\dot{\emptyset}_{l0} - 2\dot{a}\dot{u}\right) \quad 2\text{-}24$$

$$\dot{\emptyset}_{l0} = \frac{1}{1+\zeta}\left\{\left[\frac{1}{2} + \frac{1}{2}\frac{\rho_g}{\rho_l} + \zeta\right]\left(\dot{a}^2 + \frac{1}{3}\dot{u}^2\right) - \frac{\rho_g}{\rho_l}\frac{c_g}{a}\emptyset_{l0} + \frac{2\dot{u}}{3a}(1+\zeta)\emptyset_{l1} - Z\right\} \quad 2\text{-}25$$

$$\dot{\emptyset}_{l1} = \frac{1}{1+\zeta}\left[\left(1 + \frac{\rho_g}{\rho_l} + 2\zeta\right)\dot{a}\dot{u} - \frac{\rho_g}{\rho_l}c_g\left(\frac{2\emptyset_{l1}}{a} + \frac{\emptyset_{g1}}{a}\right) - \left(1 - \frac{\rho_g}{\rho_l}\right)ga\right] \quad 2\text{-}26$$

$$\dot{\emptyset}_{g1} = \frac{1}{1+\zeta}\left[\left(2+\frac{C_g}{C_l}+\zeta\right)\dot{a}\dot{u} - c_g\left(\frac{2\emptyset_{l1}}{a}+\frac{\emptyset_{g1}}{a}\right)+\frac{C_g}{C_l}\left(1-\frac{\rho_g}{\rho_l}\right)ga\right] \quad 2\text{-}27$$

Where $Z = \frac{1}{\rho_l}(P_g - p_I + \rho_l g u) + \frac{1}{3}\left[\left(\frac{\emptyset_{l1}}{a}\right)^2 - \frac{\rho_g}{\rho_l}\left(\frac{\emptyset_{g1}}{a}\right)^2\right]$, pressure p_I is a known initial hydrostatic surface pressure if $\emptyset_l = 0$, $p_I = P_{atm} + \rho_l g d_i$, and p_g is a known surface pressure of gas bubble.

$\emptyset_l$ stands for the velocity potential at the liquid particle's location, $\emptyset_g$ is the velocity potential at the gas particle's location. Considering the bubble as spherical bubble and initial condition occurring at initial time t_I, $\emptyset_l(t_I) = \emptyset_{l0}(t_I) + \emptyset_{l1}(t_I)\cos\theta$ and $\emptyset_g(t_I) = \emptyset_{g1}(t_I)\cos\theta$, where $\emptyset_{l0}(t_I)$, $\emptyset_{l1}(t_I)$and $\emptyset_{g1}(t_I)$ are described by Eq.2-28.

In order to evaluate the above equations, it is necessary to acquire the initial values of $\emptyset_{l0}$, $\emptyset_{l1}$ and $\emptyset_{g1}$ at initial time t_I, these initial values can be obtained by:

$$\emptyset_{g1}(t_I) = \frac{g}{c_g}a_I^2;\ \emptyset_{l1}(t_I) = \frac{1}{2}\frac{g}{c_l}a_I^2 \quad 2\text{-}28$$

$$\emptyset_{l0}(t_I) = -a_I\left\{\dot{a}_I\left[1+\zeta_I - \frac{1}{2}\left(1-\frac{\rho_{gI}}{\rho_l}\right)\frac{\dot{a}_I}{c_l}\right] - \frac{1}{\rho_l c_l}\times(P_{gI}-p_I) + \frac{1}{3}\left(\frac{\rho_{gI}}{\rho_l}\cdot\frac{1}{c_{gI}^2} - \frac{1}{4}\cdot\frac{1}{c_I^2}\right)\frac{1}{c_l}(ga_I)^2\right\} \quad 2\text{-}29$$

To derivative above set of equations, a finite difference scheme is implemented. With the assumption of very small time step, the equations can be written as:

$$\dot{a}_{i+1} = \frac{-1}{a}\emptyset_{l0}^i - \frac{1}{c_l}\left(\dot{\emptyset}_{l0}^i - \dot{a}_i^2 - \frac{1}{3}\dot{u}_i^2 - \frac{2\dot{u}_i}{3a_i}\emptyset_{l1}^i\right) \quad 2\text{-}30$$

$$\dot{u}_{i+1} = \frac{-2}{a_i}\emptyset_{l1}^i - \frac{1}{c_l}\left(\dot{\emptyset}_{l0}^i - 2\dot{a}_\iota\dot{u}_\iota\right) \quad 2\text{-}31$$

$$\dot{\emptyset}_{l0}^i = \frac{1}{1+\zeta}\left\{\left(\frac{1}{2}+\frac{1}{2}\frac{\rho_g}{\rho_l}+\zeta\right)\left(\dot{a}_i^2+\frac{1}{3}\dot{u}_i^2\right) - \frac{\rho_g}{\rho_l}\frac{c_g}{a_i}\emptyset_{l0}^i + \frac{2\dot{u}_\iota}{3a_i}(1+\zeta)\emptyset_{l1}^i - Z_i\right\} \quad 2\text{-}32$$

$$\dot{\emptyset}_{l1}^{i+1} = \frac{1}{1+\zeta}\left[\left(1+\frac{\rho_g}{\rho_l}+2\zeta\right)\dot{a}_\iota\dot{u}_\iota - \frac{\rho_g}{\rho_l}c_g\left(\frac{2\emptyset_{l1}^i}{a_i}+\frac{\emptyset_{g1}^i}{a_i}\right) - \left(1-\frac{\rho_g}{\rho_l}\right)ga_i\right]$$

$$\dot{\emptyset}_{g1}^{i+1} = \frac{1}{1+\zeta}\left[\left(2+\frac{C_g}{C_l}+\zeta\right)\dot{a}_\iota\dot{u}_\iota - c_g\left(\frac{2\emptyset_{l1}^i}{a_i}+\frac{\emptyset_{g1}^i}{a_i}\right)+\frac{C_g}{C_l}\left(1-\frac{\rho_g}{\rho_l}\right)ga_i\right]$$

Where $Z_i = \frac{1}{\rho_l}(P_g - p_I + \rho_l g u_i) + \frac{1}{3}\left[\left(\frac{\emptyset_{l1}^i}{a_i}\right)^2 - \frac{\rho_g}{\rho_l}\left(\frac{\emptyset_{g1}^i}{a_i}\right)^2\right]$

- ***Incident Pressure***

Geers (Hunter & Geers, 2003) showed that the significant acoustic pressure field at the ship hull standoff point (situated at a distance *r* from the charge) can be written as:

$$P_{ac}(r,t) = \rho_l \left[q(t') \frac{\partial}{\partial t'} \mathcal{Q}(r,t') + \dot{q}(t') \mathcal{Q}(r,t') + \mu(t') \frac{\partial}{\partial t'} \mathcal{M}(r,t') + \dot{\mu}(t') \mathcal{M}(r,t') + \dot{\mu}(t') \frac{\partial}{\partial t'} \mathcal{N}(r,t') + \ddot{\mu}(t') \mathcal{N}(r,t') \right] \frac{\partial t'}{\partial t}(r,t') \quad 2\text{-}33$$

Where t' is the time delay for the pressure to arrive at the observed point.

The changing distance r' from center of explosive to the observed point and the changing of depth z' from free surface during the vertical bubble migration are given explicitly by:

$$r'(r,t') = [x^2 + y^2 + z'^2(r,t')]^{\frac{1}{2}} \quad 2\text{-}34$$

$$z'(r,t') = d_i - u \quad 2\text{-}35$$

$$\text{with } t' = t - \frac{r'(r,t') - R}{c_l} \quad 2\text{-}36$$

To complete this description, the different terms used in Eq.2-33 are detailed below (Hunter & Geers, 2003):

$$q(t') = a^2(t')\dot{a}(t') \quad 2\text{-}37$$

$$\dot{q}(t') = a^2(t')\ddot{a}(t') + 2a(t')\dot{a}^2(t') \quad 2\text{-}38$$

$$\mu(t') = \frac{1}{2} a^3(t')\dot{u}(t') \quad 2\text{-}39$$

$$\dot{\mu}(t') = \frac{1}{2} [a^3(t')\ddot{u}(t') + 3a^2(t')\dot{a}(t')\dot{u}(t')] \quad 2\text{-}40$$

$$\mathcal{Q}(r,t') = \frac{1}{r'(r,t')} + \frac{z'(r,t')}{r'^2(r,t')} \dot{u}(t')/c \quad 2\text{-}41$$

$$\frac{\partial}{\partial t'} \mathcal{Q}(r,t') = \frac{z'(r,t')\dot{u}(t')}{r'^3(r,t')} + \frac{z'(r,t')\ddot{u}(t') - \dot{u}^2(t')}{cr'^2(r,t')} + \frac{2z'^2(r,t')\dot{u}^2(t')}{cr'^4(r,t')} \quad 2\text{-}42$$

$$\mathcal{M}(r,t') = \frac{z'(r,t')}{r'^3(r,t')} - \frac{\dot{u}(t')/c}{r'^2(r,t')} + \frac{3z'^2(r,t')}{r'^4(r,t')} \dot{u}(t')/c \quad 2\text{-}43$$

$$\frac{\partial}{\partial t'} \mathcal{M}(r,t') = -\frac{\dot{u}(t')}{r'^3(r,t')} + \frac{3z'^2(r,t')\dot{u}(t')}{r'^5(r,t')} - \frac{\ddot{u}(r,t')}{cr'^2(r,t')} \quad 2\text{-}44$$

$$\_\_\_\_\_ + z'(r,t') \times \frac{3z'^2(r,t')\ddot{u}(t') - 8\dot{u}^2(t')}{cr'^4(r,t')} + \frac{12z'^3(r,t')\dot{u}^2(t')}{cr'^6(r,t')}$$

$$\mathcal{N}(r,t') = \frac{z'(r,t')}{cr'^2(r,t')} \quad 2\text{-}45$$

$$\frac{\partial}{\partial t'}\mathcal{N}(r,t') = -\frac{\dot{u}(t')}{cr'^2(r,t')} + \frac{2z'(r,t')\dot{u}(t')}{cr'^4(r,t')} \quad 2\text{-}46$$

$$\frac{\partial t'}{\partial t}(r,t') = \left[1 - \frac{z'(r,t')}{r'(r,t')}\dot{u}(t')/c\right]^{-1} \quad 2\text{-}47$$

Assuming that the sound speed in the seawater is closed to infinity, the terms which are related with the sound speed c can be ignored. Therefore, above Eqs.2-41, 2-43, and 2-45 become:

$$\mathcal{Q}(r,t') = \frac{1}{r'(r,t')} \quad 2\text{-}48$$

$$\frac{\partial}{\partial t'}\mathcal{Q}(r,t') = \frac{z'(r,t')\dot{u}(t')}{r'^3(r,t')} \quad 2\text{-}49$$

$$\mathcal{M}(r,t') = \frac{z'(r,t')}{r'^3(r,t')} \quad 2\text{-}50$$

$$\frac{\partial}{\partial t'}\mathcal{M}(r,t') = -\frac{\dot{u}(t')}{r'^3(r,t')} + \frac{3z'^2(r,t')\dot{u}(t')}{r'^5(r,t')} \quad 2\text{-}51$$

$$\mathcal{N}(r,t') = 0 \quad 2\text{-}52$$

$$\frac{\partial}{\partial t'}\mathcal{N}(r,t') = 0 \quad 2\text{-}53$$

$$\frac{\partial t'}{\partial t}(r,t') = \left[1 - \frac{z'(r,t')}{r'(r,t')}\dot{u}(t')/c\right]^{-1} = 1 \quad 2\text{-}54$$

Taking into account the above equations, Eq. can be simplified to following equation:

$$P_{ac}(r,t) = \rho_l\left[q(t')\frac{\partial}{\partial t'}\mathcal{Q}(r,t') + \dot{q}(t')\mathcal{Q}(r,t') + \mu(t')\frac{\partial}{\partial t'}\mathcal{M}(r,t') + \dot{\mu}(t')\mathcal{M}(r,t')\right] \quad 2\text{-}55$$

2.3.2. Empirical method

- ***Bubble pressure pulse***

Webster (Webster, 2007) used the peak approximation method, based on empirical coefficients, to determine the pressure-time history generated by an underwater explosion. The equation proposed by the author to obtain the incident pressure of bubble pulse is shown hereafter (Cole, 1948). The units in the following expression, valid for TNT explosive only, are in lb/in^2:

$$P_{max} - P_0 = \left[2.26 \cdot 10^{-6} \cdot k \left(4.19 \cdot 10^7 rQ \frac{\gamma_E - 1}{k} \right)^{1+\frac{2}{3(\gamma_E - 1)}} \cdot \frac{W^{\frac{1}{3}}}{R} \right] \quad \text{2-56}$$

Where:

γ_E: Ratio of specific heats for TNT gas products, $\gamma_E = 1.25$

k: Parameter employed for TNT, k =7.83 × 10^9

r: Fraction of the detonation energy Q expressed in cal./gm of explosive, where rQ= 440.

Besides, impulse is one of the most important factors when discussing the bubble pulse behavior, the prolonged wave will have different impulse compared with first shock wave. The impulse of bubble pulse can be calculated as:

$$I_2 = K_{bp} \cdot Z_0^{A_{bp}} \left(\frac{W^{\frac{2}{3}}}{R} \right) \quad \text{2-57}$$

Where K_{bp} and A_{bp} are 12.148 and -1/6 respectively, the constants for secondary pressure pulse; whereas Z_0 = D + 33ft is the initial depth from level of zero pressure (Cole, 1948).

The estimated pulse velocity can be written as:

$$u = \frac{\pi}{2} \left(\frac{A_{M1} - \left(\frac{W}{\rho_{TNT} \cdot g} \right)^{\frac{1}{3}}}{t_{bM1}} \right) \quad \text{2-58}$$

Thus, the arrival time of the secondary pressure pulse at location R is given as:

$$t_{2p} = \frac{R}{u} \quad \text{2-59}$$

- ***Bubble dynamics***

Many parameters are associated with the pulsations of the gas bubble generated by an underwater explosion. The first step before calculating the pressure associated to bubble pulses is to study the bubble radius variation.

According to Webster (Webster, 2007), the first oscillation period (t_{b1}) and the first maximum bubble radius (A_{M1}) may be written as:

$$t_{b1} = 1.14 \cdot \rho_0^{\frac{1}{2}} \frac{Y_0^{\frac{1}{3}}}{(\rho_0 \cdot g \cdot z_0)^{\frac{5}{6}}} \quad 2\text{-}60$$

$$A_{M1} = \left[\left(\frac{4\pi}{3}\rho_0 \cdot g \cdot z_0\right)^{-1} \cdot Y_0\right]^{\frac{1}{3}} \quad 2\text{-}61$$

Where $z_0 = D + 33\ ft$ and $Y_0 = \frac{W}{g} \cdot Q_0 + \frac{4\pi}{3} \cdot \rho_0 \cdot \frac{W}{\rho_{TNT}} \cdot z_0$

The initial energy per mass for TNT charge Q_0 can be expressed as:

$$Q_0 = \frac{K_J}{\gamma - 1}\left(\frac{4\pi}{3} \cdot \frac{W}{\rho_{TNT} \cdot g}\right) \quad 2\text{-}62$$

Where K_J is the Jones constant given as 2712.28 $m^{11/4}/s^2$ (Cole, 1948)

Regarding the second period of oscillation and corresponding maximum bubble radius, the scale factor indicates the percentage of energy loss as follows: (Cole, 1948)

$$Q_1 = 0.34 \cdot Q_0 \quad 2\text{-}63$$

$$Y_1 = 0.34 \cdot Y_0 \quad 2\text{-}64$$

A second pulse occurs at the second contraction of the gas bubble and corresponding period and maximum bubble radius can be expressed as:

$$t_{b2} = 1.14 \cdot \rho_0^{\frac{1}{2}} \frac{Y_1^{\frac{1}{3}}}{(\rho_0 \cdot g \cdot z_0)^{\frac{5}{6}}} \quad 2\text{-}65$$

$$A_{M2} = \left[\left(\frac{4\pi}{3}\rho_0 \cdot g \cdot z_0\right)^{-1} \cdot Y_1\right]^{\frac{1}{3}} \quad 2\text{-}66$$

Furthermore, the approximation time for the gas bubble at its first and second maximum radius can be estimated as:

$$t_{bM1} = \frac{1}{2} t_{b1} \quad \text{2-67}$$

$$t_{bM2} = \frac{1}{2} (t_{b2} - t_{b1}) \quad \text{2-68}$$

The bubble oscillation periods are then $T_1 = t_{b1}$ and $T_2 = (t_{b2} - t_{b1})$.

The duration of the secondary bubble pulse can be expressed as: $T_2 = I_2 / P_{2max}$

2.4. Pressure on Finite Element Model

With the consideration of the pressure expressed as a spherical wave in the fluid field, Barras (Barras, 2012) proposed the spherical wave approximation (SWA) with two-dimensional configuration by submarine explosion problem. In Figure 2.9, assuming D is the depth of charge from free surface, R is the distance from charge location to standoff point which is perpendicular to the structure, and $P_I(t)$ stands for the incident pressure to standoff point in terms of time steps. In order to calculate the incident pressure to each point of the wetted structure, considering $\vec{n}_i$ represents the normal vector to each element on finite element model, $\vec{R}_i$ is the vector from charge to each element i, whereas $\alpha_i$is the angle between two vectors $\vec{n}_i$ and $\vec{R}_i$. With this consequence, the incident pressure which is perpendicular to each element can be obtained as $P_I \cos\alpha_i$.

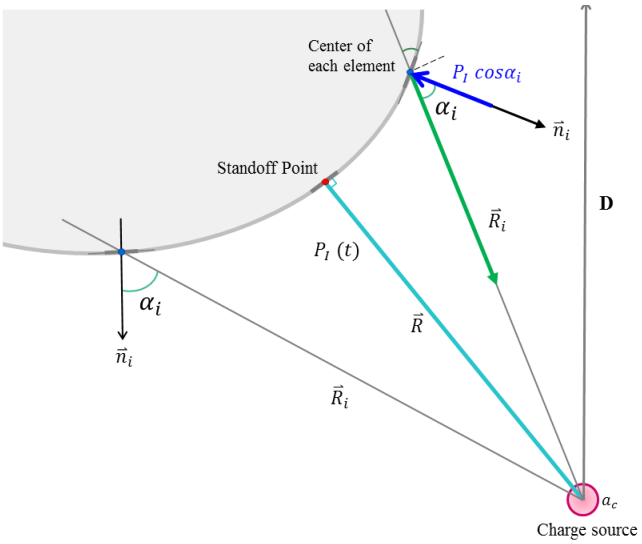

Figure 2.9: General two-dimension configuration of underwater explosion problem

Due to the strong impact from extremely high pressure loads by underwater explosion, the fluid- structure interaction cannot be neglected. Here the interaction process is considered as shock wave phase and bubble oscillation phase respectively.

First of all, in order to acquire the effect by non-contact underwater explosion in shock wave phase, the pressure applied to each element at point *i* can be written as: (Hollyer, 1959)

$$P_{element,sh} = 2P_I(t) - \frac{\rho c v_i}{\sin\alpha_i} \qquad 2\text{-}69$$

Where

$$v_i = \frac{2\sin\alpha_i P_0}{m}\frac{\theta}{1-\beta_i}\left(e^{-\beta_i t/\theta} - e^{-t/\theta}\right) \qquad 2\text{-}70$$

Thus, Eq. 2-69 can be rewritten as:

$$P_{element,sh}(t) = 2P_I(t) - \frac{2\rho c\theta P_0}{m(1-\beta_i)}\left(e^{-\beta_i t/\theta} - e^{-t/\theta}\right) \quad 2\text{-}71$$

Moreover, the approximation of fluid-structure interaction is also taken into account in bubble oscillation phase, Eq.2-72 represents the pressure effect on each element in secondary phase (Barras, 2012):

$$P_{element,bub}(t) = 2P_I(t) - \rho c\left[\frac{dW}{dt}(t) + \frac{2}{\theta_d}W(t-\theta_d) - \frac{2}{{\theta_d}^2}\int_{t-\theta_d}^{t} W(\tau)d\tau\right] \quad 2\text{-}72$$

Where

$\theta_d = \mathrm{a}/\mathrm{c}$, the diffraction time which is corresponding to the time taken by a wave due to propagate from the point *i* to the center.

W: the deflection at the center of the element at instant explosion

According to Eq. 2-71 and 2-72, the second term of both equations are such a small value that could not make obvious influence on the results of pressure to each element which means can be ignored, as a consequence, the final pressure apply to each element can be simplified as:

$$P_{element}(t) = 2P_I(t) \quad 2\text{-}73$$

3. INCIDENT PRESSURE OF BUBBLE MIGRATION

3.1. Results and Comparison of Existing Approaches

Due to the well-developed methodology to calculate the pressure due to first shock wave in a short time period, the calculation process is considered from previous section 2.2.

This chapter will focus on the procedure to figure out the most suitable approach to obtain the pressure of nonlinear bubble oscillation phase. According to section 2.3, three main possible approaches are taken into account in this study: analytical Waveless, DAA model and empirical model, all the above approaches have been programmed by a MATLAB in the present master thesis. In addition, corresponding formulations for incident pressure, bubble radius, bubble radius velocity and vertical bubble displacement have been applied to three examples related to three different initial conditions as follows:

- ***Example* 1:** Initial condition proposed by (Barras, 2012)

The initial settings presented in Barras's research were referred as the initial condition in this example, the details are listed as Table 3-1:

Table 3-1: Initial condition of Example 1

	Description
$\mathbf{m_c}$	TNT charge mass, m_c= 500 kg
$\mathbf{d_i}$	Distance from charge to free surface, $\boldsymbol{d_i}$ = 50 m
r	Distance from charge to standoff point, r = 50 m
$\boldsymbol{\rho_c}$	Density of charge, $\boldsymbol{\rho_c}$= 1600 kg/m^3
SF	Shock factor = 0.447

- ***Example* 2**: Initial condition proposed by (Hunter & Geers, 2002) (Hunter & Geers, 2003)

Table 3-2 presented in the study of Hunter and Geers was considered as initial conditions of case 2 and corresponding parameters are listed below:

Table 3-2: Initial condition of Example 2

	Description
$\mathbf{m_c}$	TNT charge mass, mc= 0.3 kg
$\boldsymbol{d_i}$	Distance from charge to free surface, $\boldsymbol{d_i}$ = 92 m
$\boldsymbol{\rho_c}$	Density of charge, $\boldsymbol{\rho_c}$= 1500 kg/m3
SF	Shock factor = 0.012

- ***Example 3***: Initial condition proposed by (Webster, 2007)

Table 3-3 proposed by Webster was taken into account for the initial conditions. Corresponding values are listed below:

Table 3-3: Initial condition of Example 3

	Description
$\mathbf{m_c}$	TNT charge mass, m_c= 1.45 kg
$\boldsymbol{d_i}$	Distance from charge to free surface, $\boldsymbol{d_i}$ = 178 m
$\boldsymbol{\rho_c}$	Density of charge , $\boldsymbol{\rho_c}$= 1500 kg/m^3
$\boldsymbol{R}$	Radial distance from charge, $\boldsymbol{R = 0.8\,m}$
SF	Shock factor = 0.007

3.2. Results and Comparison of Three Examples

- ***Example 1***

Figure 3.1 plots the comparison of bubble radius obtained from waveless and DAA analytical models (Figure 3.1 (a)) as well as the bubble radius measured from underwater explosion test (Figure 3.1 (b)) (Barras, 2012). It appears clearly that the time history calculated from DAA model matches much better with the experimental curve. It is also noticeable that the maximum bubble radius obtained from the waveless model in the second period is even larger than the first bubble maximum radius, which seems to be unrealistic as the bubble loses energy during the pulsation process.

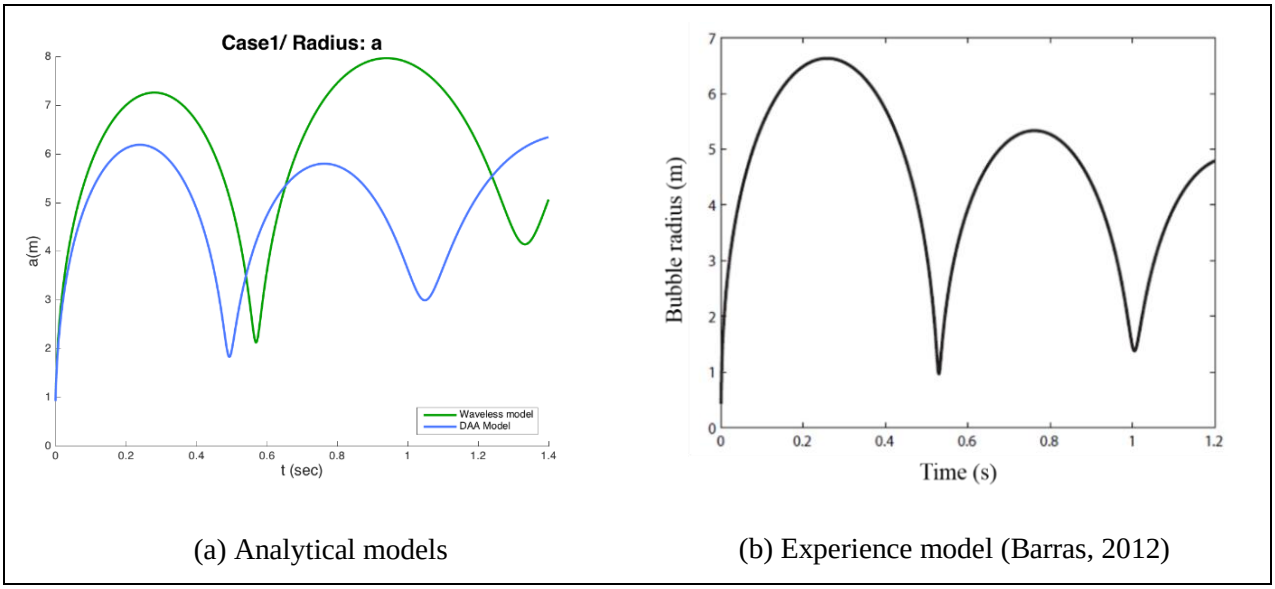

(a) Analytical models (b) Experience model (Barras, 2012)

Figure 3.1: Comparison of bubble radius: analytical models and experience (Example 1)

In Figure 3.2, the bubble vertical migration obtained by both analytical models are compared to the measured one and it appears that DAA model result matches also better with experimental result.

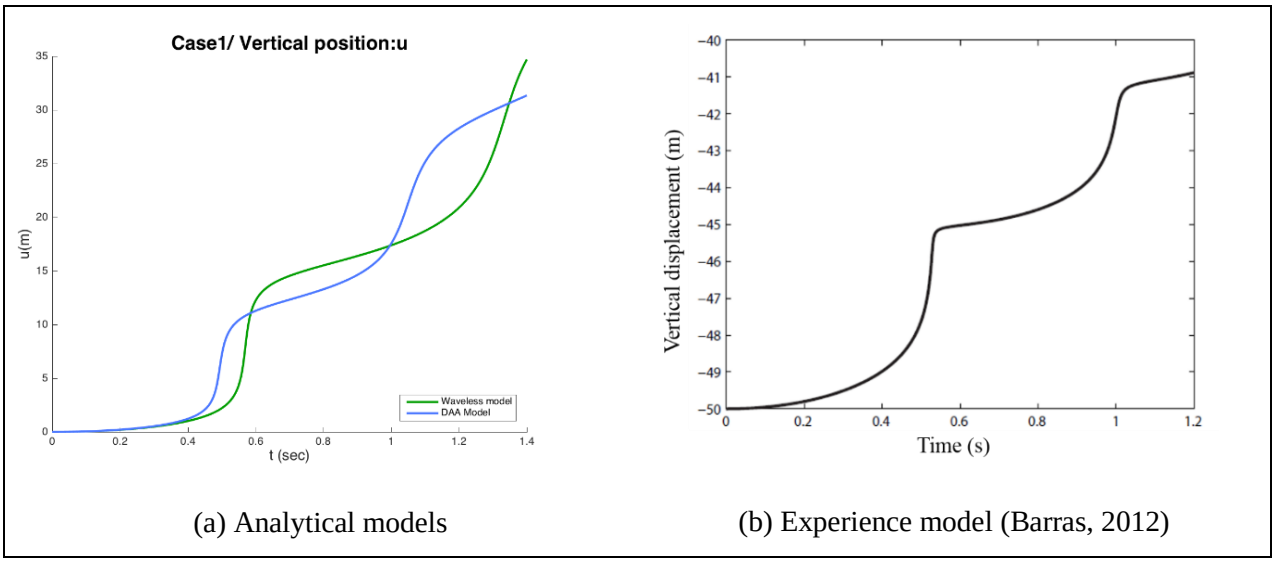

(a) Analytical models (b) Experience model (Barras, 2012)

Figure 3.2: Comparison of vertical displacement: analytical models and experience (Example 1)

Finally, the incident pressure time evolutions calculated during the first two time periods by analytical and empirical models are compared in Figure 3.3 to the measured incident pressure. This figure shows that the DAA model gives here again more realistic results.

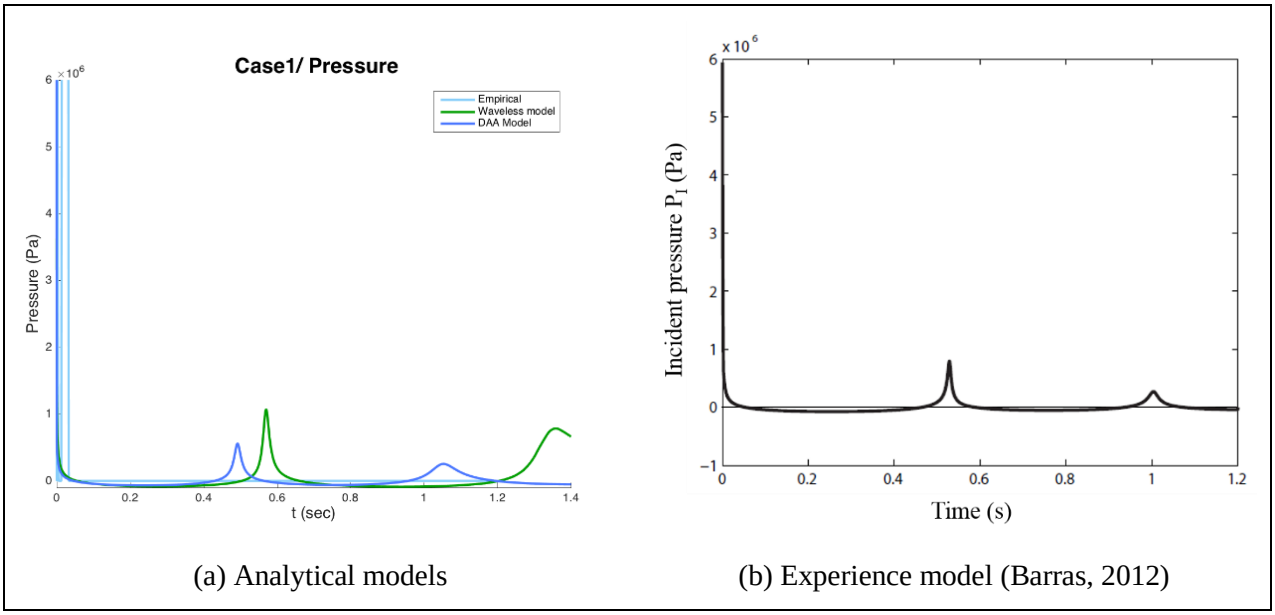

(a) Analytical models (b) Experience model (Barras, 2012)

Figure 3.3: Comparison of incident pressure: analytical, empirical and experience (Example 1)

- ***Example 2***

Regarding the analytical models, it is obvious that the DAA model leads again to more realistic results than the waveless one. The damping effect, which is taken into account by DAA model but not by waveless model, appears clearly in Figure 3.4. In the same way, the energy-loss is represented more rationally by DAA model as shown in Figure 3.6 (a). The peak pressure associated with the secondary bubble pulse decreases sensitively as compared to the fist pulse and the maximum bubble radius is decreased as well. Comparing empirical model and analytical models, Figure 3.6 (b) also shows that even if the occurrence of the first bubble peak obtained by the empirical model is close to the one obtained by DAA model, its level is unrealistically high. These figures illustrate the fact that empirical coefficients associated to the empirical model are not appropriate for this example.

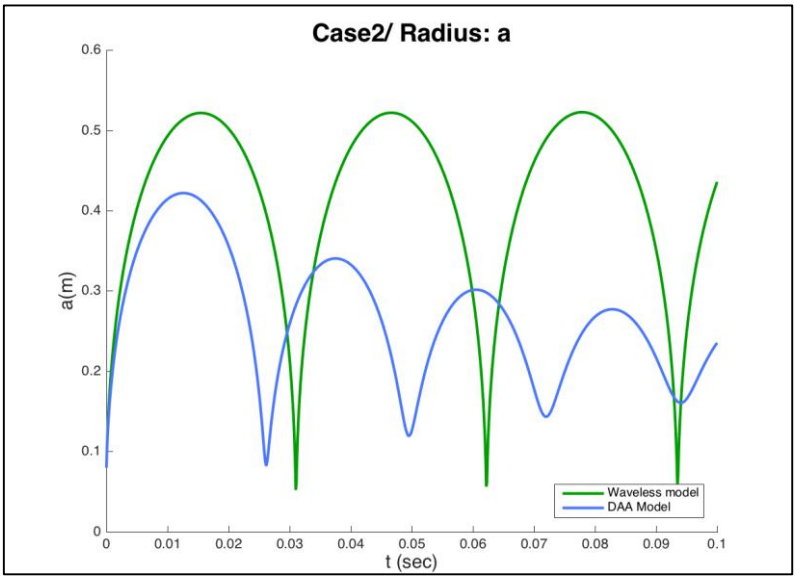

Figure 3.4: Comparison of bubble radius for analytical models (Example 2)

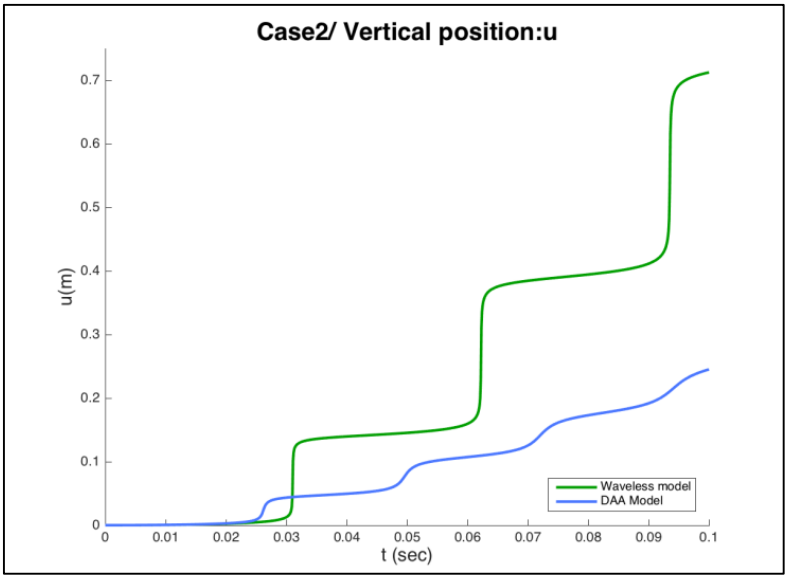

Figure 3.5: Comparison of vertical displacement for analytical models (Example 2)

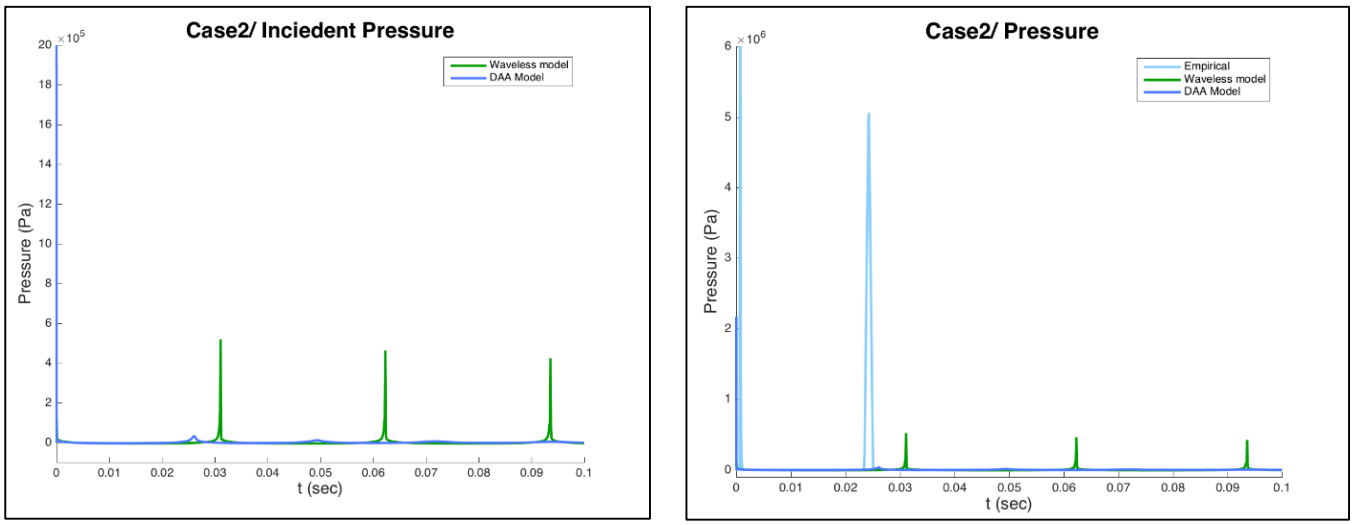

(a) (b)

Figure 3.6: Comparison of incident pressure: analytical and empirical models (Example 2)

- ***Example 3***

The results are very similar to the ones obtained for the previous example. Damping and energy loss are clearly captured by DAA model, but not by the waveless one Figure 3.7 and Figure 3.8. Figure 3.9 presents the incident pressures between two analytical models, whereas Figure 3.10 illustrates the incident pressure by empirical and waveless models. It shows that the empirical model has unrealistically high-pressure peak with the comparison of analytical models.

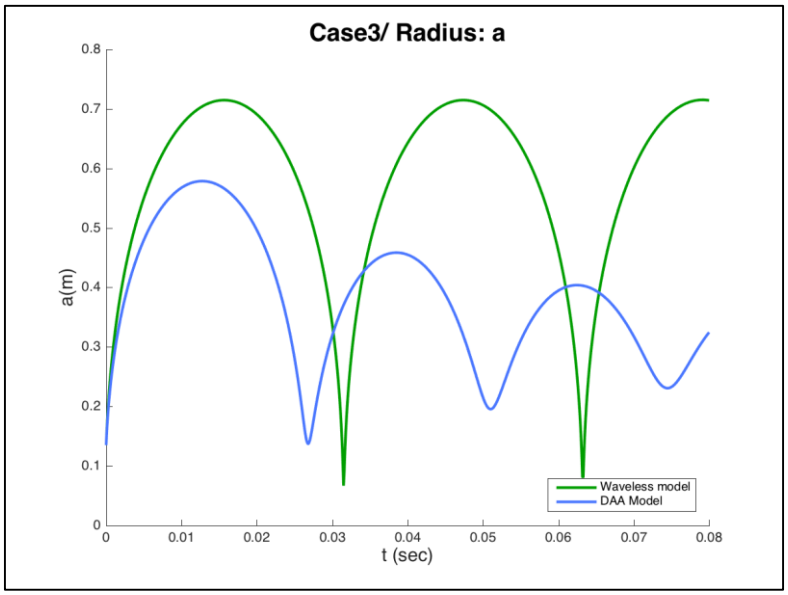

Figure 3.7: Comparison of bubble radius: analytical models (Example 3)

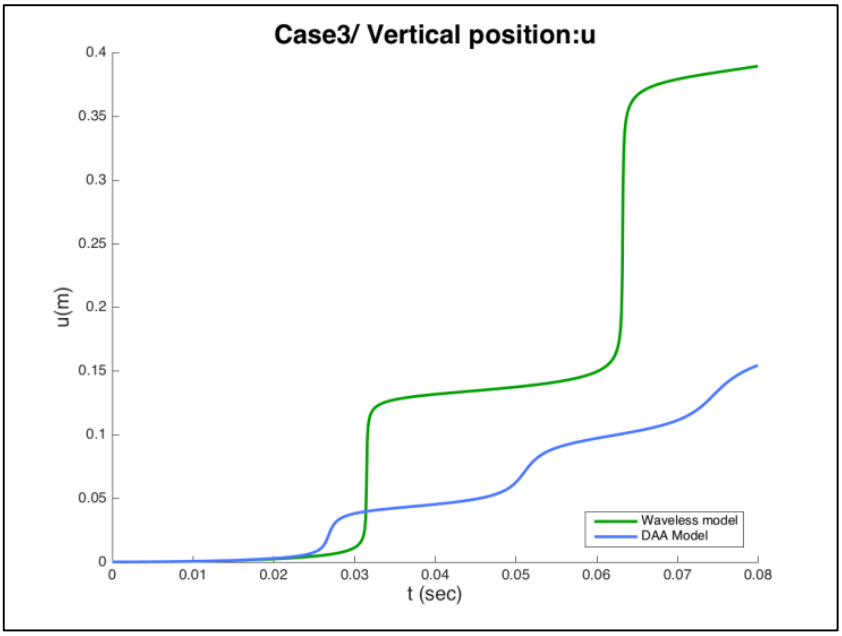

Figure 3.8: Comparison of vertical displacement: analytical models (Example 3)

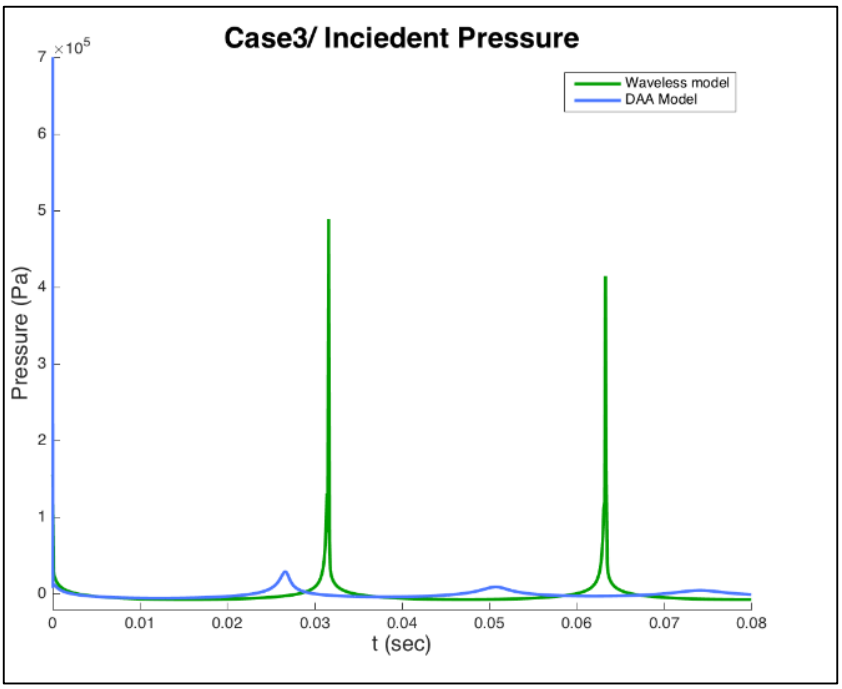

Figure 3.9: Comparison of incident pressure: analytical models (Example 3)

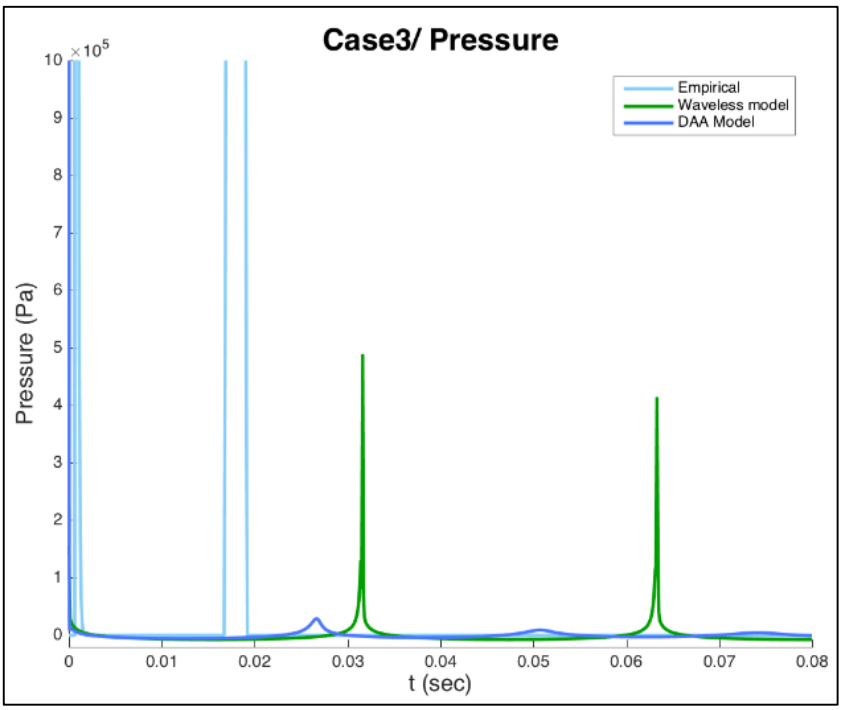

Figure 3.10: Comparison of incident pressure: analytical and empirical models (Example 3)

3.3. Conclusion

Taking into account the results presented before, the following conclusions can be drawn:

As the empirical model (Webster, 2007) is taken into account, empirical coefficients are required to calculate the bubble radius for each time period, which means that this model is not suited when the type of explosive material is changed. Moreover, resulting incident pressure seems to be unrealistic as compared to the pressure measured experimentally.

It is more flexible to use analytical models for any condition of explosive charge depth, material, weight and density instead of applying empirical values which depend on a specific case.

The simplified waveless model does not take into account damping and energy loss between two successive bubble pulsations.

By considering the damping effect as it is done in the DAA model, the interaction between the fluid and the gas bubble behaviors can be simulated properly. The finite difference method was applied in this study to solve the corresponding non-linear equations.

In conclusion, the analytical DAA model is undoubtedly the best one of these three methods. It is able to simulate correctly the radius migration of the bubble, its vertical displacement as well as the pressure arriving at the ship hull. However, Cole (Cole, 1948) mentioned that the ratio of forward and after period is about T_2/T_1=70%, whereas the time period ratio obtained

using DAA model is about 100%. This should be investigated further in more detail. On the other hand, the bubble is considered as spherical in the proposed models, whereas the bubble is compressible in reality and takes the shape of a torus during the compression phase. It can, however be shown that this assumption leads to conservative results when compared to experimental ones. Finally, it can be said that the DAA model can be applied for any type and location of charge.

4. RESPONSE ANALAYSIS OF A STRUCTURE EXCITED BY BUBBLE OSCILLATIONS

Once the different approaches have been compared, the DAA method is chosen to calculate the incident pressure due to the bubble oscillations and migration; the initial conditions related to Example 1 are taken into account for the following analyses. Once the developed MATLAB program is run, the resulting pressure is automatically distributed on the wetted part of a simple structure discretized in finite elements. The simulation of the structure response is then performed using the nonlinear explicit solver LS-DYNA.

In the framework of the author internship performed in STX Europe shipyard, a complete procedure was developed for analyzing the whipping response of a surface ship submitted to an underwater explosion. As the finite element software which is used in STX Europe is ANSYS, it was necessary to convert in ANSYS language the MATLAB code developed in ICAM in order to calculate the pressure distribution on the wet part of the studied structure.

The different structures analysis which have been performed during the master thesis work and the internship are as follows:

- **Clamped quarter plate model (LS-DYNA):** A clamped plate model was considered in order to validate qualitatively the deformation of a structure submitted to both the first shock wave and the secondary bubble pulsations.
- **Semi-cylinder model (LS-DYNA):** A simplified semi-cylinder model representing the hull beam of a ship was developed, including some transverse and longitudinal bulkheads. In the second stage, the pressure load due to underwater explosion was applied to the wetted part of this model and its whipping response was analyzed using LS-DYNA nonlinear transient simulations.
- **Semi-cylinder model (ANSYS):** in a similar way, the first objective was here to transfer the code from MATLAB to ANSYS format and to validate the developments in ANSYS language, making sure that the resulting pressure-time distributions calculated by MATLAB and ANSYS are same. Applying the pressure load to the cylinder model, the second objective was to calculate the ship response with ANSYS and to compare the resulting structural response with LS-DYNA results.
- **Real reference ship model:** Once the ANSYS program for generating the pressure distribution was validated, the final stage consisted in applying the entire procedure to a real finite element ship model provided by STX Europe.

4.1. Plate Response F.E. Simulation using LS-DYNA

4.1.1. Analysis procedure

In order to simulate the whipping response of a structure submitted to an underwater explosion, MATLAB and LS-DYNA were used at ICAM Nantes campus and the following steps were successively performed during the analysis process:

1) Model preparation: Create a finite element model in MSC Patran, export model information such as nodes and element lists as *.keyword files for MATLAB and LS-DYNA
2) Pressure load calculation: Calculate the pressure time evolution to be applied on each wetted finite element of the plate by means of analytical DAA model already programmed in MATLAB
3) Structural response analysis: Apply the pressure loads to the plate model in LS-DYNA, and run the simulation
4) Check results: In the post-processing stage, it is important to check the structural response behavior, such as vertical displacement, effective plastic strain and total energy in the system.

4.1.2. Model and loads

First of all, one consider a ship bottom plate assumed to be clamped on two consecutive frames and two longitudinal girders as shown in Figure 4.1 (a). In this simulation, only a quarter of the plate with length 8.4 m and width 4.9 m is modeled and symmetry boundary conditions are applied. The plate thickness is 30 mm and a steel material is considered. Besides, Figure 4.1 (b) represents the boundary condition imposed on each edge: two edges are clamped by restraining translation and rotation degrees of freedom, whereas symmetry boundary conditions are imposed on two remaining edges by restraining Tx translation and Ry, Rz rotations on one edge and Ty translation and Rx, Rz rotations on the other edge.

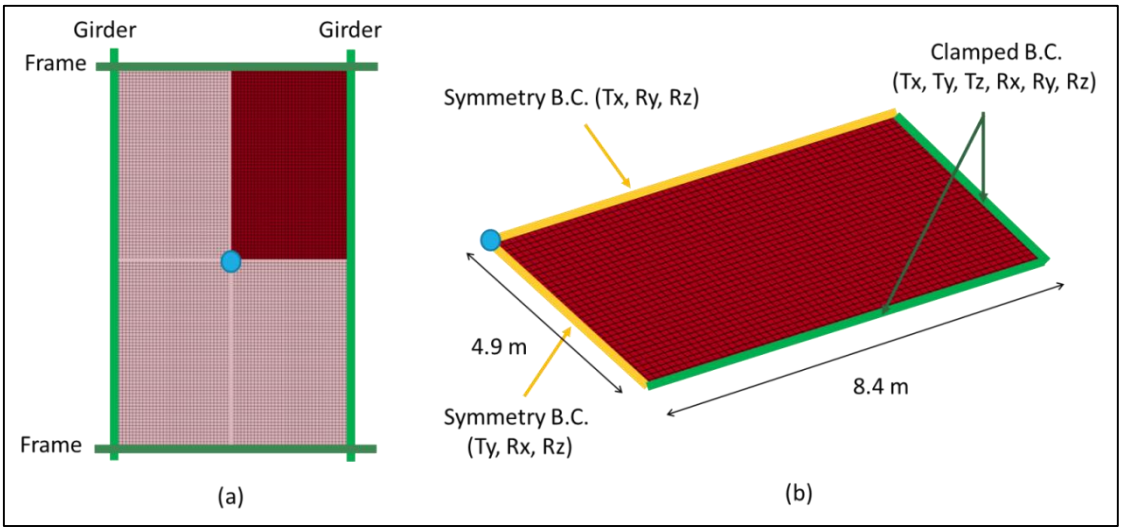

Figure 4.1: Finite element model of clamped plate

- ***Pressure Loads***

Assuming that the explosive charge is located 50 meters below the ship bottom, the pressure load to apply to the plate elements is computed by MATLAB. Figure 4.2 plots the time evolution of the pressure which is received by the center of plate (blue point in Figure 4.1). From this curve, it appears that:

- the maximum of the pressure,12 MPa, occurs at the beginning of the shock wave,
- the first bubble pulse happens after 0.5 seconds and leads to an incident pressure of 1.3 MPa,
- the second pulse occurs after 1.04 seconds and leads to an incident pressure of 0.6 MPa.

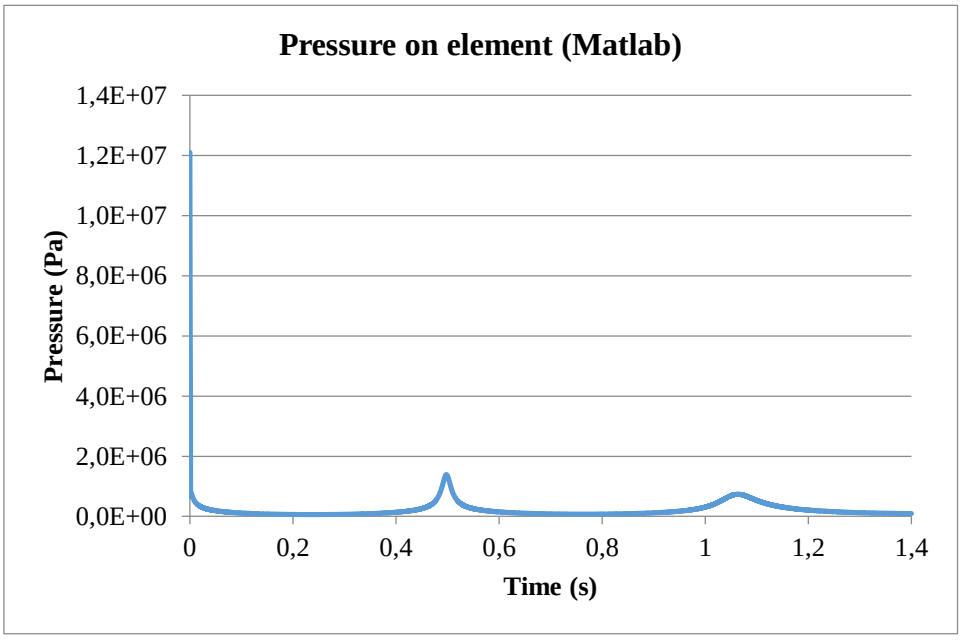

Figure 4.2: Pressure load distribution on center element (Plate model)

4.1.3. Results

Once the F.E. model is prepared and each wetted element is loaded, the numerical analysis of plate structural response can be carried out in LS-DYNA. Figure 4.3 shows the vertical displacement of the plate center node. This curves clearly shows that the main displacement is caused by the shock wave and a second displacement occurs during the first bubble pulse (0.5s). On contrary, the second bubble pulse (1.04s) seems to have any effect on the plate deformation, even if a slight increase of the total energy is observed on Figure 4.8. Figure 4.4 to Figure 4.6 also show the vertical displacement of the plate at different instants.

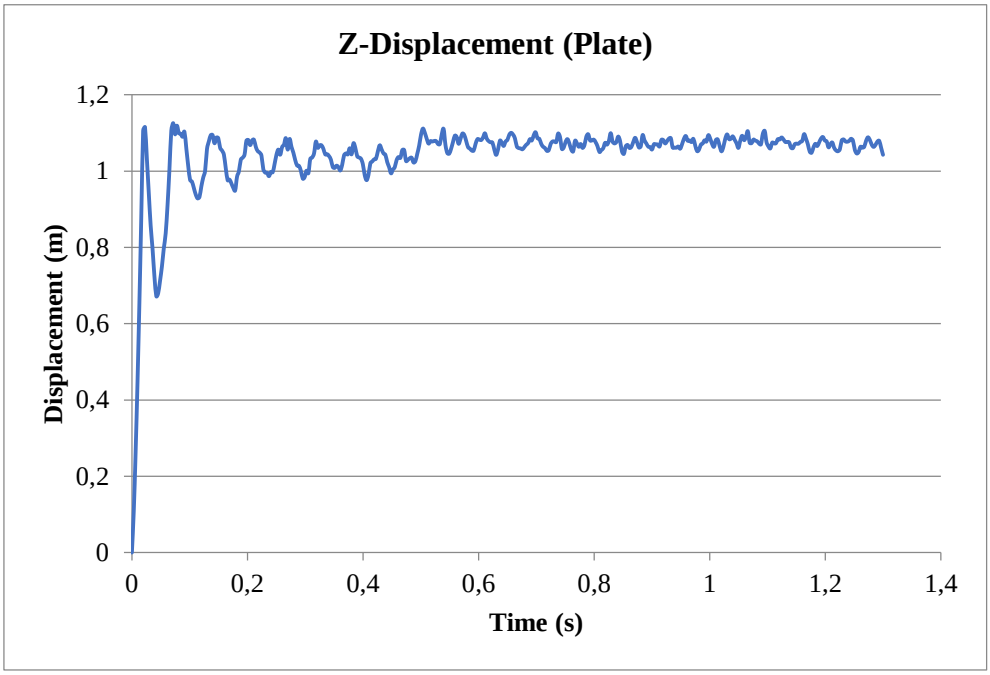

Figure 4.3: Z-displacement at the center of plate

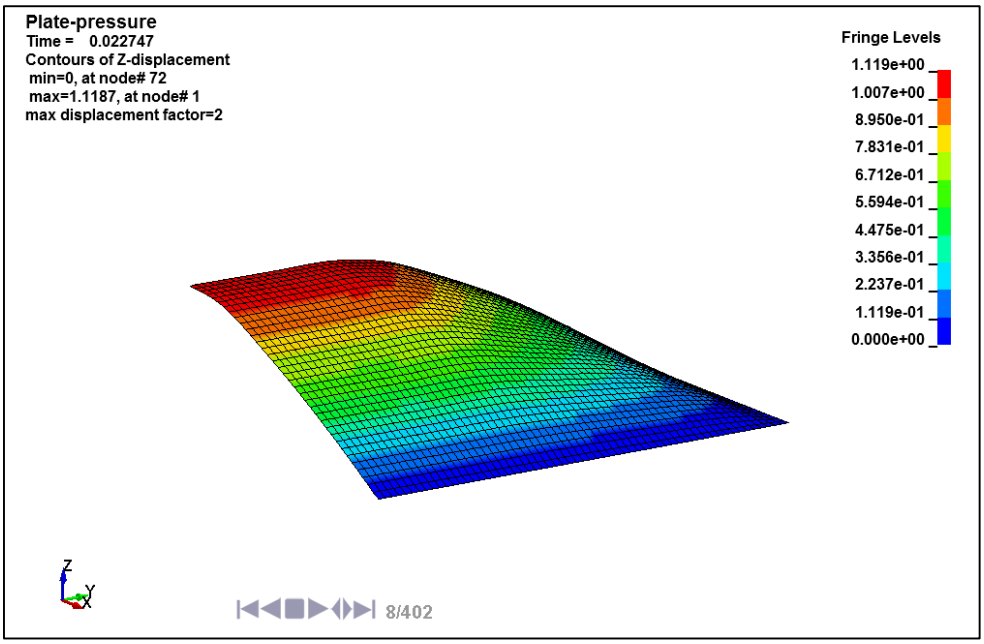

Figure 4.4: Deformation of plate model after first shock wave (LS-DYNA)

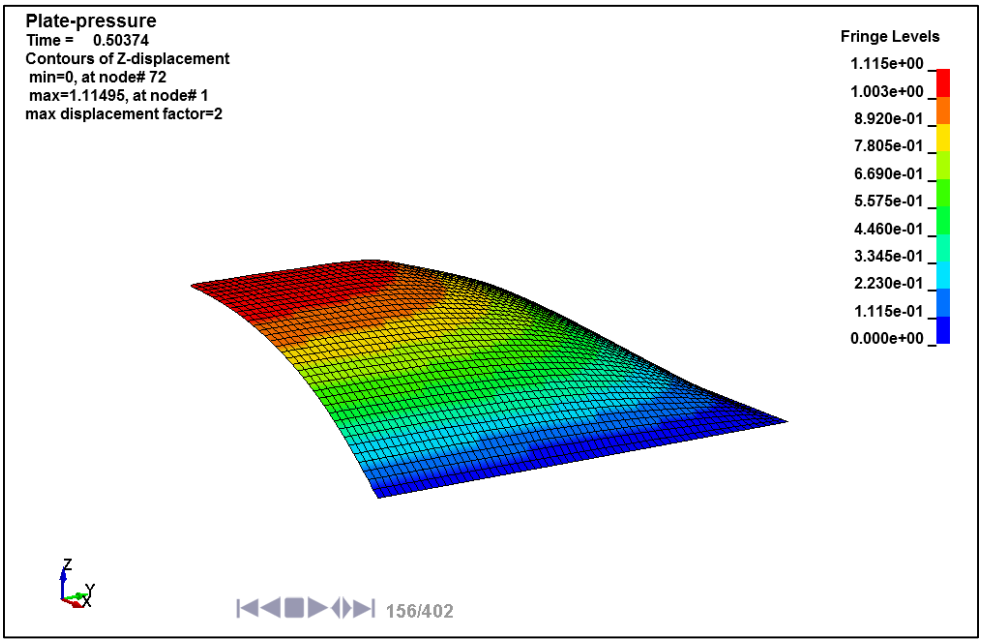

Figure 4.5: Deformation of plate model after first bubble pulse (LS-DYNA)

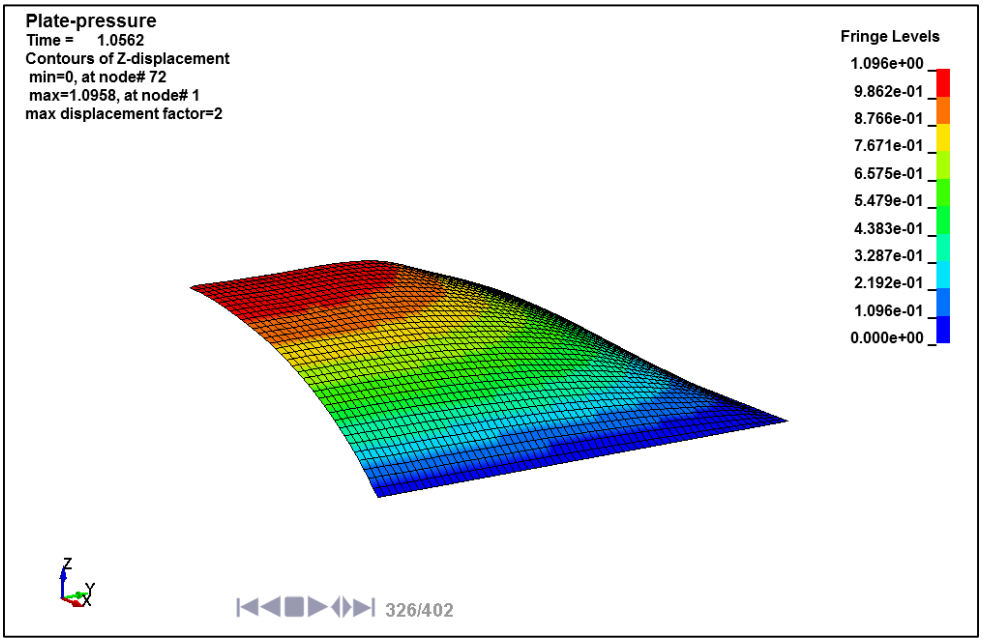

Figure 4.6: Deformation of plate model after second bubble pulse (LS-DYNA)

Furthermore, the structure will have permanent deformation once plastic strain occurs. Figure 4.7 presents the evolution of effective plastic strain at the plate center element. The plastic wave develops from the beginning of the explosion and the plastic strain level increases up to 6%. When the first bubble pulsation occurs, the plastic strain at the center of the plate increases suddenly up to 7%, then remains constant despite the occurrence of the second bubble pulse.

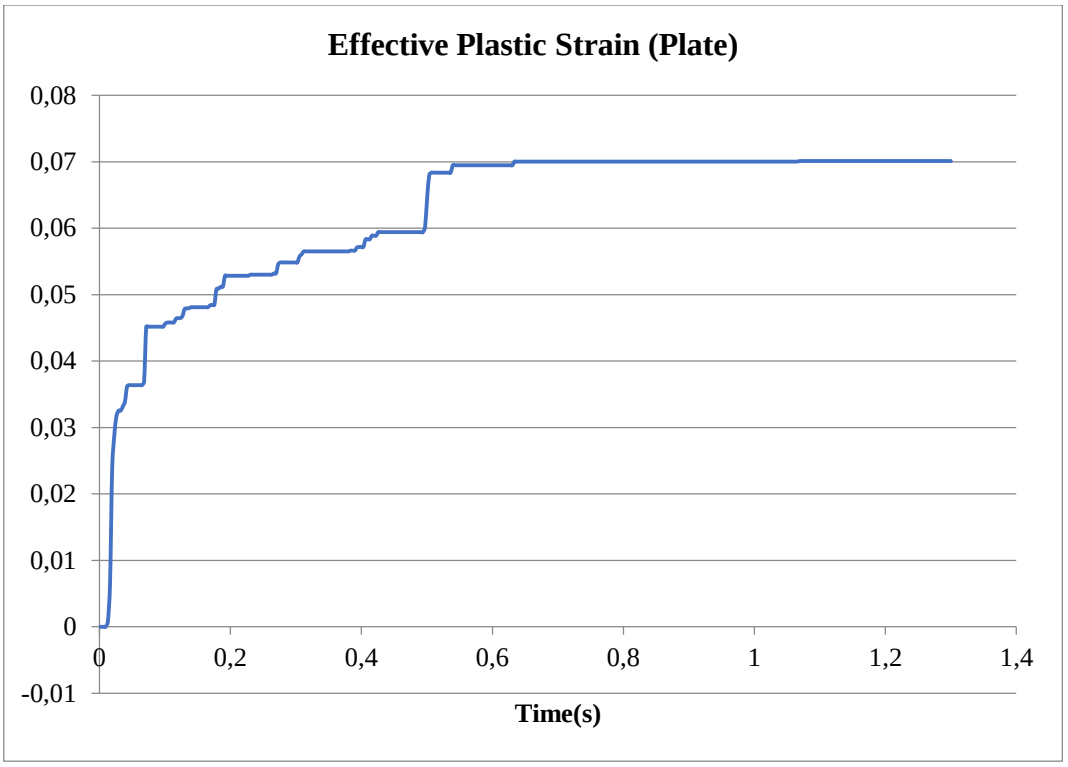

Figure 4.7: Effective plastic strain at the center of plate

Figure 4.8 plots the time evolution of the total energy. The first bubble pulse peak value occurs around 0.5 seconds with energy 1.9×10^7 J and a slightly rise happens during the second bubble pulse at 1.095 seconds.

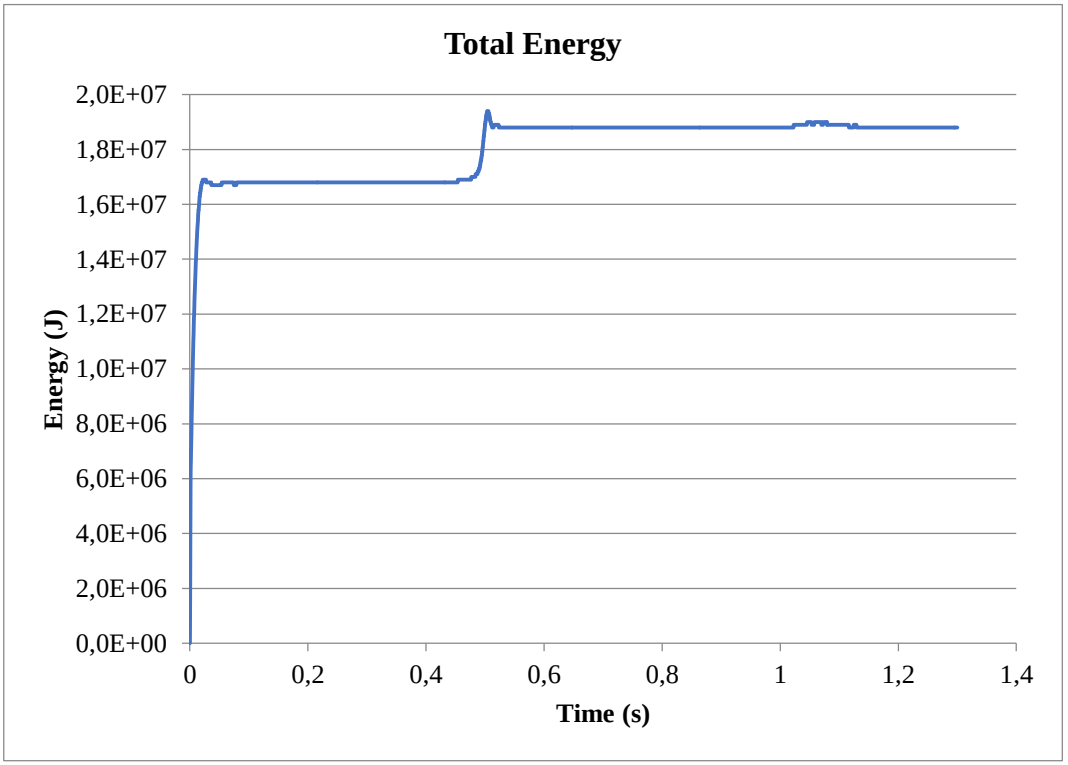

Figure 4.8: Total energy at the center of plate

4.2. Semi-cylinder F.E. Simulation using LS-DYNA

4.2.1. Model and pressure loads

- ***Model and boundary condition***

With the validation of plate model, the next stage consists in applying the developed methodology to a semi-cylinder model which is supposed to model a ship hull. Figure 4.9 presents the finite element model of the semi-cylinder "representing" 150 meters long surface ship. The ship breath is equal to 20 meters and its draft 8 meters (Table 4-1). The internal stiffening system is supposed to include transverse bulkheads every 10 meters along the ship, as well as longitudinal bulkheads every 3 meters. Regarding the thicknesses, 10 mm thick plate is used for the deck, 20 mm for all transverse and longitudinal bulkheads and the hull thickness is increased up to 80mm in order to account for the presence of secondary stiffeners.

Table 4-1: Principle dimension of cylinder model

Item	Description
Length overall	150.0 m
Breadth	20.0 m
Draught	8.0 m

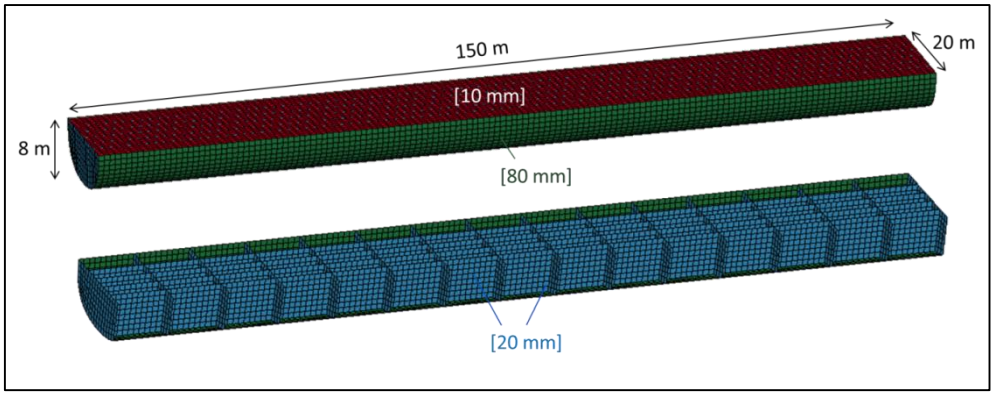

Figure 4.9: Finite element model of cylinder model (Patran)

In order to confirm that the results are realistic in every stage (shock wave, 1st and 2nd bubble pulses), specific elements are chosen as the reference so as to check and compare the results with further ANSYS simulations results. Figure 4.10 and Figure 4.11 show the referent points of the semi-cylinder deck, bottom and side shell. Assuming that the charge is located 50 meters below the bottom, the pressure load decreases when the angle between the vector of charge to the elements and the normal vectors of each element increases. Moreover, let us name elements at midship section D1, B1, and S1 for deck, bottom and side shell respectively;

similarly, D2, B2, and S2 locate at the quart of ship length from midship, whereas D3, B3 and S3 locate at the end of ship which is half length of ship from midship. Besides, Table 4 2 lists the element ID and primary node ID in correspondence with each reference point.

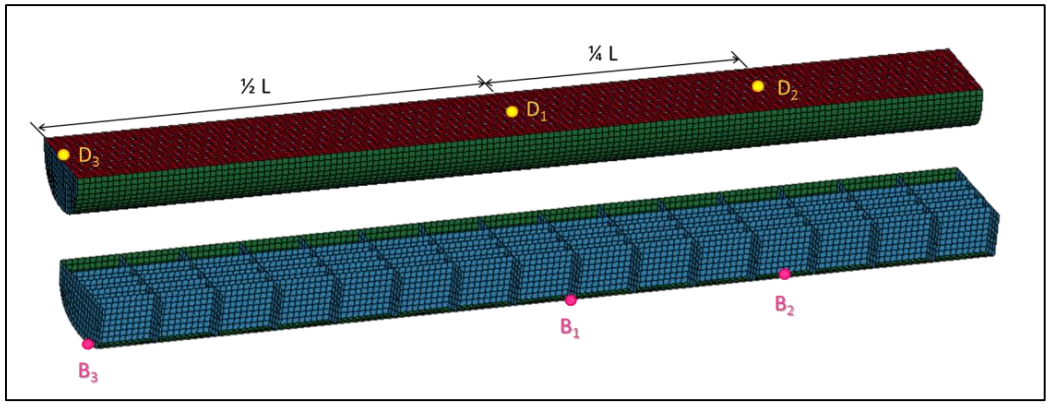

Figure 4.10: Location of reference points on bottom and deck (Patran)

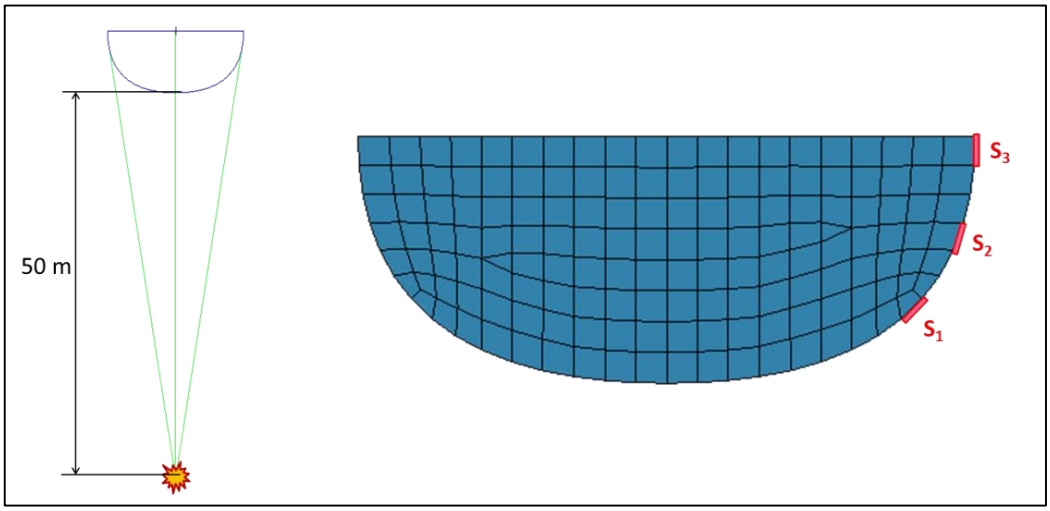

Figure 4.11: Location of reference points on side at midship section

Table 4-2: Element IDs at bottom, side shell and deck of cylinder model (LS-DYNA)

Bottom	Elem. ID	Side	Elem. ID	Deck	Elem. ID
B_1	9906	S_1	12306	D_1	9454
B_2	10020	S_2	12309	D_2	9565
B_3	9681	S_3	12312	D_3	9229

- ***Pressure Loads***

From the calculation of pressure loads by DAA model performed in MATLAB, Figure 4.12 and Figure 4.13 present the time evolution of pressure loads at bottom and side shell respectively. First of all, it is clear that the pressure loads decreases when the distance of the post-processed point to the charge increases: for the midship location at the bottom, element B1 receives a pressure of about 12 MPa when first shock wave hits the structure, then 1.15 MPa at the first bubble pulse (0.44 second) and 0.05 MPa just after the second bubble pulsation. At 1/4 ship length, bottom element B2, receives a first shock wave pressure of 6.42 MPa, 0.73 MPa just after the first bubble pulse and 0.11 MPa at the second pulse. Moreover, at the end of ship element B3 has pressure loaded with a pressure of 3 MPa when first shock wave arrives, 0.13 MPa just after the first bubble pulsation and 0.09 MPa at second bubble pulsation.

As the hull side is concerned, the pressure distribution will decrease according to the angle between the direction normal to the element and line joining the element to charge. Figure 4.13 plots the pressure distribution for three locations S1, S2, and S3. Firstly, at location S1 which is close to the bottom at midship, a significant high pressure loads 6.74 MPa appears when first shock wave happens, 0.6 MPa just after the first bubble pulse, and 0.3 MPa when second bubble pulsation happens. Secondly, 3.7 MPa pressure load is applied to S2 which is located at one-third distance from free surface to the end of bottom at first shock wave whereas 0.1 MPA and 0.075 M Pa are the peak values for first and second bubble pulsations. Finally, the pressure distribution for S3 point becomes zero because the angle αi is larger than 90^{o} between the element normal and the line joining the element to the charge. It points out that the pressure loads decreases when the angle between element normal vector and the vector from located element to the charge increases.

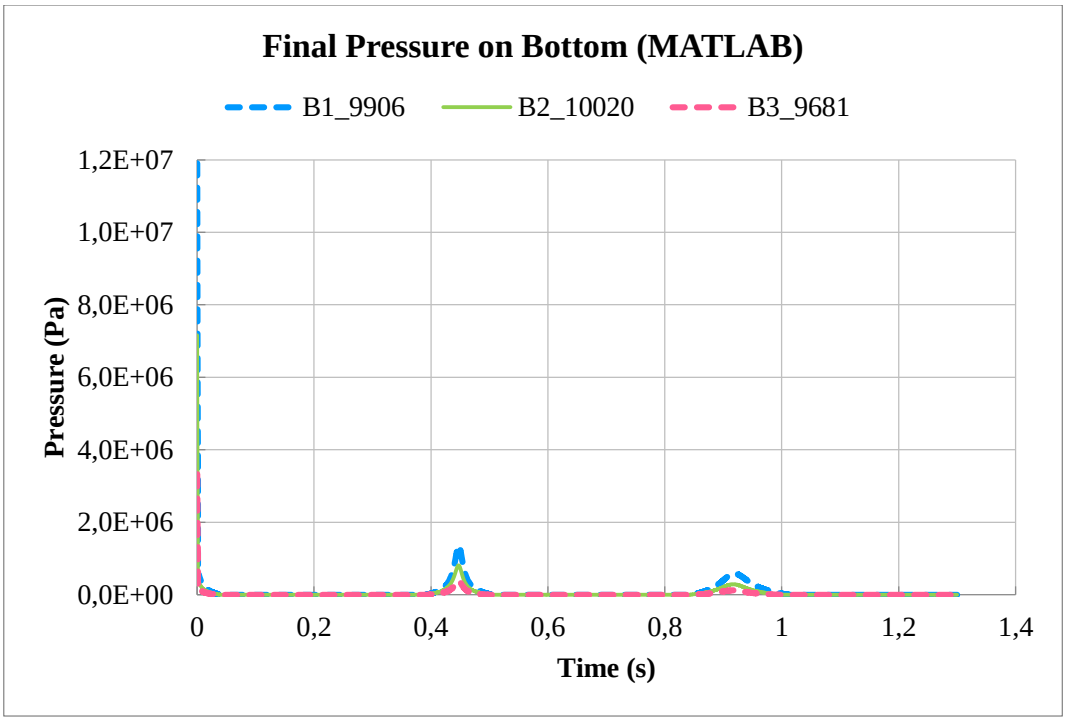

Figure 4.12: Pressure loads on bottom of cylinder model

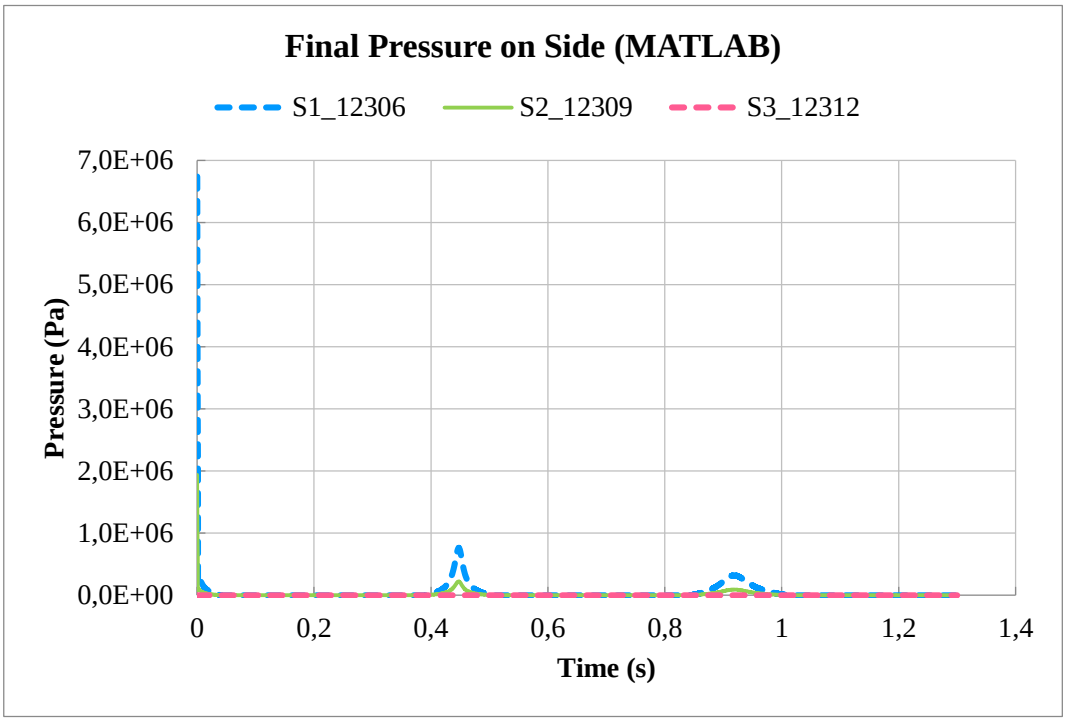

Figure 4.13: Pressure loads on hull side of cylinder model

Moreover, it is known that with the sufficient accumulation of energy during the bubble propagation. The impulse and energy can be calculated from Eqs.2-8 and 2-9, besides, by calculating the area under the pressure curve. In the present example, it is calculated that the area below the pressure curve at first bubble pulse and second bubble pulse peak are about five times higher than the area associated with the first shock wave. It proves that the bubble oscillations have the significant influence on the ship structure and might cause severe

structural damage that cannot be ignored when analyzing the ship response to an underwater explosion.

4.2.2. Results

In LS-DYNA, the total energy is the summation of internal energy, kinetic energy, deformation energy and external works, which describe how the structural absorb the energy with submitted to the underwater explosion.

Figure 4.14 shows the time evolution of kinetic energy, the internal energy of deformation, external energy, hourglass energy and total energy which represent the transfer of energies between the explosion and model. In this diagrams, three obvious peak values appear corresponding to the three important phenomena which happen to kinetic, external and total energy: first shock wave, first bubble pulsation, and second bubble pulsation. According to Figure 4.14, it is clear that there have almost 1.5 times energy happened for secondary bubble oscillation phase compared with the first shock wave, with this consequence, it indicates that it cannot be ignored and should consider it as serious for the influence of secondary bubble pulsation. Similarity, the total energy which includes inertial energy, kinetic energy hourglass energy also on. From this diagram, it has 4×107 J at 0.014 seconds, 1×108 J at 0.5 seconds and 1.32 ×108 J at 0.98 seconds. It represents the bubble oscillation phase; it has more than 1.5 times total energy than first shock wave phase as well.

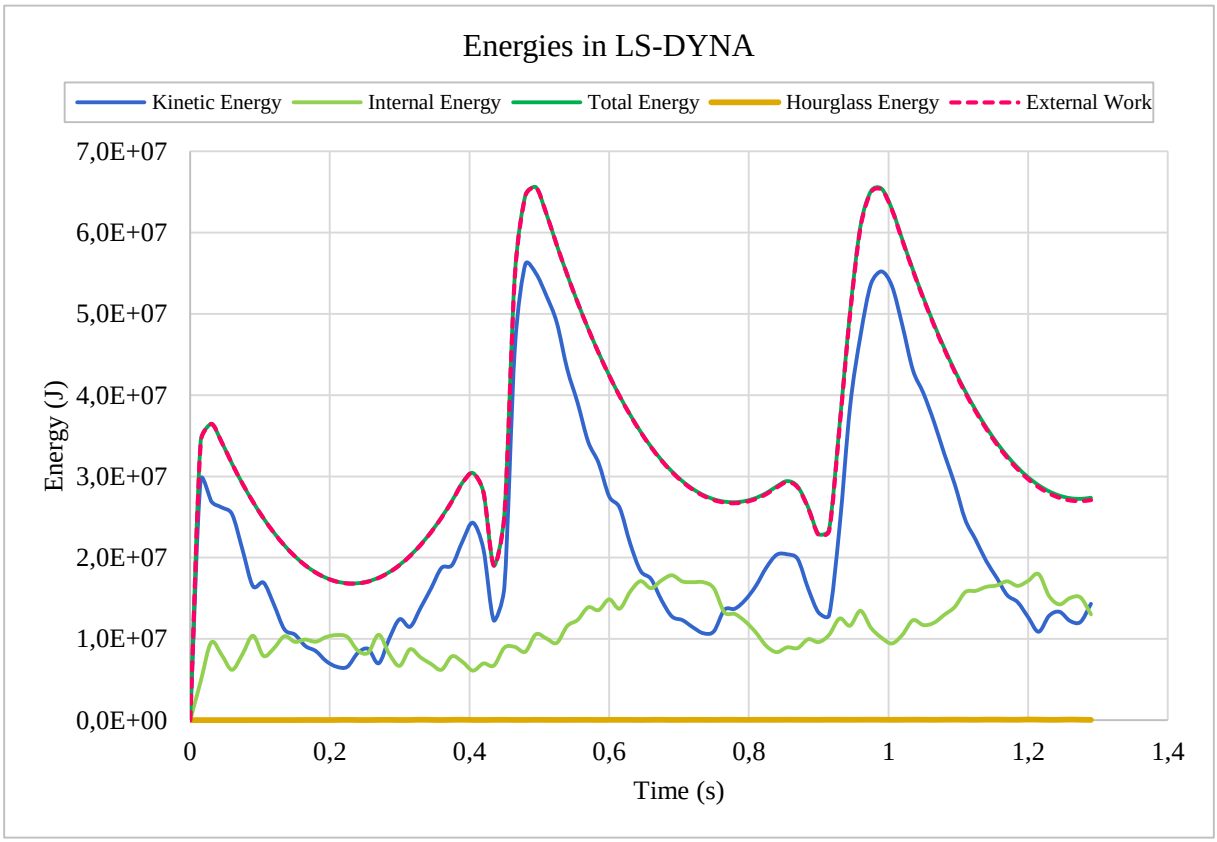

Figure 4.14: Energies of cylinder model (LS-DYNA)

Furthermore, in order to check that the ship deformation is realistic, Figure 4.15 to Figure 4.17 plot the time evolutions vertical z- displacement at the reference points on the bottom, side shell, and deck.

First of all, Figure 4.15 plots the time evolution of the vertical displacement of the three bottom reference points during the bubble migration. At the midship location, the vertical bottom displacement increases up to 0.36 m, 0.73 m and 1.2m at shock wave, first and second bubble pulses instants respectively. It is worth noting that these displacements includes the overall displacement of the ship which is not compensated by the gravity force as the gravity is not taken into account in these simulations. Figure 4.16 and Figure 4.17 show that the vertical displacement of the side shell and the deck follows more or less the displacement of the bottom.

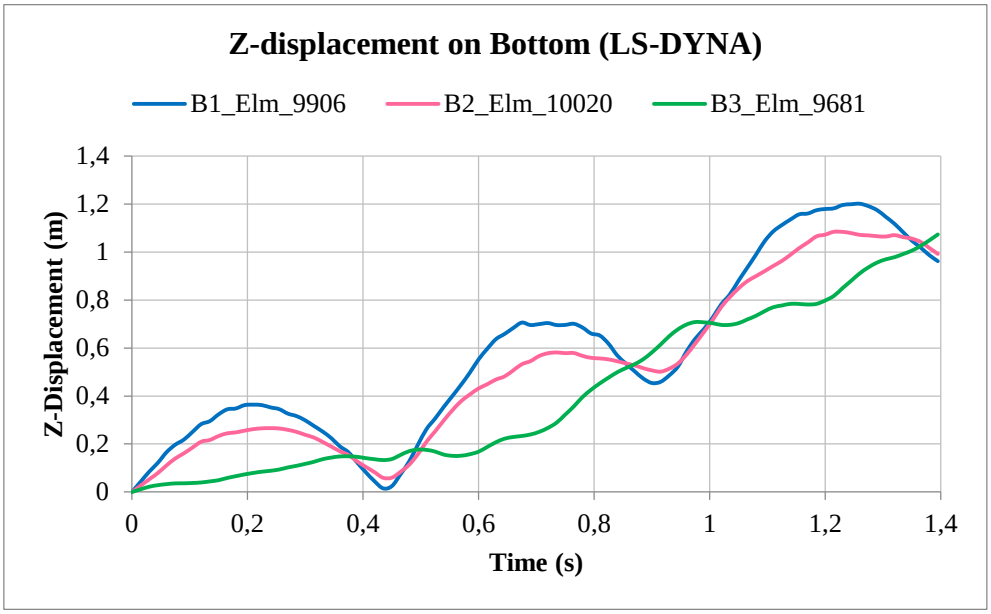

Figure 4.15: Z-displacement at bottom of cylinder model (LS-DYNA)

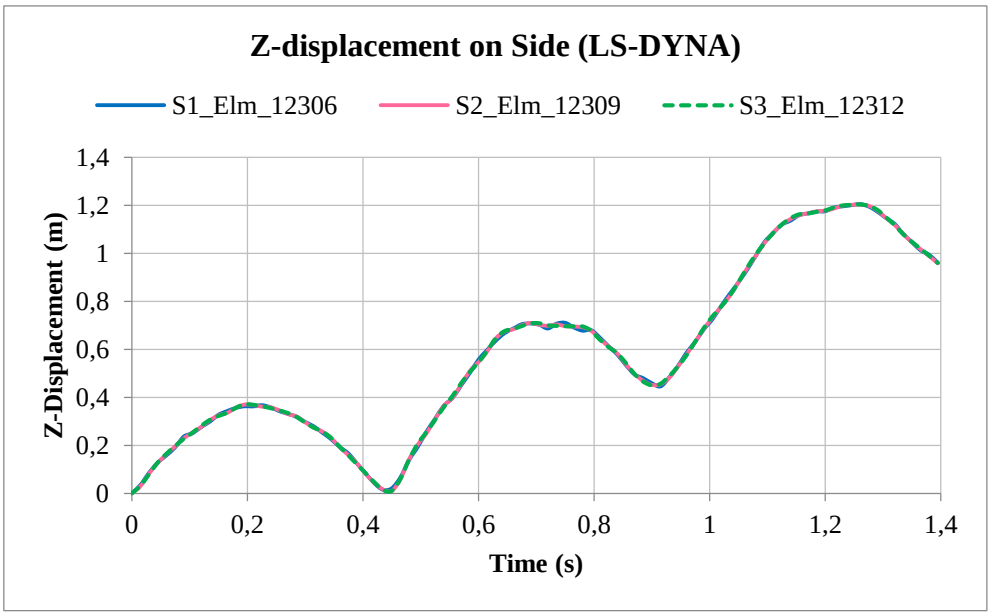

Figure 4.16: Z-displacement at side shell of cylinder model (LS-DYNA)

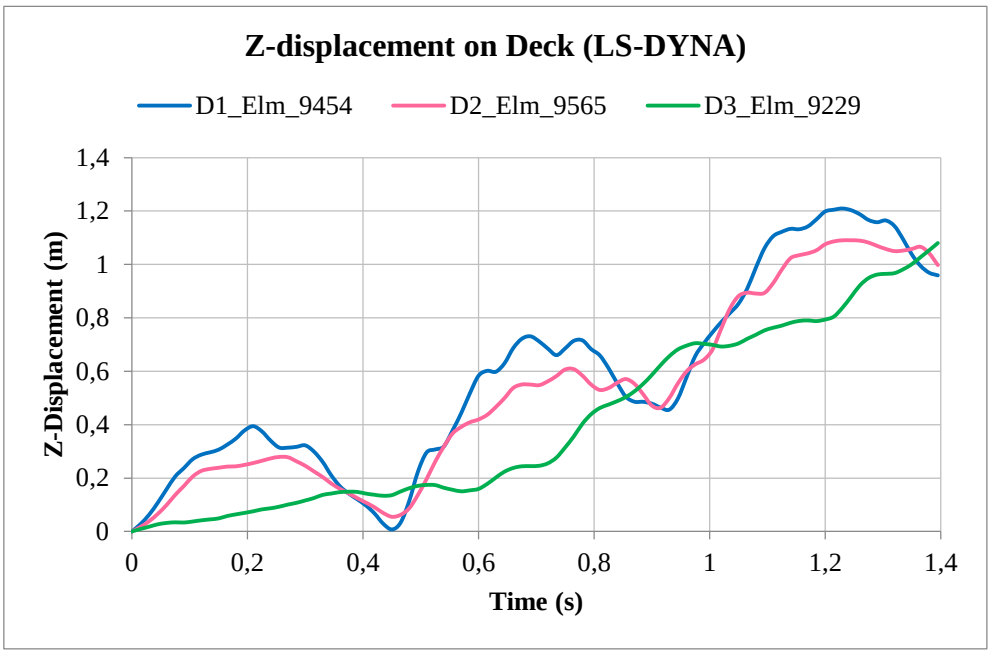

Figure 4.17: Z-displacement at deck of cylinder model (LS-DYNA)

In order to extract the overall displacement of the ship from this results, Figure 4.18 plots the difference between midship the bottom vertical displacement (location B1) and the afterward ship one (location B3). These results show that the overall deflection of the hull beam increases up to 30 cm after the shock wave, 45 cm after the first bubble pulse and 38 cm after the second one. These results will be further compared with ANSYS results. It appears that these curves seem to be quite realistic, even if the simulations performed using LS-DYNA do not consider the fluid-structure interaction. Let us remember that these simulations have been carried out with the objective to verify the quality of the pressure distribution and to put in evidence the influence of the bubble oscillations.

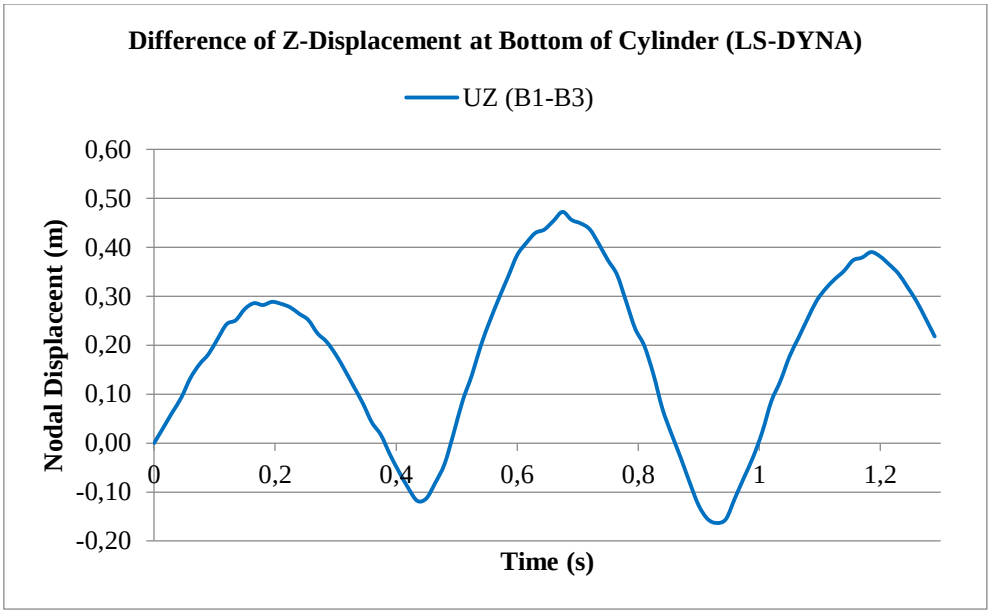

Figure 4.18: Difference of Z-displacement between B1 and B3 points (LS-DYNA)

In correspondence with the vertical displacements plotted in Figure 4.15 to Figure 4.17, Figure 4.19 to Figure 4.21 show the deformation of semi-cylinder model as post-processed using the interface of LS-DYNA. These three plots represent the deforming model at particular time 0.2 s, 0.7s and 1.2 s which have the peak value of displacement respectively. It is clear that the highest displacement occurs in the middle of the ship which is at the closest distance to the charge (50 m).

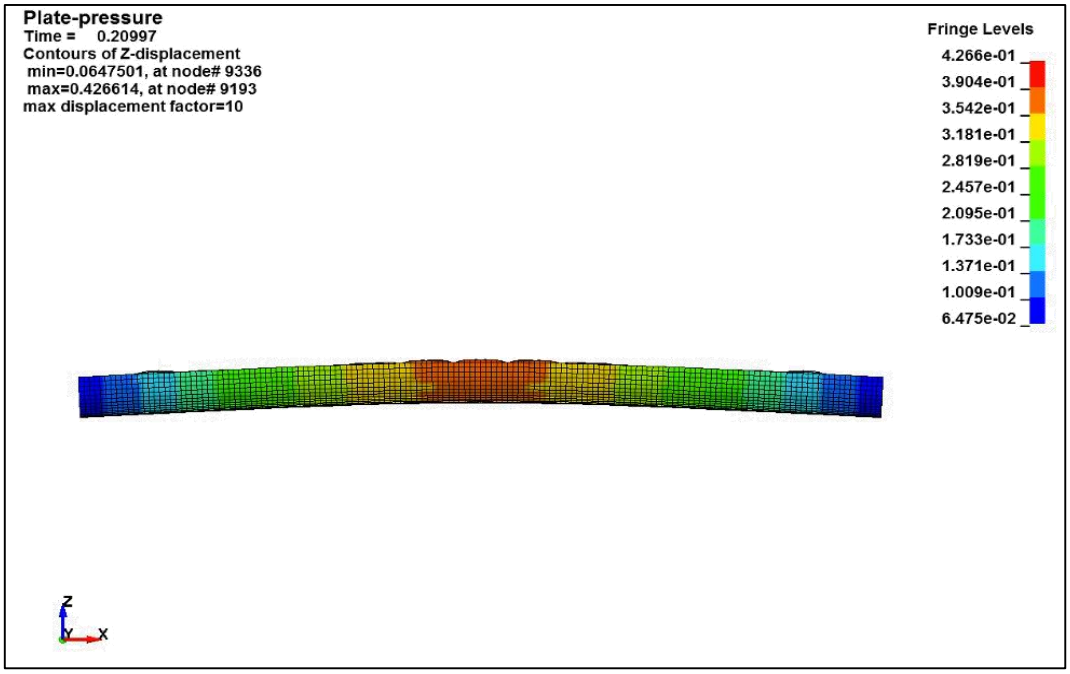

Figure 4.19: Deformation of Z-displacement after first shock wave at 0.2 s (LS-DYNA)

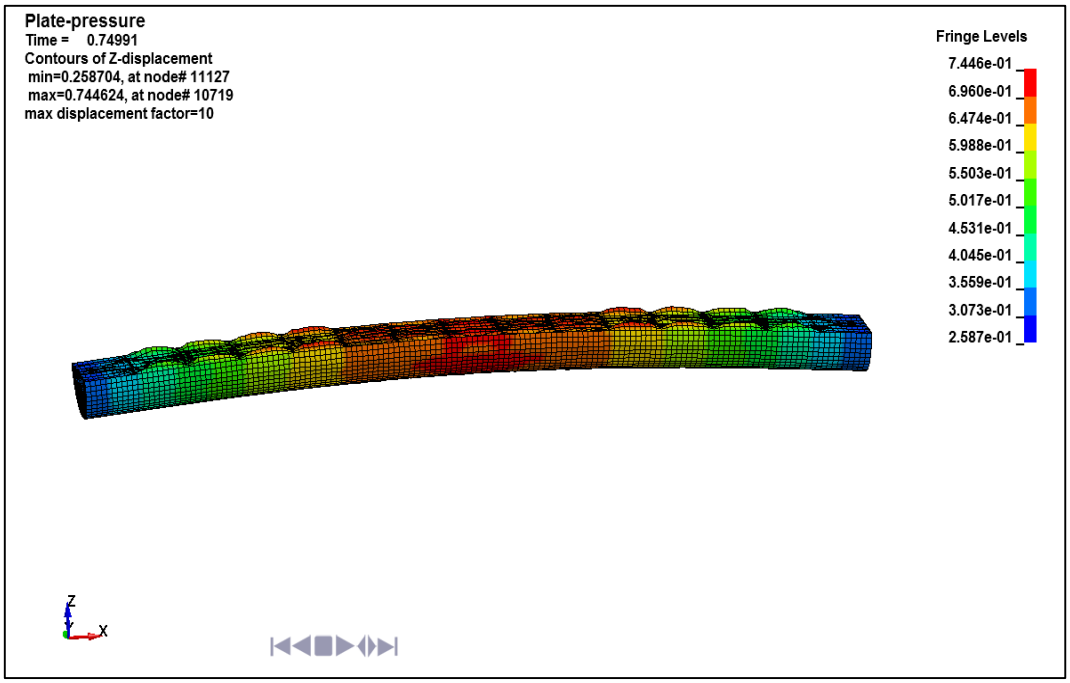

Figure 4.20: Deformation of Z-displacement after first bubble pulse at 0.7 s (LS-DYNA)

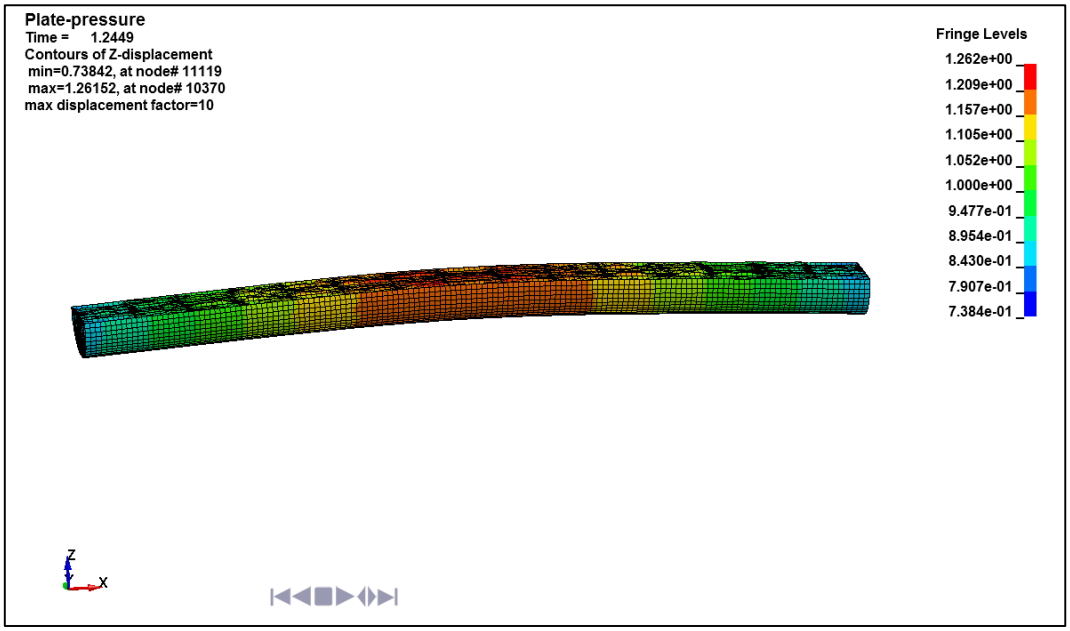

Figure 4.21: Deformation of Z-displacement after second pulse at 1.24 s (LS-DYNA)

Furthermore, as mentioned before, the elastoplastic strain is one of the important guidance to check whether the structure has classified or not. In this case, the effective plastic strain is zero during the overall bubble progression, which means that the structure remains without any permanent deformation. That is to say, the chosen structure is strength enough to stay in the elastic domain, which seems to be logical knowing that the hull thickness has been taken equal to 80 mm.

4.3. Semi-cylinder F.E. Simulation using ANSYS

4.3.1. Analysis method and procedure

The main objective of the internship performed in STX Europe was to develop a complete analysis procedure of the surface ship whipping response when it is submitted to an underwater explosion effect. Before all calculations, the very first step was to write the program for ANSYS, by converting the MATLAB code into ANSYS language which is the numerical code commonly used in STX Europe.

Hence, with the purpose of carrying out the analysis process in implicit numerical software ANSYS, it is important to clarify each step to make sure that ANSYS results compare correctly, at each step, with the results obtained in ICAM with LS-DYNA. Figure 4.22 presents the analysis procedure which was implemented in ANSYS.

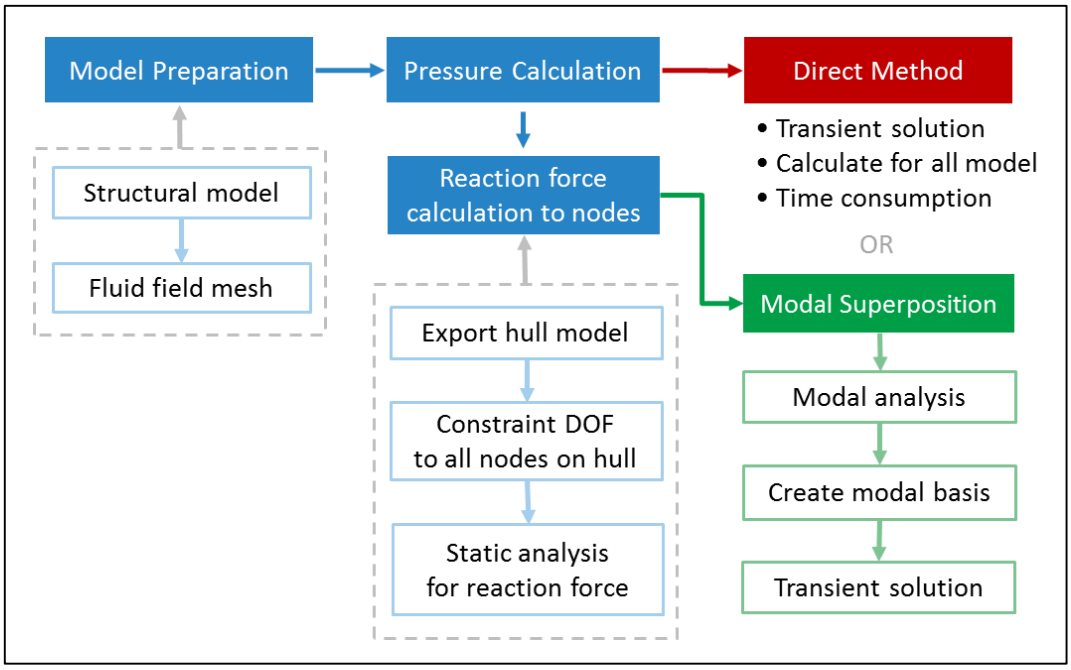

Figure 4.22: Configuration of analysis procedure in ANSYS

There are three main stages to process a complete analysis using ANSYS finite element code: model preparation, pressure loads calculation and simulation using one of two possible calculation methods.

Model preparation: In order to perform a numerical analysis with ANSYS, not only the structural mesh for the semi-cylinder model or surface ship model but also the surrounding water mesh are built in order to take into account the fluid-structure interaction. The detail description of model definition, such as structural mesh, fluid mesh and boundary condition are presented in the following section.

Pressure loads calculation: From the MATLAB code which has been previously developed to calculate pressure loads based on analytical DAA model, a procedure in ANSYS language has to be built in order to generate, directly in ANSYS, the correct pressure on each wetted finite element. This work will be discussed in the later section.

Analysis methods: Two approaches are available in ANSYS F.E. code to simulate the whipping response of a semi-immerged structure: the direct integration method and the modal superposition method.

Direct integration method: In this solution, applying pressure loads to the entire model and doing transient solution directly. It analyzes the structural response for all elements with every time step, which is more convenient and less step to perform the analysis. Nevertheless, due to the direct method will calculate the deformation of all elements of the entire model for each time step, which has huge time consumption to accomplish all process. With the assumption of direct integration method, it is suitable for any movements of fluid and structure, no matter large or small displacement of the structure, as well as the large velocity of fluid particles. Moreover, it has no limitation to linear behavior only, which means it allows for non-linear material behavior, such as contacts and non-linear loadings. However, this method requires specific expertise, the post-treatments of calculations are delicate that regulations do not apply this method currently.

Modal superposition method: With the consideration of time consuming, the other solution is to analyze with the modal analysis.

Firstly, a static solution must be carried out in order to acquire the reaction forces on each node of the ship hull. The pressure loads are applied to the center of elements with the fixed six degrees of freedom to all nodes. Then, by performing a static analysis, the reaction force on nodes due to the pressure loads by the underwater explosion in time steps can be obtained.

Afterward, performing modal analysis without any pressure loads and force on finite element model, considering the 80% modal mass as some modes as the preparation, with this consequence, with the summation deformation for ship model due to the modal superposition of each mode can be considered as the modal basis.

Finally, reaction forces are imported to all nodes on ship hull, executing transient solution with the summation deformation by modal superposition. With this method, the consuming of time is quite less than the direct method which saves lots of time even it takes more steps to achieve the calculation.

The principle of the modal method is to write the fluid-structure coupling system movement equations on the natural modes basis, in order to break down the analysis of N single degree of freedom oscillators. With this method, it assumes the fluid and structure are linear behavior with the small movement of perfect fluid and elastic structure. With the calculation of natural modes of the fluid-structure system, natural frequencies, and mode shapes can be carried out during this process. Afterward, projecting the movement equations in the modal space, which means the vector space is created by using the calculated mode shapes. Lastly, determining the system response in the modal space by using the spectral method or a modal superposition method.

Nevertheless, even though this method is more simple and easier to implement than direct integration method, it has limitation to execute this analysis, such as it is necessary to make sure it has enough modes to handle correct modal truncation. Also, the refinement of finite element mesh size must sufficient and enable to capture all the required modes. Lastly, it allows for small displacements of the fluid-structure system and linear behavior only.

4.3.2. Model and analysis process in ANSYS

- ***Model Preparation***

Figure 4.23 shows the cylinder model created using ANSYS pre-processor with the same dimension as mentioned in Table 4-1. The distance from explosive to the structure remains 50 m, and the charge is kept at the midship under the bottom. Moreover, with the consideration of the interaction between the structure and the sea water, it is necessary to create a fluid mesh in ANSYS. Figure 4.24 plots the interface mesh between the structure and the fluid. Lastly, Figure 4.25 presents the fluid-field mesh surrounded the semi-cylinder, knowing that 50 m is considered as the radius of fluid-field mesh in this case.

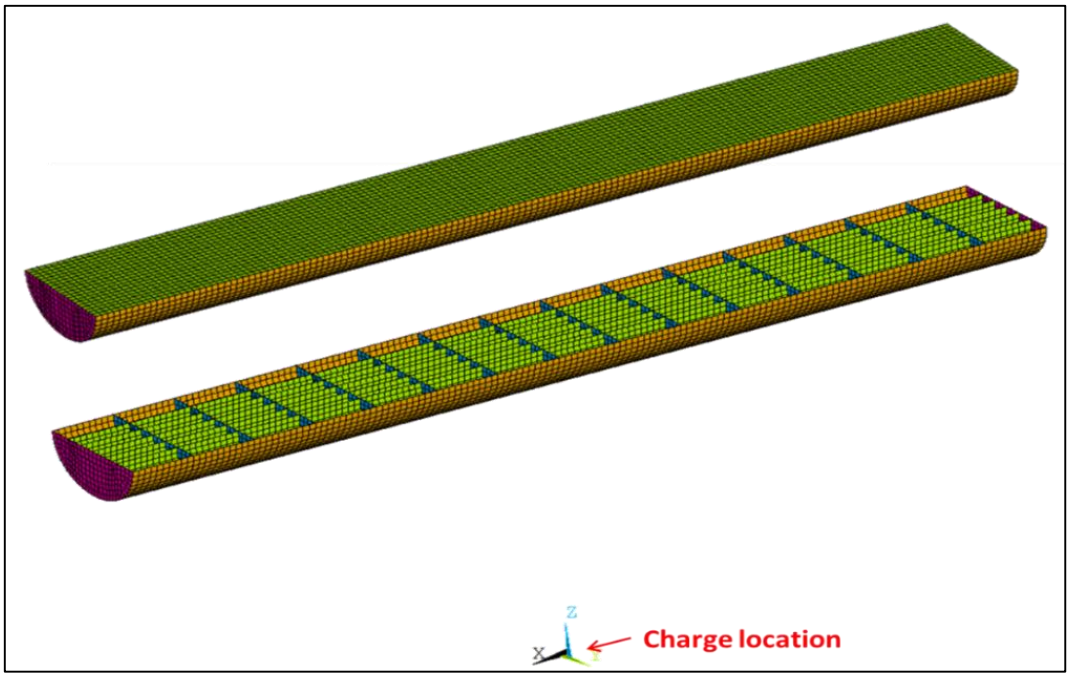

Figure 4.23: Cylinder model with meshes

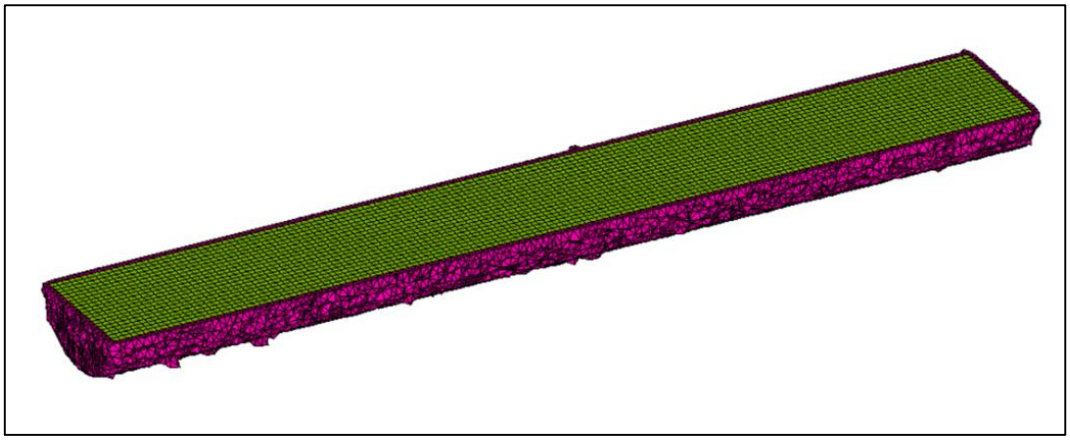

Figure 4.24: Fluid-structure interface mesh

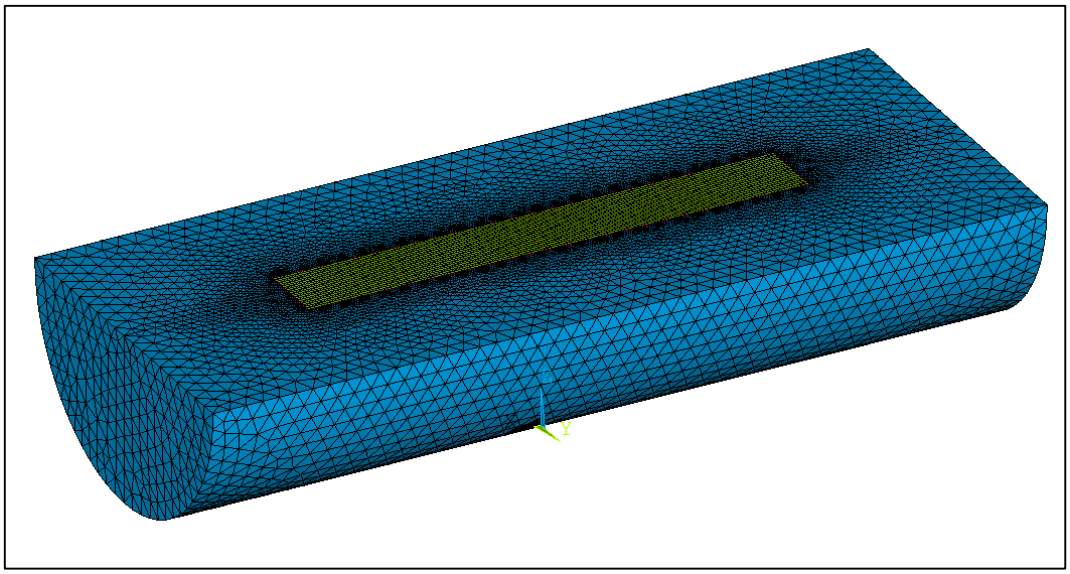

Figure 4.25: Fluid field mesh

Similarly to the semi-cylinder response simulation performed with LS-DYNA, the reference points are at the same relative place as plotted in Figure 4.10 and Figure 4.11, whereas the corresponding element and node IDs are listed in Table 4-3 as below.

Table 4-3: Referred element and node IDs at bottom, side shell and deck of cylinder model in ANSYS

Bottom	Elem. ID	Node ID	Side	Elem. ID	Node ID	Deck	Elem. ID	Node ID
B_1	8670	1404	S_1	6749	6907	D_1	3798	4160
B_2	9002	1761	S_2	6779	6910	D_2	4361	4806
B_3	7897	8001	S_3	6809	6913	D_3	2633	3006

- ***Pressure Loads***

Once the procedure in ANSYS language has been run, Figure 4.26 and Figure 4.27 plot the pressure loads distribution at the reference points located on bottom and side shell of the semi-cylinder. Compared with Figure 4.12 and Figure 4.13, which are the pressure loads distribution on bottom and side by using MATLAB code; for instance, curve B1 in Figure 4.12 and Figure 4.26, they have same pressure distribution with time evolution, the pressure peaks are occurred at same time step and with same amount values. Whereas the distributions in Figure 4.13 and Figure 4.27 have slightly different due to the curvature of the model is slightly different design.

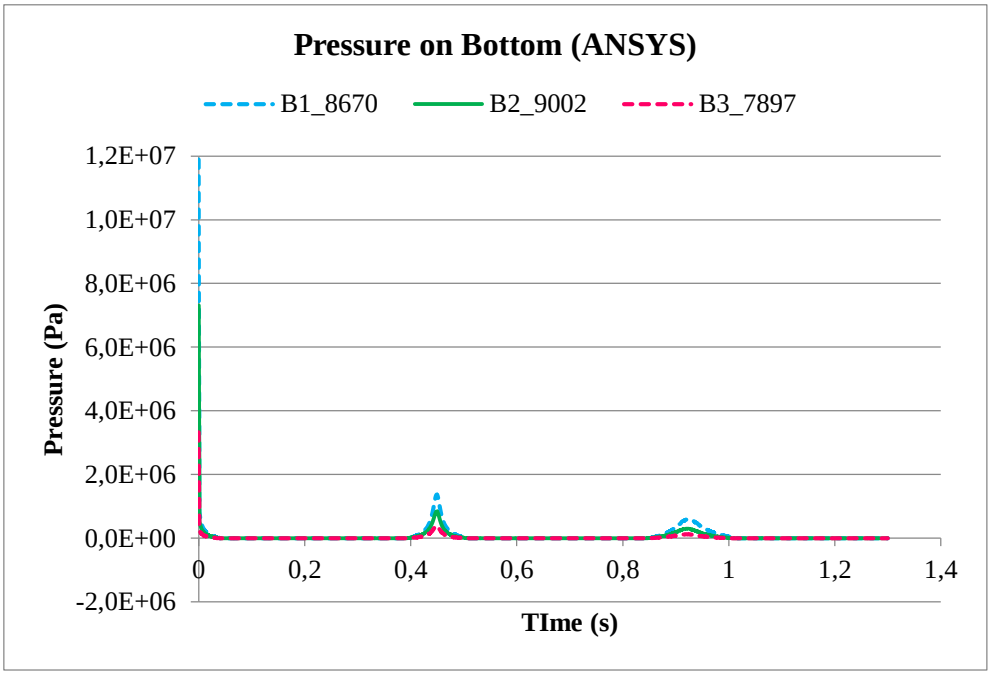

Figure 4.26: Pressure loads on bottom of cylinder model (ANSYS)

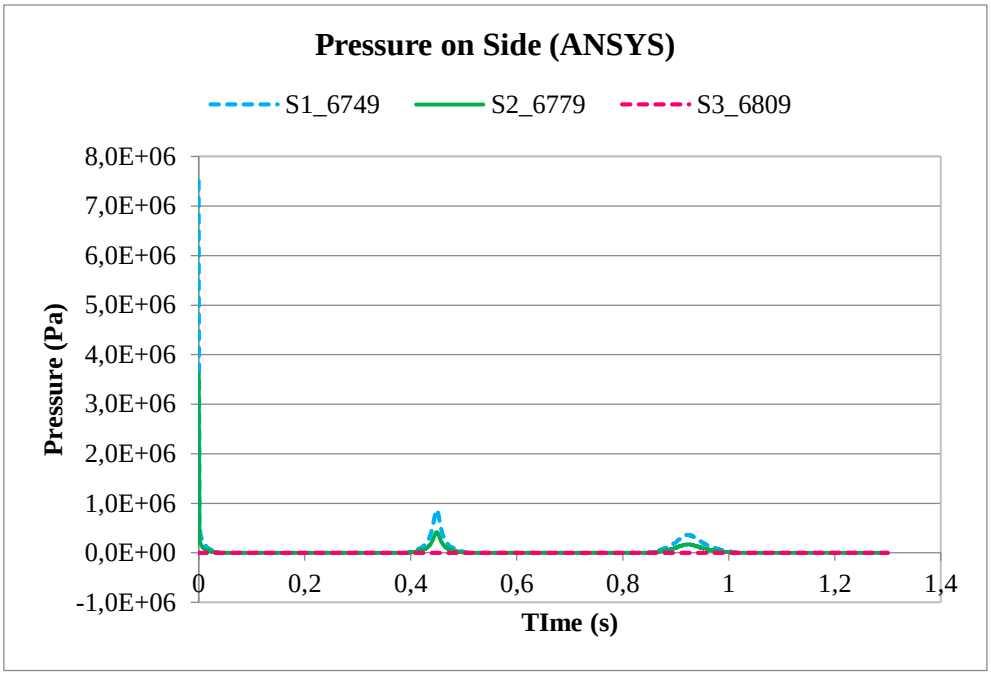

Figure 4.27: Pressure loads on side of cylinder model (ANSYS)

- ***Analysis Procedure***

In order to calculate the structural response of the semi-cylinder submitted to the calculated pressure field, five steps are requested using ANSYS code:

Constraint nodes: In this step, the reaction forces on each node are calculated according to the pressure loads applied on elements. Thus, the nodes are then completely restrained (6 d.o.f) and the hull elements are exported as a single model for obtaining the reaction forces.

Static solution: Once the boundary condition is set, a static solution in ANSYS allows to calculate the reaction forces at each node and at each time step. The obtained distribution is plotted in Figure 4.28.

Modal analysis: Modal superposition method is taken into account as the main method for this study because the procedure will require less time consumption. The first step consists then in running a modal analysis on the entire model, without considering any pressure loads and forces. The mode shapes can then be post-processed with corresponding natural frequencies. The number of modes to consider in the transient response calculation must represent at least 80% of the model mass. Figure 4.29 plots first mode shape which is the first vertical bending mode.

Apply reaction force: This step consist in importing the reaction forces into the semi-cylinder model instead of the pressure loads on elements.

Transient solution: Based on the mode shapes obtained from the modal analysis, the transient response of the semi-cylinder, loaded by the time evolution of the reaction forces, is performed using the modal superposition method. As a result, the deformed model is obtained at each time step.

Figure 4.28 presents the nodal constraints and reaction force distribution for cylinder model. In this diagram, each node is fixed with six degrees of freedom (UX UY, UZ, RX, RY, RZ). It is clear that the highest reaction force magnitude appear in the middle of the ship and decrease toward to the end of both sides.

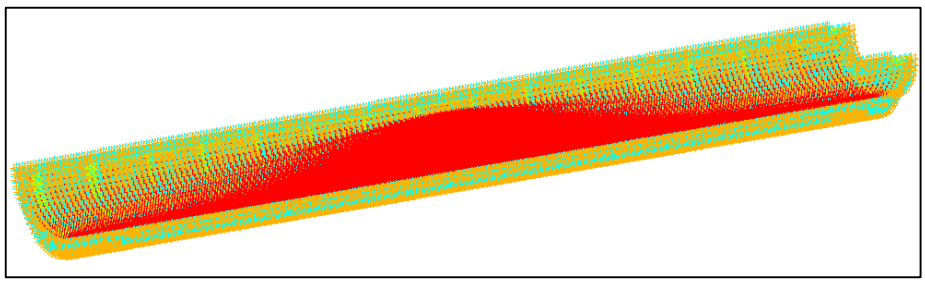

Figure 4.28: Nodal constraints and reaction forces distribution

As mentioned previously, before applying the reaction forces to the model, a modal analysis should be performed. In the present case, 676 modes are calculated up to 10 Hz. Figure 4.29 and Figure 4.30 plot the global modes shapes of cylinder model. Figure 4.29 shows the deformation of the first mode with the two-node vertical bending moment, whereas Figure 4.30 indicates the three-node is bending moment for the deformation of cylinder model.

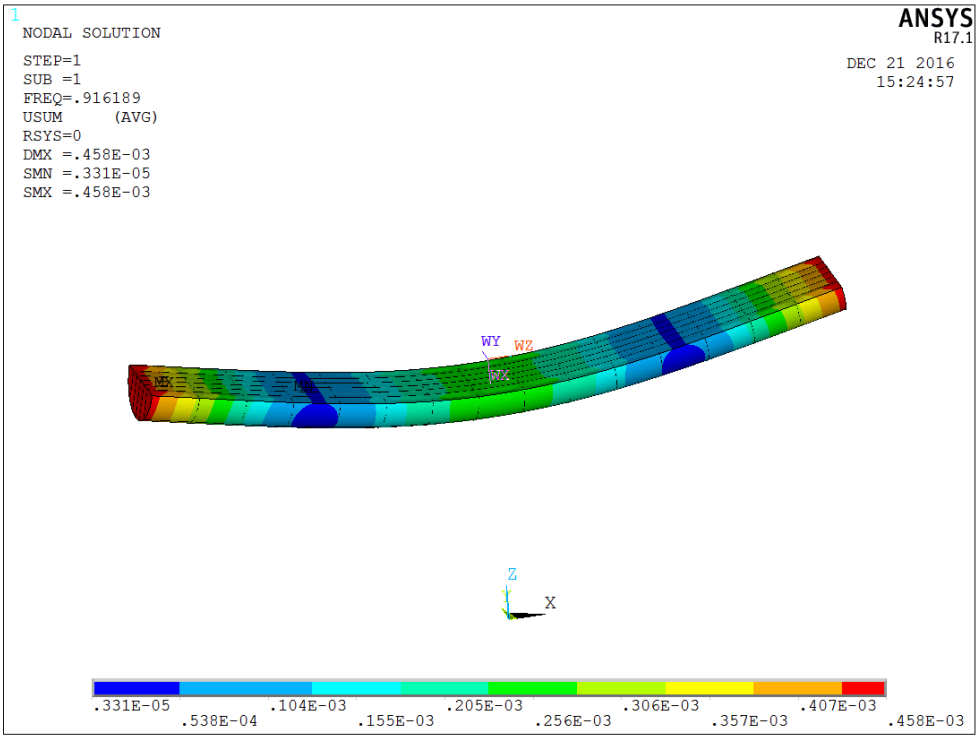

Figure 4.29: Deformation of 1st mode of cylinder model

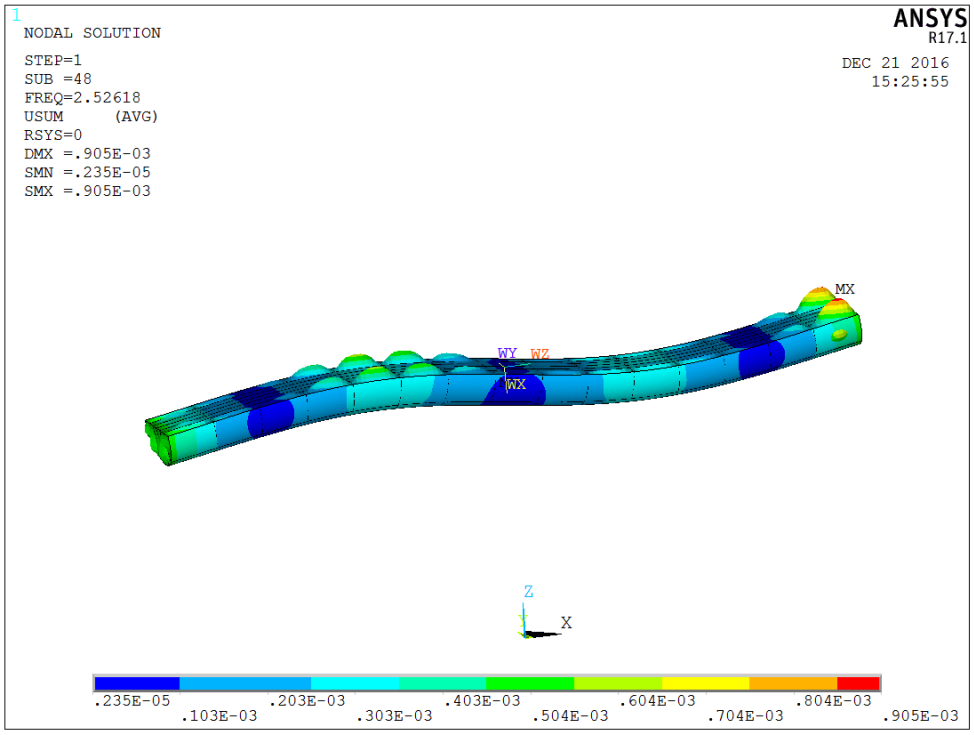

Figure 4.30: Deformation of 48th mode of cylinder model

By applying the reaction force time evolutions to the semi-cylinder model, a transient solution is run to obtain the structural response. From this analysis, nodal translational displacements along the three axes are post-processed for nine specific reference points and plot on Figure A1.1 to Figure A1.9 in Appendix A1. Furthermore, Figure 4.31 to Figure 4.33 present the comparison of Z-displacements at references nodes located respectively at the bottom, side and deck, whereas Figure 4.34 shows the difference between points B1 (midship) and B3 (end of ship) vertical displacements.

Apart from the fact that the resulting displacements time evolutions are sinusoidal as expected, these results seem to be completely unrealistic for two reasons:

- Firstly, the displacements of the different points are maximum at t=0, while they should be null at the initial time.
- Secondly, the maximum displacement levels (several meters) are completely unrealistic, contrary to the results obtained with the explicit direct integration solver LS-DYNA (see Figure 4-19 for instance). Moreover, taking into account the fluid structure interaction cannot explain such high displacement levels

This result analysis shows that further investigation has to be done regarding the transient response analysis based on the modal superposition method. More precisely, the suitability of such method must be verified since the modal method is limited to “small displacements”, which is not the case in this example (regarding LS-DYNA results, the deck displacement is almost 40 times higher than its thickness). One perspective of the work presented in this master thesis is to run a direct integration implicit simulation using ANSYS solver, even if the calculation time is much higher, in order to see if the problems come from some limitation of the modal superposition method or some error of implementation.

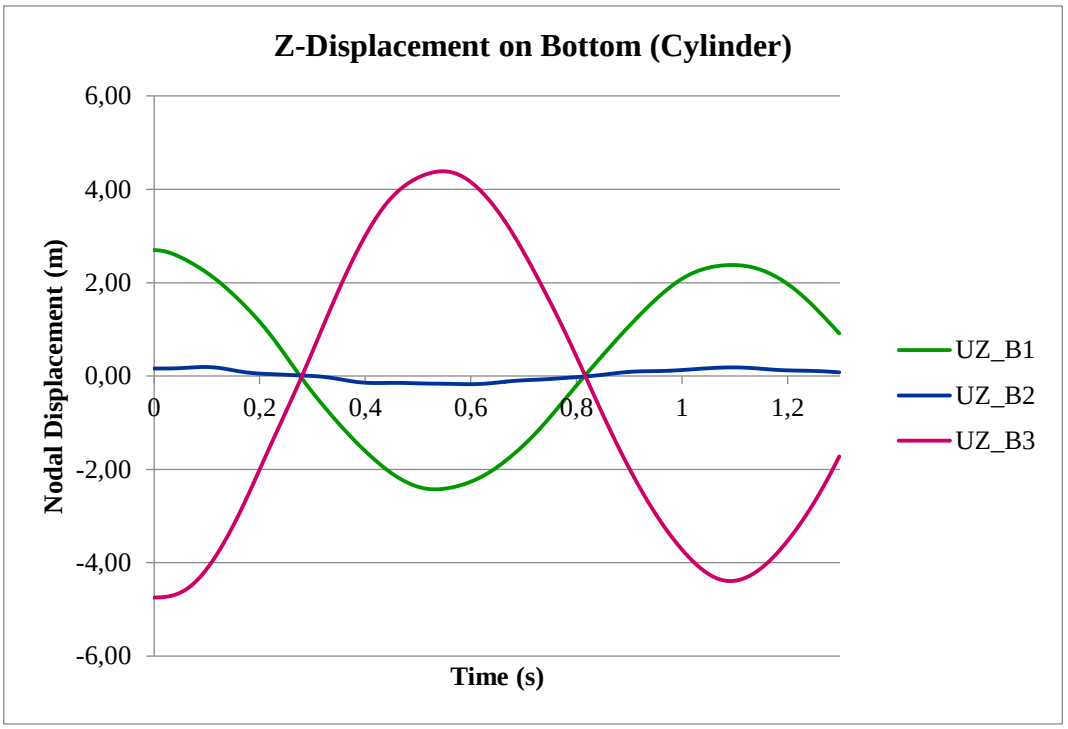

Figure 4.31: Z-displacements at bottom for cylinder model (ANSYS)

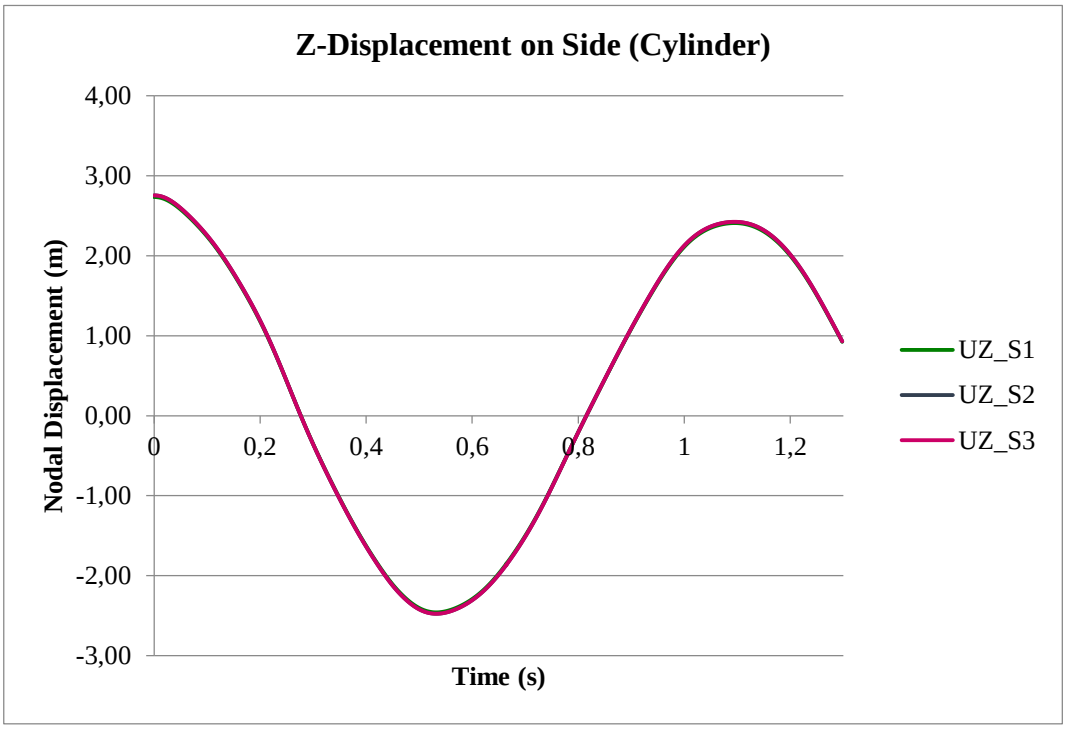

Figure 4.32: Z-displacements at side for cylinder model (ANSYS)

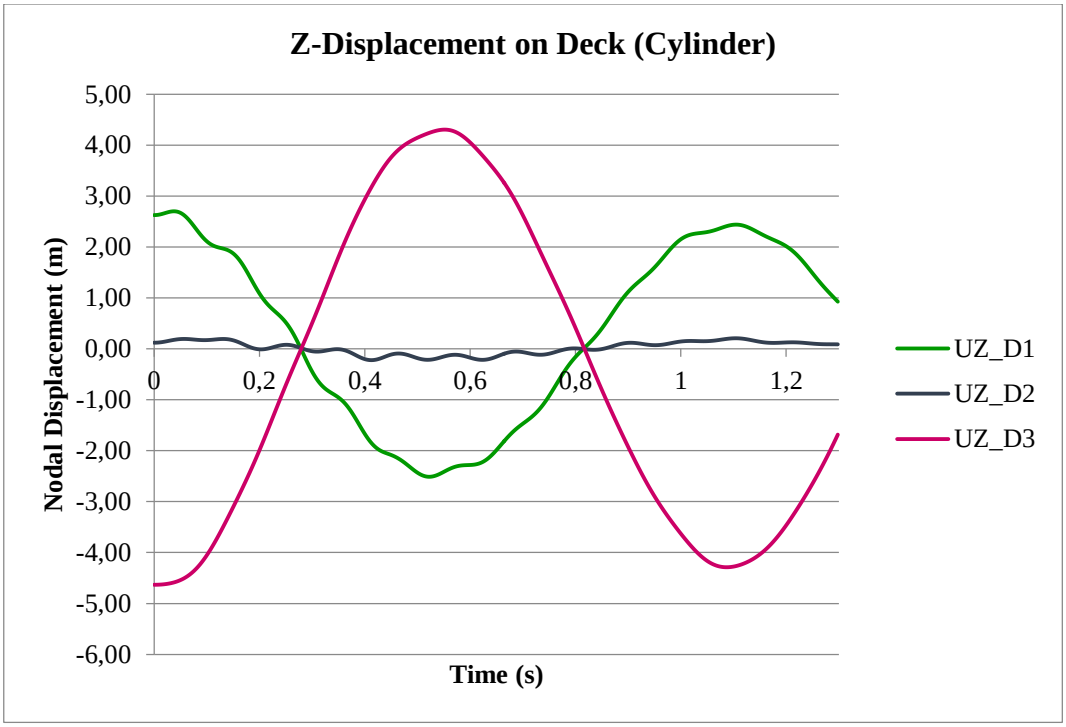

Figure 4.33: Z-displacements at bottom for cylinder model (ANSYS)

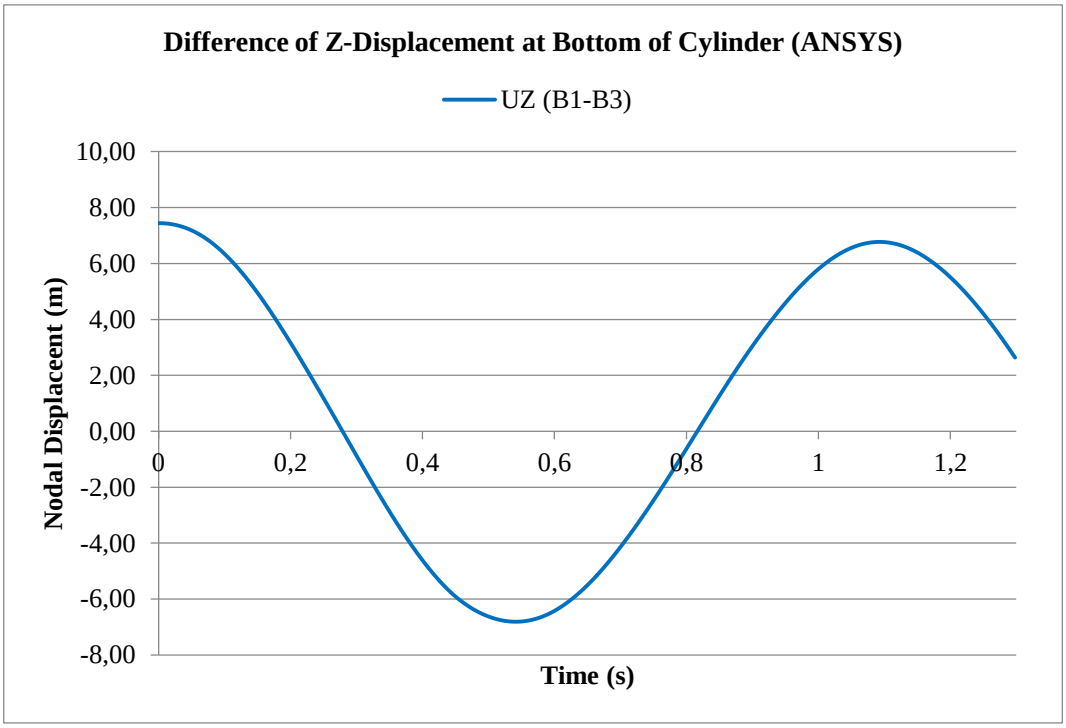

Figure 4.34: Difference of Z-displacement between B1 and B3 points (ANSYS)

This page is intentionally left blank.

5. CASE STUDY: FRIGATE SHIP

5.1. Reference Ship Information

In this chapter, the frigate ship which is provided by STX Europe is considered as the reference ship for the following study. As listed in Table 5-1, the overall length of the frigate ship is 95 m, its breadth is 40 m, and its draft is 4.75 m.

Table 5-1: Principle dimension of frigate model

Item	Description
Length overall	95.0 m
Breadth	40.0 m
Draught	4.75 m

Moreover, the details of initial conditions regarding the underwater explosion scenario are listed in Table 5-2. In this case, considering a shock factor equal to 0.6, a charge of 1296 kg of TNT is supposed to explode at 64.75 m below the free surface and 60 m bellow the ship bottom.

Table 5-2: Initial condition of frigate model

	Description
$\mathbf{m_c}$	TNT charge mass, m_c= 1296 kg
$\mathbf{d_i}$	Distance from charge to free surface, $\boldsymbol{d_i}$ = 64.75 m
r	Distance from charge to standoff point, r = 60 m
$\boldsymbol{\rho_c}$	Density of charge, $\boldsymbol{\rho_c}$= 1600 kg/m^3
SF	Shock factor = 0.6

Figure 5.1 shows the coarse mesh finite element model of frigate ship which is prepared by STX. The charge is assumed to be located at the original point of the coordinate system as illustrated in Figure 5.2.

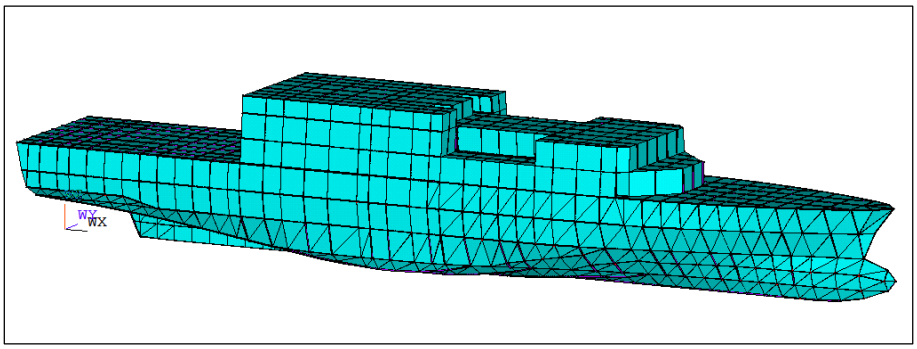

Figure 5.1: Finite element model of frigate ship

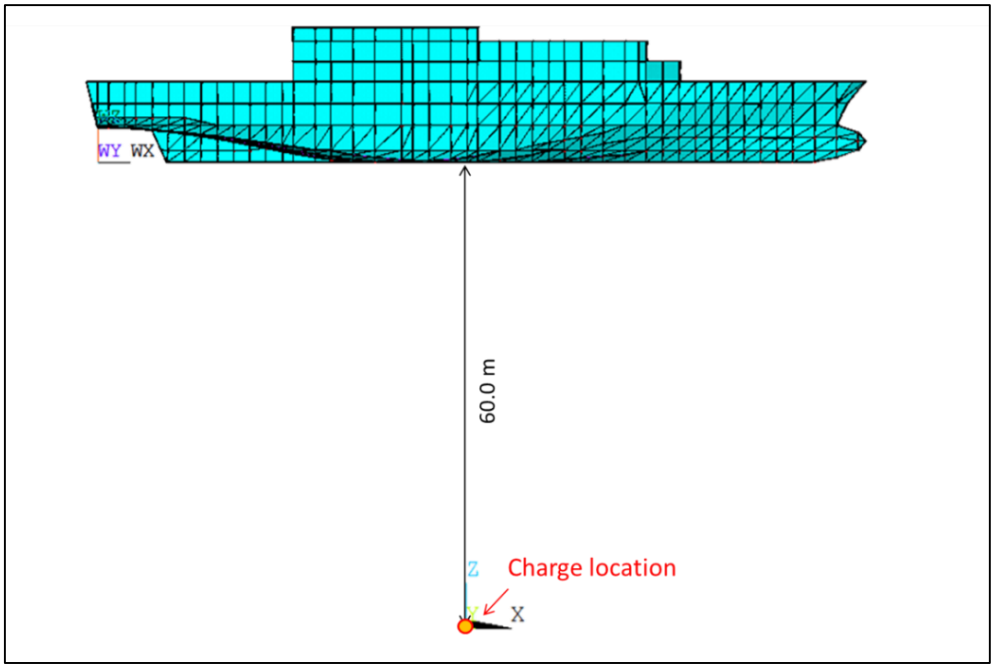

Figure 5.2: Profile view of model and the location of charge

With the consideration of fluid-structure interaction (FSI), it is necessary to create in ANSYS a fluid-field mesh and an interface mesh between fluid and structure meshes. Figure 5.3 represents the design of fluid-field and structure meshes. In this plot, the pink stands for the interface mesh between fluid and structure mesh, whereas the blue mesh represents the sea water with the radius of 40 m surrounding to the ship.

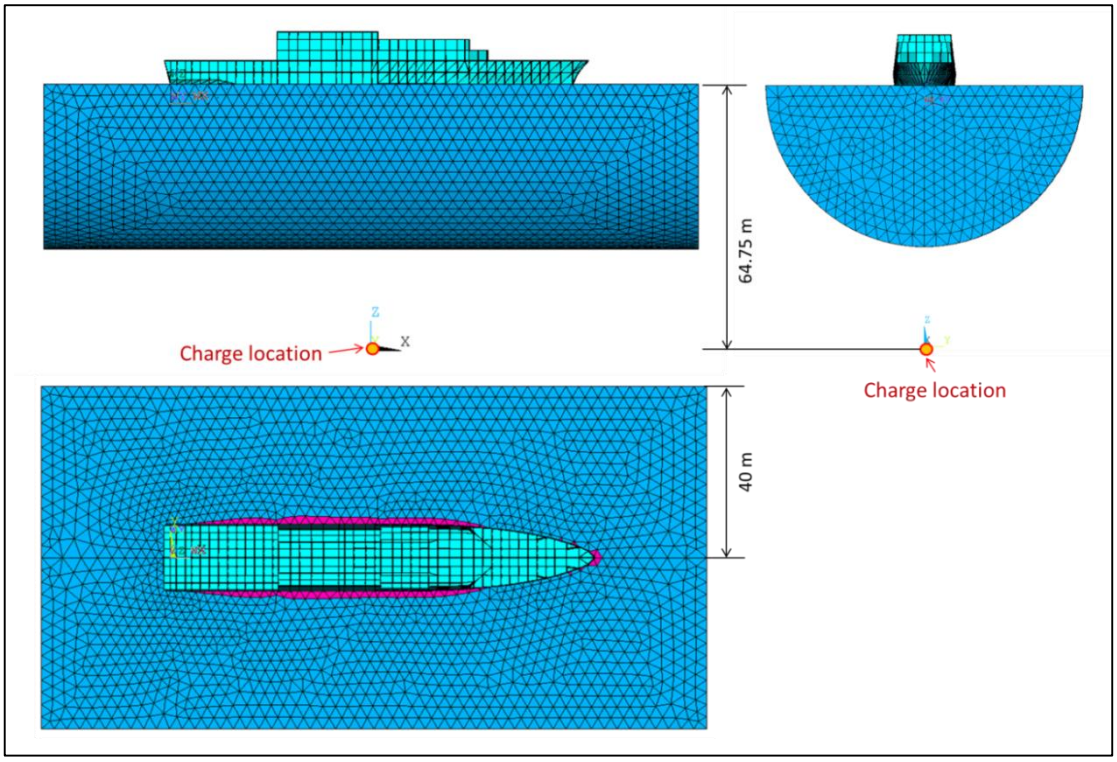

Figure 5.3: Overview of fluid-field mesh and structural mesh

In addition, in order to check the values of the ship model after analyzing, several reference points are selected on the ship bottom, hull side and deck. Figure 5.4 indicates the reference location of each point at the bottom, deck, and side shell, whereas Table 5-3 lists the element and node IDs for each location of frigate model in ANSYS.

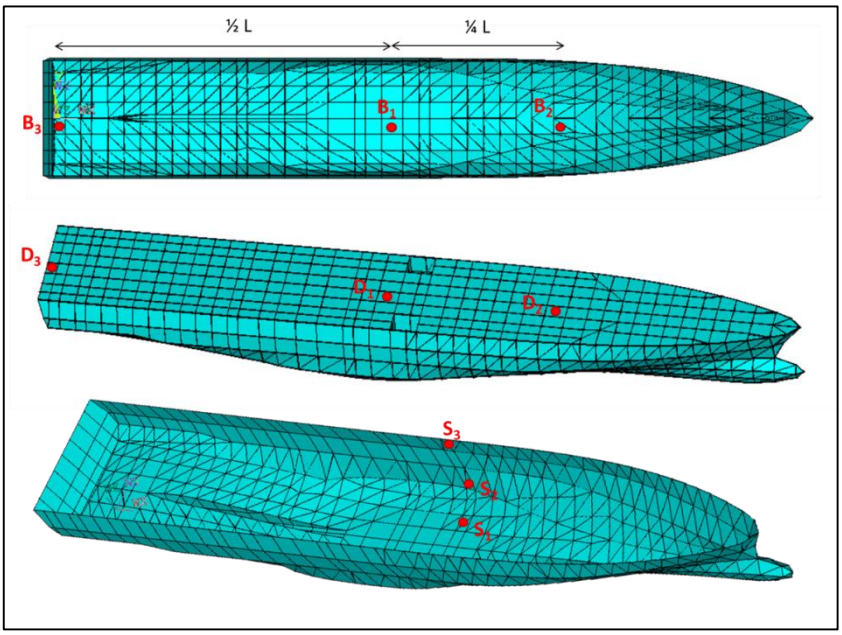

Figure 5.4: Reference points for frigate ship model

Table 5-3: Referred element and node IDs at bottom, side shell and deck of frigate model in ANSYS

Bottom	Elem. ID	Node ID	**Side**	Elem. ID	Node ID	**Deck**	Elem. ID	Node ID
B_1	22	128	S_1	8129	143	S_1	361	889
B_2	8237	2001	S_2	8140	406	S_2	256	749
B_3	7886	54	S_3	8107	492	S_3	4233	2011

5.2. Analysis Process and Results

This section presents the different results obtained from the analysis procedure already described in section 4.3.2:

1) Pressure loads distribution calculated by the ANSYS procedure written in the framework of the present work
2) Reaction forces post-processed from a static calculation
3) Global vertical bending mode shapes post-processed from a modal analysis
4) Nodal vertical displacements post-processed from transient solution

5.2.1. Pressure load distribution

Figure 5.5 and Figure 5.6 plot the pressure load distributions at bottom and side of ship model when submitted to the underwater explosion which parameters are described in Table 5-4.

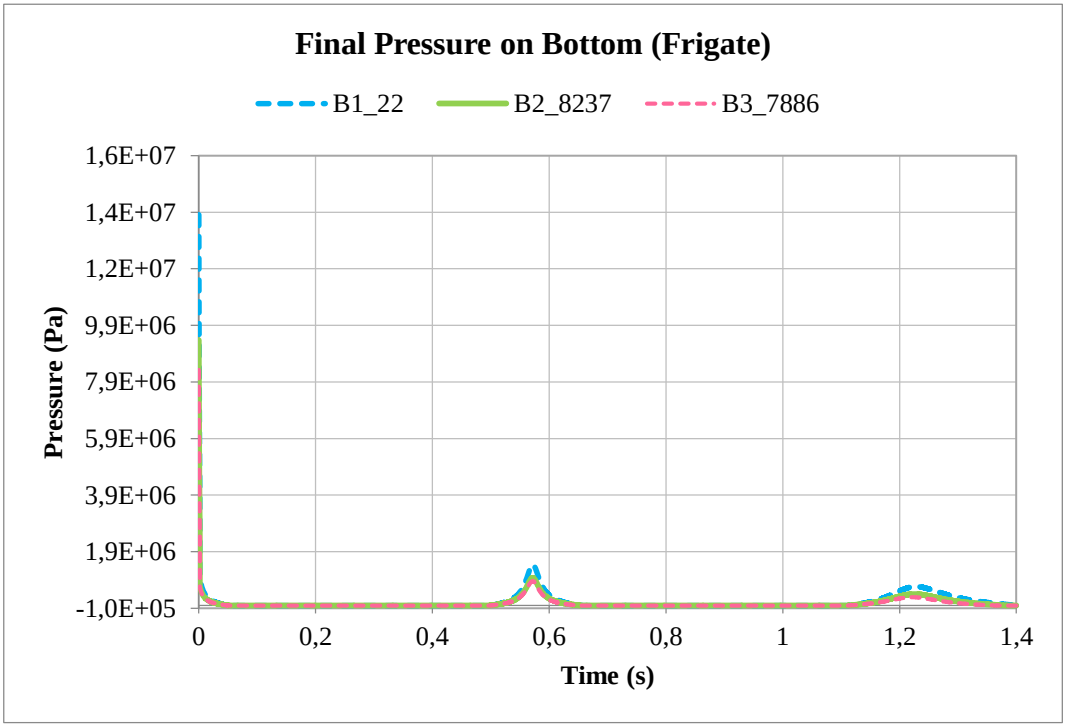

Figure 5.5: Pressure loads on bottom of frigate model (ANSYS)

On the other hand, Figure 5.6 illustrates the pressure loads distribution for the side shell in the midship section.

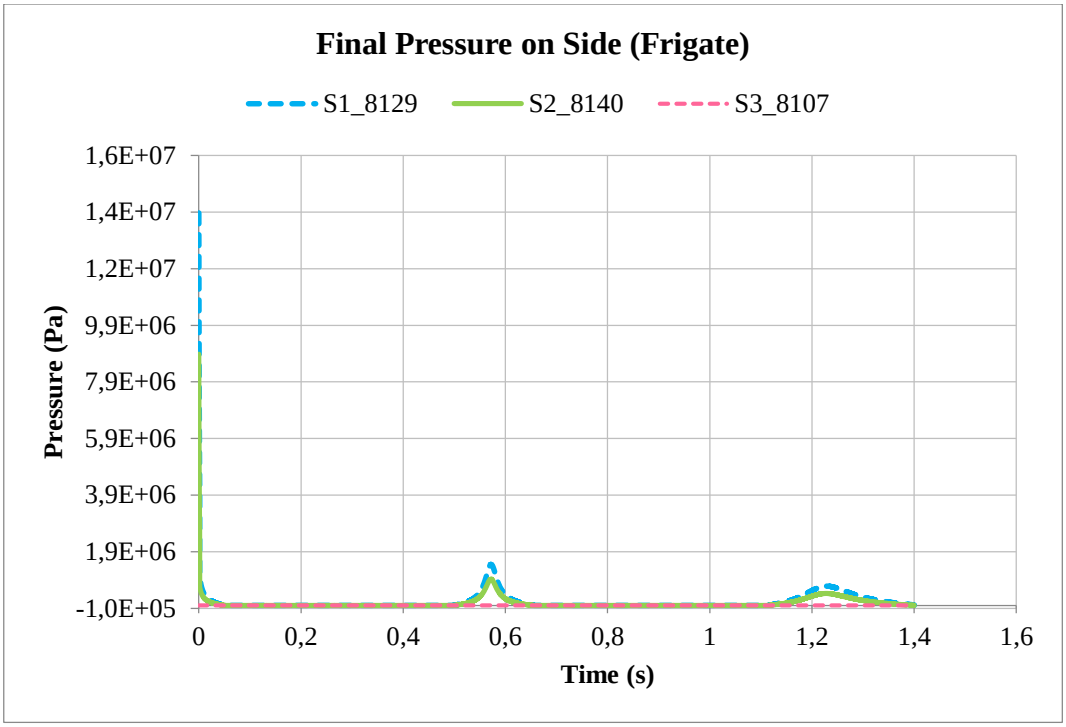

Figure 5.6: Pressure loads at side of frigate model (ANSYS)

Table 5-4: Maximum values of pressure loads on bottom and side for frigate ship

Location	1st shock wave	1st bubble pulse	2nd bubble pulse
B1	14.0	1.44	0.67
B2	9.38	0.97	0.40
B3	8.32	0.86	0.30
S1	13.8	1.45	0.68
S2	8.87	0.93	0.42
S3	0.0	0.0	0.0

Unit: MPa

5.2.2. Results of static analysis

With the limitation of ANSYS, it is necessary to apply reaction forces into nodes instead of pressure loads to shell element if we want to implement transient response analysis.

Therefore, the results retrieved from the static analysis are presented. Since the charge is located below the midship section, reaction forces are more significant amidships as it is confirmed in Figure 5.7. Moreover, the free surface constraint is represented by green triangles where the pressure load is zero.

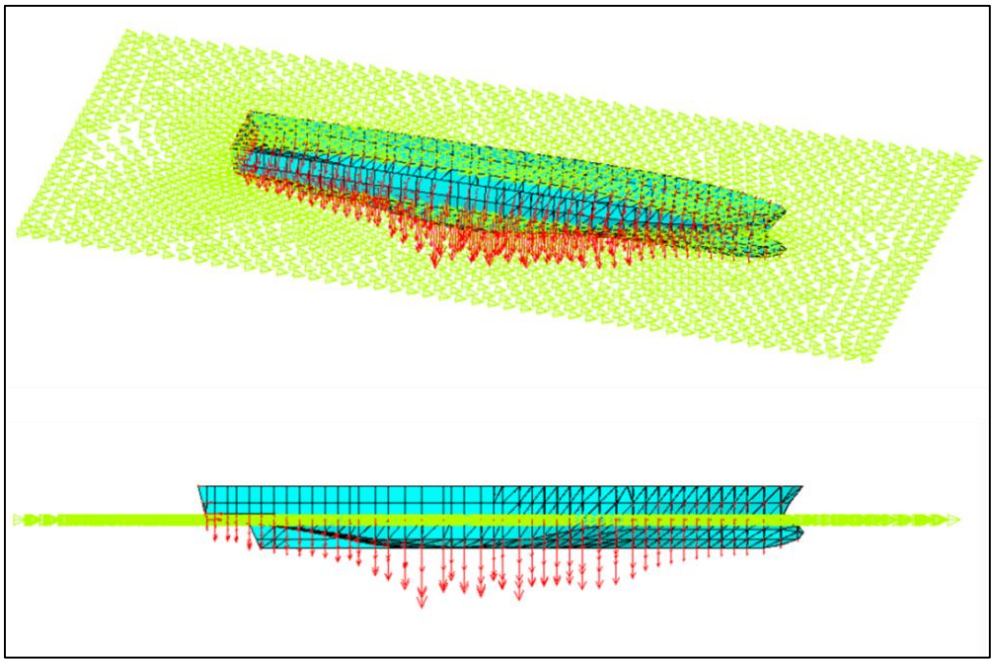

Figure 5.7: Distribution of reaction forces on hull model (Frigate)

Figure 5.8 to Figure 5.10 illustrate the reaction forces to nodes on the bottom in three reference points. According to these diagrams, the reaction force has the most contribution in z-direction which parameters are described in Table 5-5Table 5-4. According to the distribution of reaction force curves, it is clear that the trends are like pressure loads distribution with the time evolution.

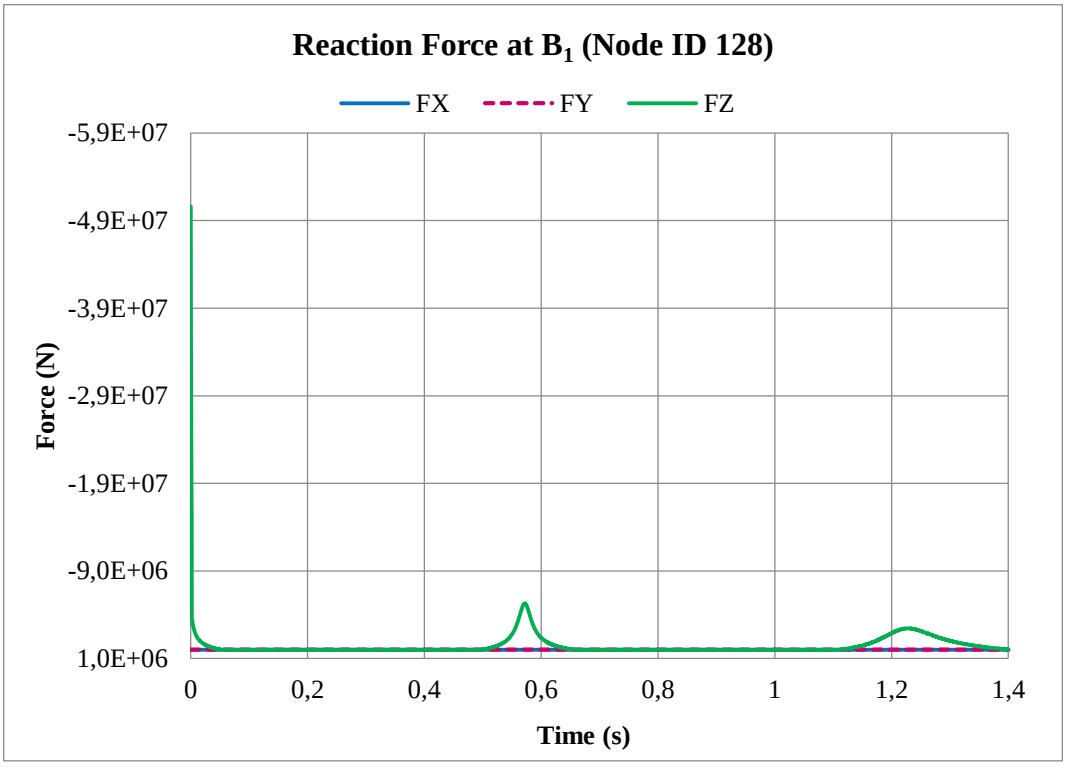

Figure 5.8: Reaction forces at middle of bottom B_1 (Node ID 128)

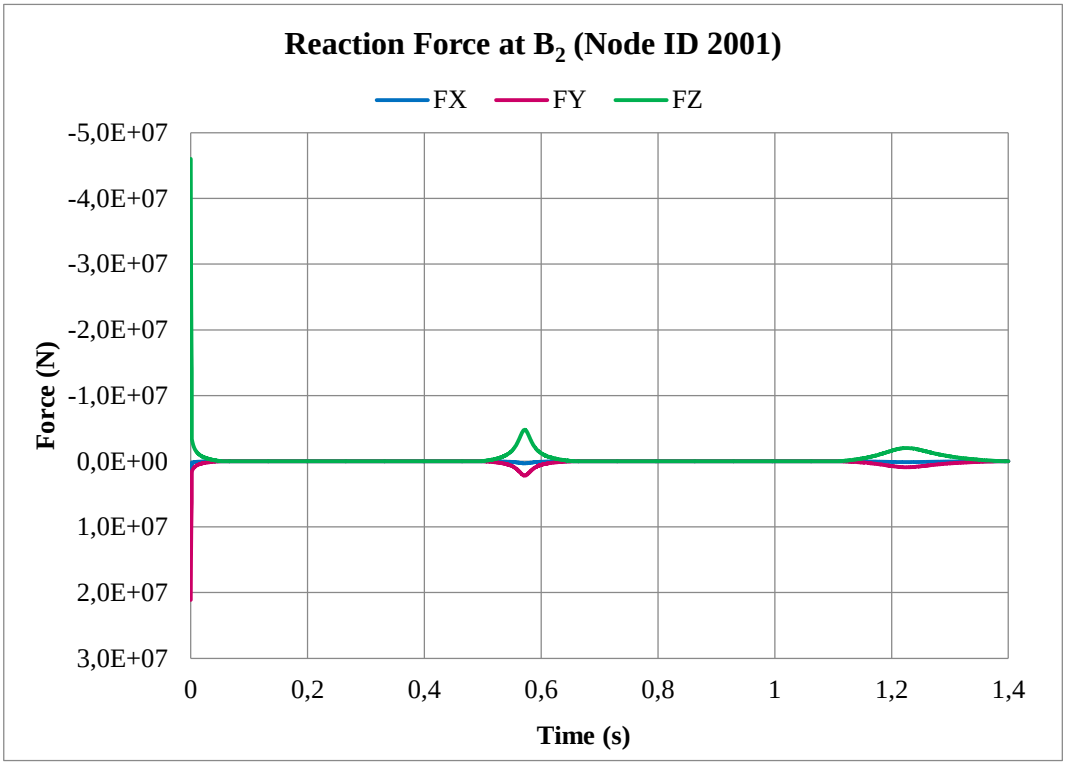

Figure 5.9: Reaction forces at 1/4 L of bottom B_2 (Node ID 2001)

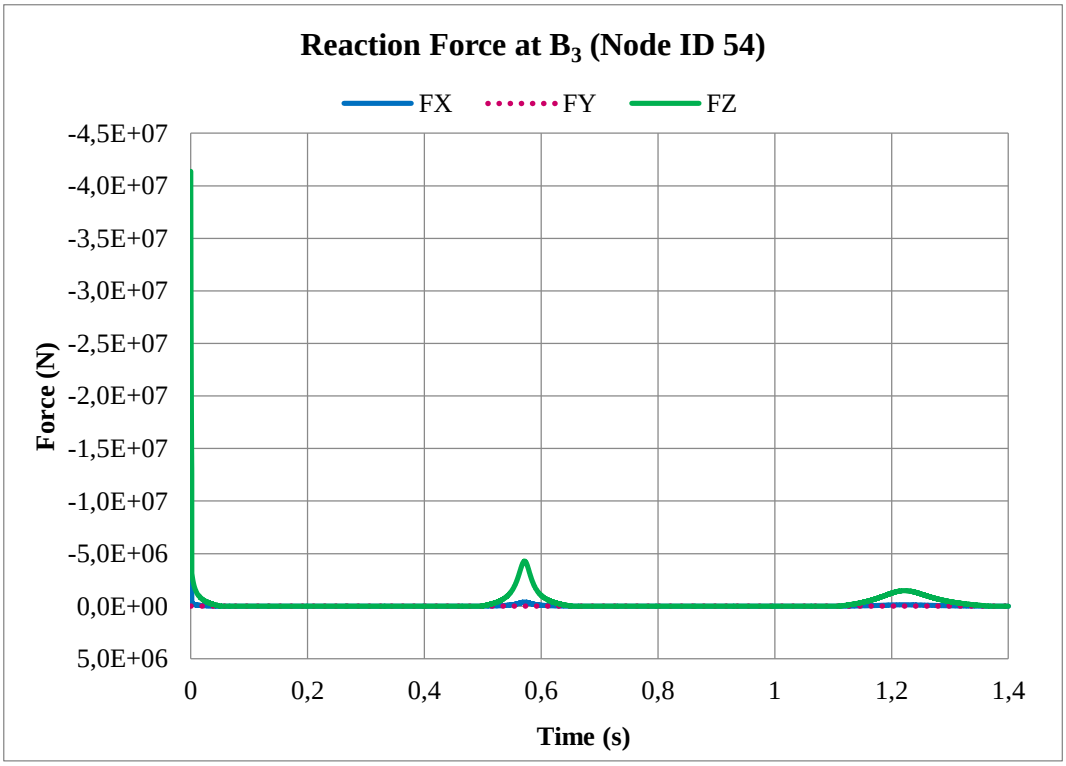

Figure 5.10: Reaction forces at end of bottom B_3 (Node ID 54)

On the other hand, Figure 5.11 to Figure 5.13 show the reaction forces for side shell at the amidships section. For the peak values of each location, the parameters are listed in Table 5-5 as well.

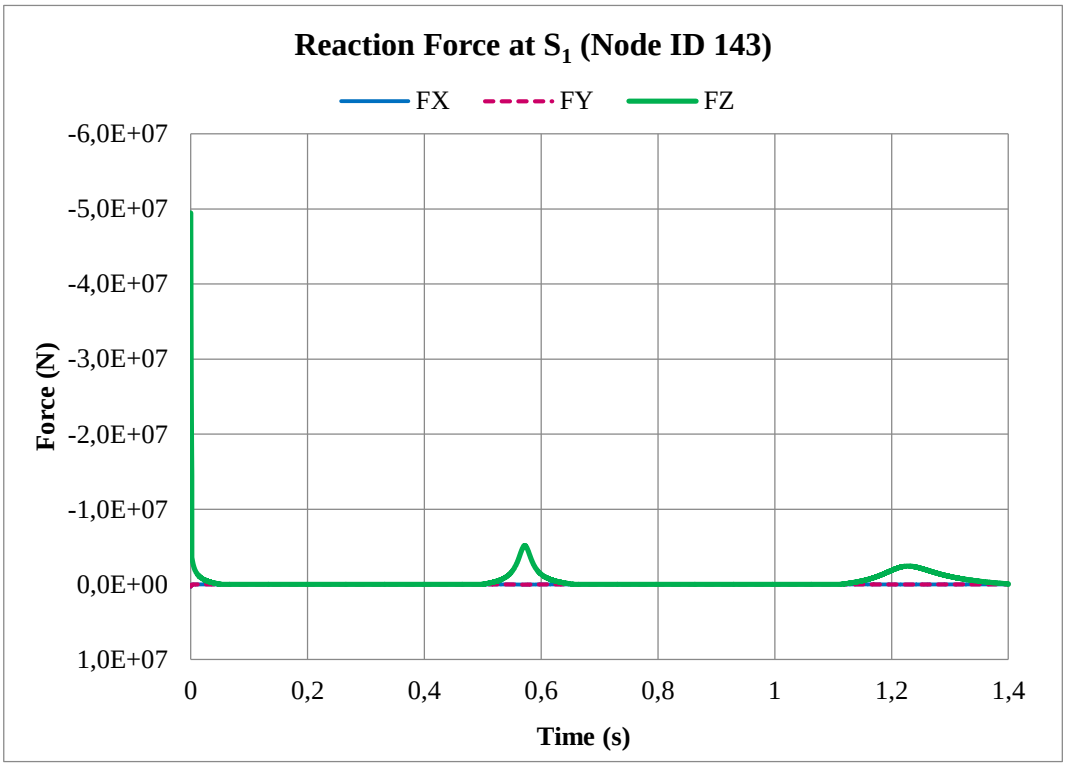

Figure 5.11: Reaction forces at side shell S_1 (Node ID 143)

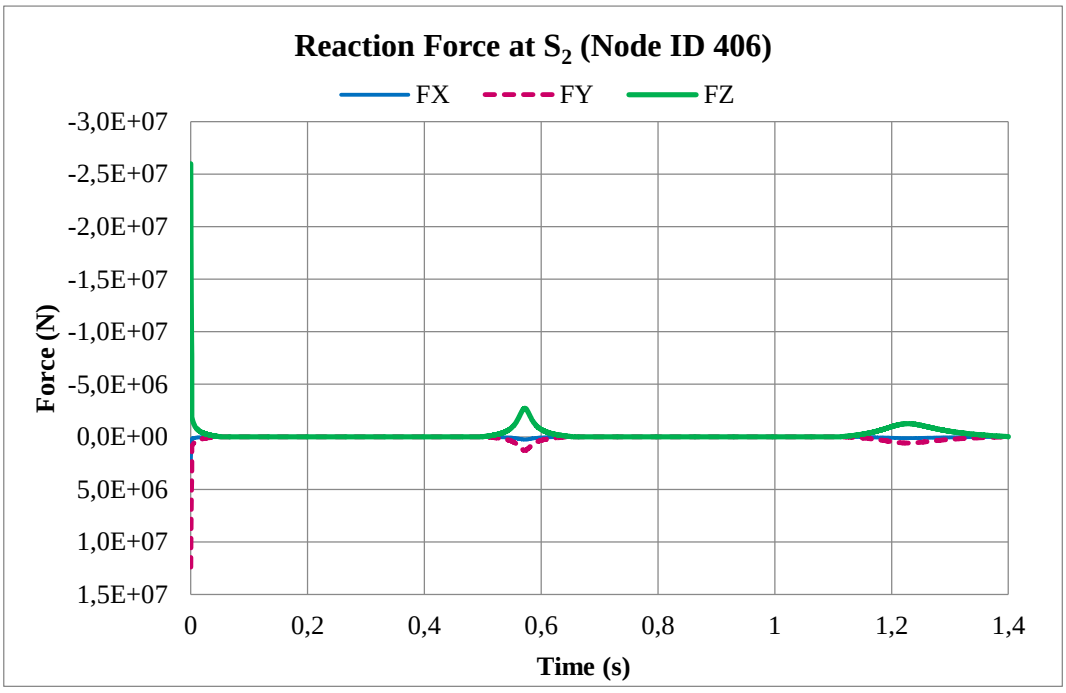

Figure 5.12: Reaction forces at side shell S_2 (Node ID 406)

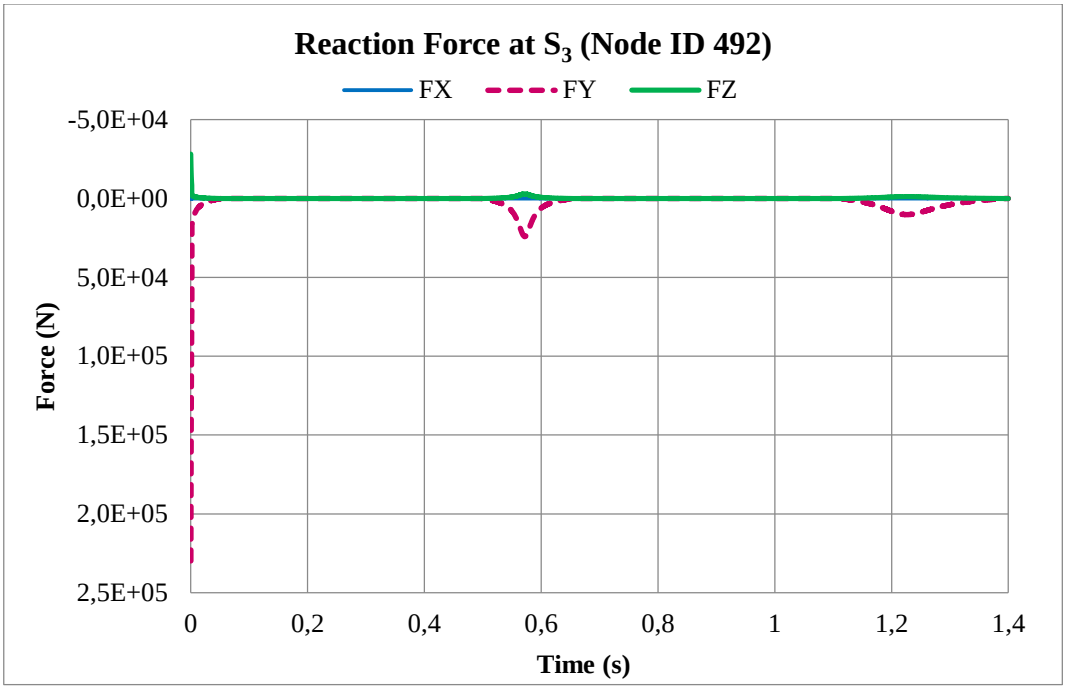

Figure 5.13: Reaction forces at side shell S_3 (Node ID 492)

Table 5-5: Maximum values of raction force on bottom and side for frigate ship

Location	Direction	1st shock wave	1st bubble pulse	2nd bubble pulse
B1	FZ	5.1×10^{7}	5.1×10^{6}	2.4×10^{6}
B2	FZ	4.6×10^{7}	4.7×10^{6}	1.8×10^{6}
B3	FZ	4.1×10^{7}	3.8×10^{6}	1.5×10^{6}
S1	FZ	5.0×10^{7}	3.5×10^{6}	2.3×10^{6}
S2	FZ	2.5×10^{7}	1.6×10^{6}	1.1×10^{6}
S3	FY	2.3×10^{5}	2.0×10^{4}	9.6×10^{3}

Unit: N

5.2.3. Results of modal analysis

In order to acquire deformation of each mode for modal superposition, it is necessary to perform modal analysis before applying reaction forces for the transient solution. In this case, 360 natural modes up to frequency 12 Hz are taken into consideration for participation in the modal superposition procedure. Figure 5.14 shows the global bending modes within 360 modes. As it can be seen, Figure 5.14(a) plot the first vertical bending global mode (4^{th} mode) at 2.69Hz, which has the main contribution in the z-direction; the second global mode (20^{th} mode) is a horizontal bending mode at 3.7 Hz and depicted in Figure 5.14 (b). Furthermore, Figure 5.14 (c) to Figure 5.14 (f), present three vertical bending modes respectively at 4.35 Hz, 6.23 Hz, 8.09 Hz and 9.80 Hz.

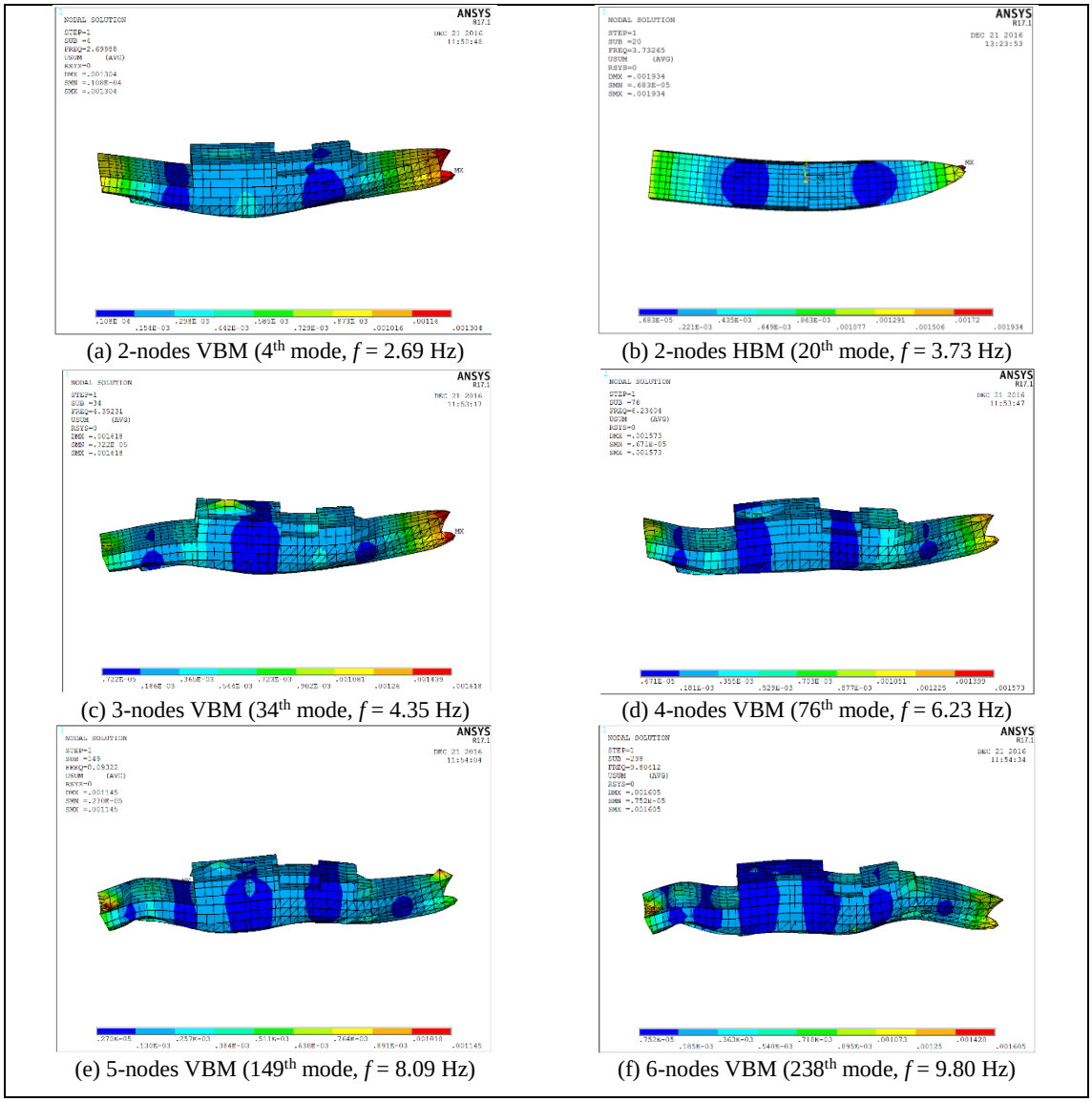

(a) 2-nodes VBM (4th mode, f = 2.69 Hz)

(b) 2-nodes HBM (20th mode, f = 3.73 Hz)

(c) 3-nodes VBM (34th mode, f = 4.35 Hz)

(d) 4-nodes VBM (76th mode, f = 6.23 Hz)

(e) 5-nodes VBM (149th mode, f = 8.09 Hz)

(f) 6-nodes VBM (238th mode, f = 9.80 Hz)

Figure 5.14: Deformation of global modes for frigate ship model

5.2.4. Results of transient solution

The transient solution is run using the reaction forces as loading and the superposition of considered mode shapes. The nodal displacement along the three directions UX, UY, and UZ are presented in Figure A2.1 to Figure A2.9. The main displacements are vertical direction, and Figure 5.15 to Figure 5.17 present the vertical displacements at reference nodes located at the bottom, the side shell, and the deck. According to these three diagrams, it is obvious that bottom and deck have higher displacement for z-direction compared with side shell. In Figure 5.15, the displacement of B1 varies from -50 mm to 50 mm; whereas the most severe displacement occurs on B3 varying between -100 mm to 100mm.

Lastly, Figure 5.18 presents the difference between the vertical displacement at midship B1 and aft point B3. Obviously, the damping effect has an influence on the deformation as the curve is decreasing with the time.

Although the results depicted in Figures 5-15 to 5-28 seem to be more realistic regarding the displacement amplitudes than the one observed for the semi-cylinder, the same problem than the one encountered in the semi-cylinder study can be observed, that is the displacement is not zero at the initial time. As for the conclusion related to the semi-cylinder study, it is clear that the transient response based on modal superposition must be further investigated as the resulting displacements are not realistic.

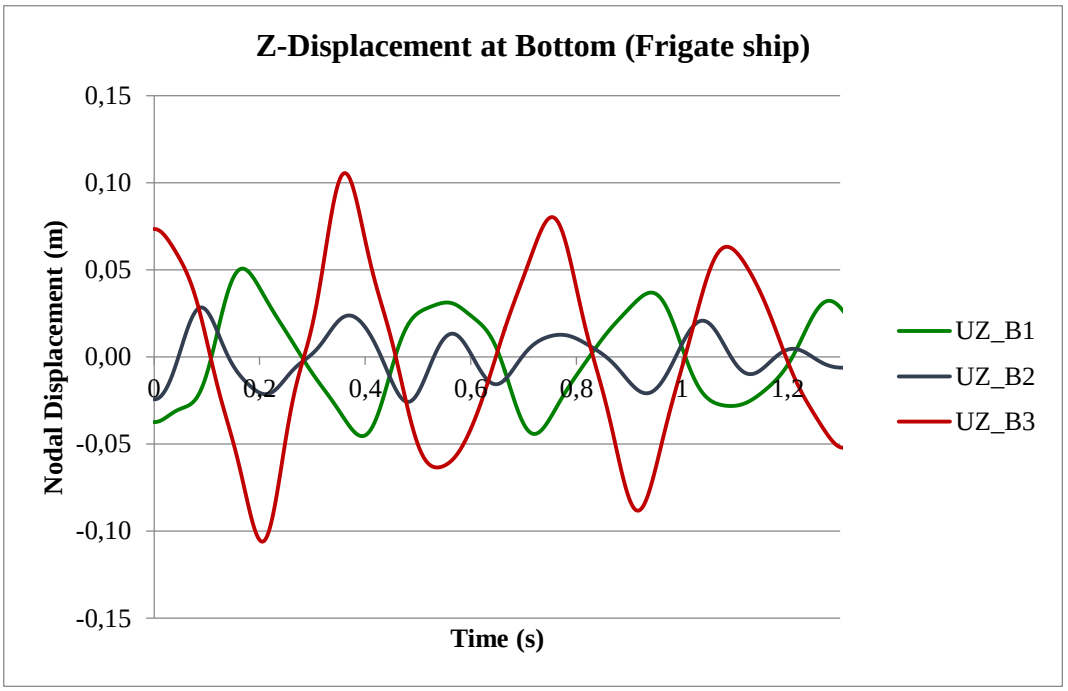

Figure 5.15: Z-displacements at bottom for frigate ship

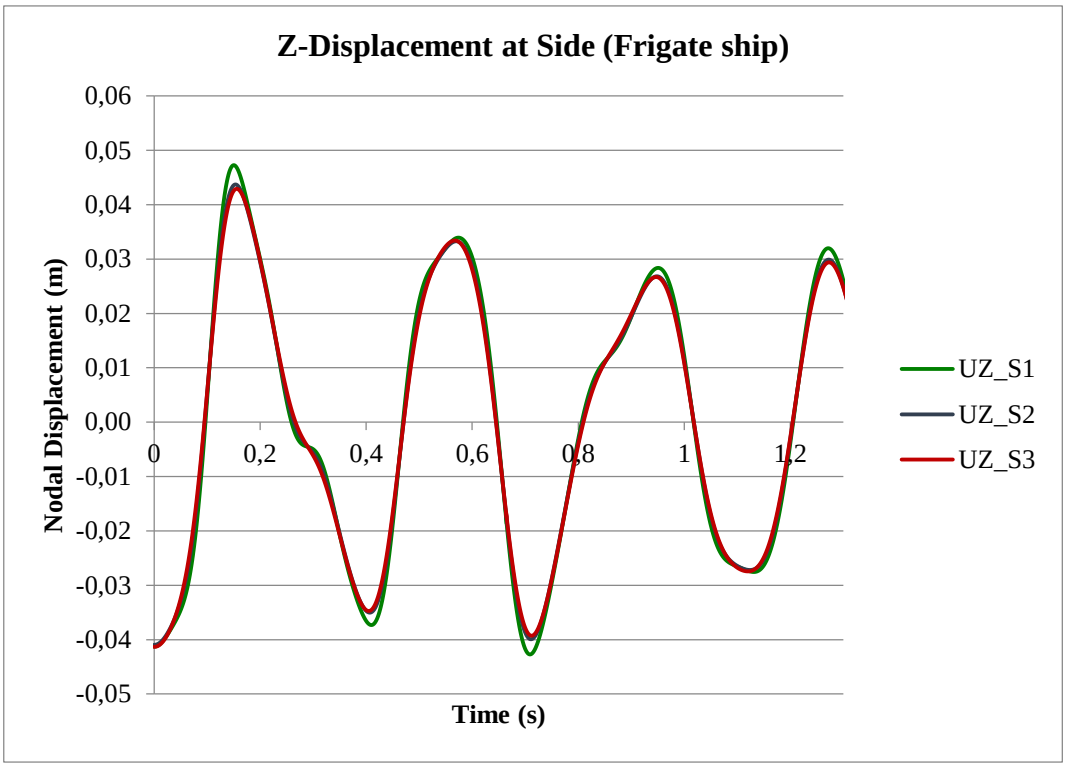

Figure 5.16: Z-displacements at side for frigate ship

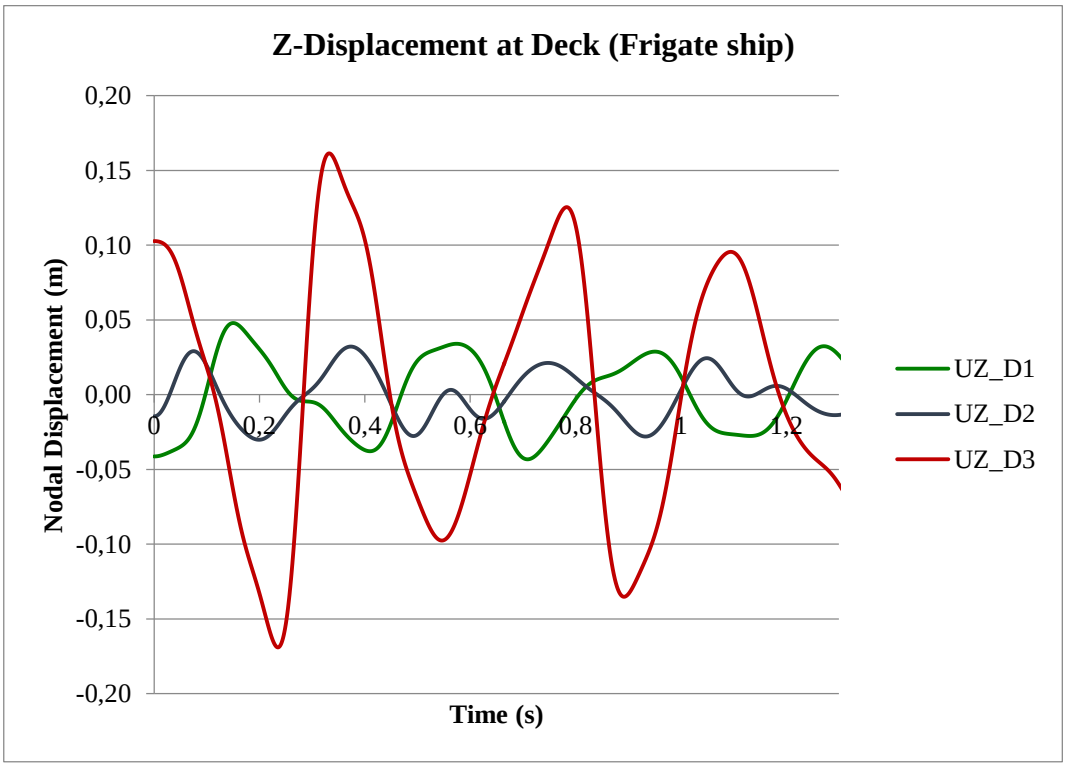

Figure 5.17: Z-displacements at deck for frigate ship

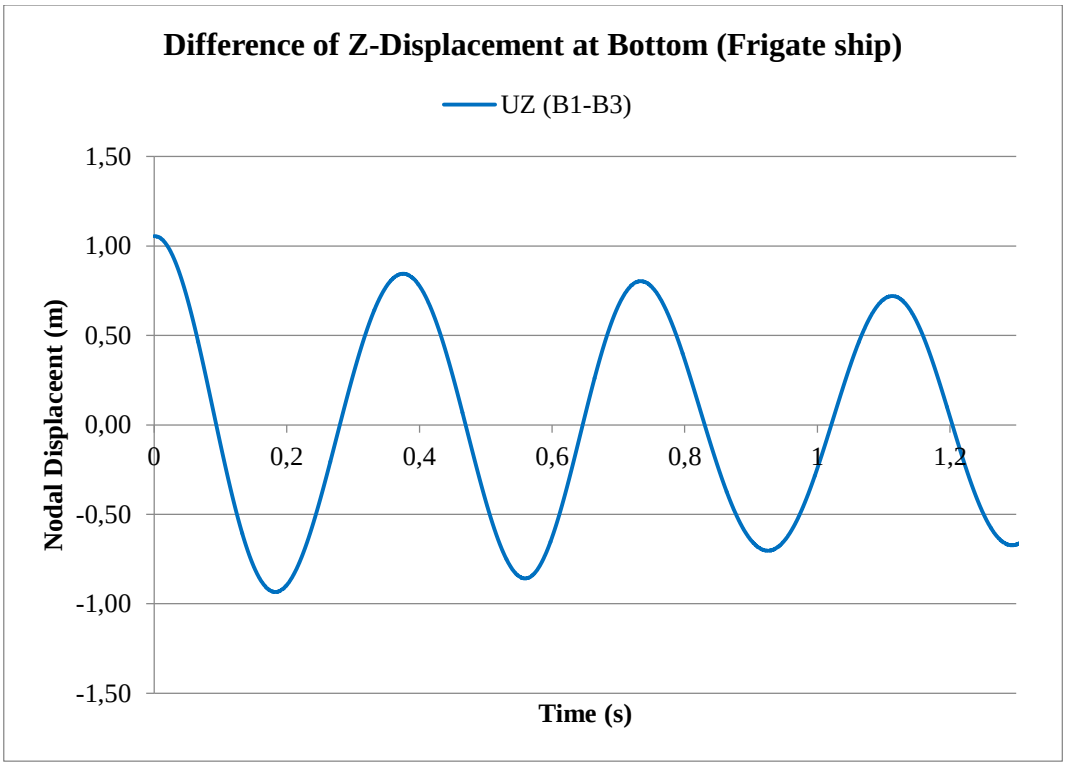

Figure 5.18: Differnece of Z-displacements between B1 and B3 for frigate ship

6. CONCLUSIONS

After analyzing the most important existing methodologies, it has been found that DAA model is the most suitable approach in order to predict the whipping response on ship structures submitted to the underwater explosion. In this study, a complete scheme is developed in order to perform the structure response by means of explicit and implicit numerical methods. The main conclusions drawn from the present research are summarized below:

1. A detailed assessment has been undertaken to compare empirical and analytical methods taken from existing literature so as to find out the most suitable methodology for obtaining the pressure exerted by the oscillations of the bubble generated by an underwater explosion.

2. In this thesis, it is confirmed that DAA analytical model provides more accurate and rational pressure distribution results than other empirical or analytical approaches. DAA model is also very flexible to estimate bubble behavior according to arbitrary initial settings such as explosive mass, the density of charge, and speed of sound in sea water and charge depth. In addition, a good agreement has been observed between DDA model and empirical results when setting identical initial conditions. Hence, it has been proven that DAA model can be used to acquire accurate pressure load distribution induced by the underwater explosion.

3. According to pressure load distribution diagram gathered from LS-DYNA simulation, it is clear that the impulse I of first and second bubble pulse peaks is five times more than first shock wave phase, which means that the energy is much higher during the bubble oscillation phase. Furthermore, the total energy diagram obtained from LS-DYNA points out that the energy increases dramatically within secondary bubble pulsation phase; hence, it has been demonstrated that secondary bubble pulsation phase has the significant influence on ship structure. It might cause severe structural damage to the ship and cannot be neglected in such simulations.

4. On the other hand, it should be highlighted that DAA analytical model can also be implemented in ANSYS software package by means of an implicit numerical finite element method. In order to predict the structure whipping response in ANSYS software, pressure loads are firstly computed by means of a code developed inside ANSYS; Then, once natural frequencies and mode shapes have been calculated, a transient solution based on modal superposition is run to calculate the response of the ship submitted to

both the shock wave and the bubble oscillations pressures. However, the resulting vertical displacement are, for the moment, not realistic. This can be due to either a wrong utilization of the transient solver or to some limitation of the superposition method. This aspect will be investigated in collaboration with STX in the last part of the master thesis.

7. FURTHER WORK

I. Nodal displacement has been presented in this research as the result of the transient analysis; nevertheless, a more detailed post-processing can be performed with the assistance of the "expansion function" in ANSYS software package so as to obtain stresses, elastic/plastic strains, and elements displacements. It would be interesting to extend the post-processing stage, gathering more results and therefore assessing more thoroughly the behavior of the structure.

II. Furthermore, when the problem related to the transient response will have been solved, velocities and accelerations at different points of the structure (bottom, decks, bulkheads, etc.) could be post-processed as well. Shock response spectra (SRS) could then be calculated based on above information and applied at the base of embarked materials. The dynamic design analysis method (DDAM) would then be applied to simulate the response of the material (displacements, velocities, accelerations, stresses, etc.) in the case of an underwater explosion.

8. ACKNOWLEDGEMENT

Firstly, I would like to express my sincere gratitude to my supervisor Prof. Hervé Le Sourne for the continuous support of my master study, for his patience, motivations, and instructions throughout the eight months I have spent in ICAM. His guidance helped me in all the time of research and writing of this thesis.

Besides, I would also like to thank all members of the Department of Acoustic and Vibrations in STX Europe, who provided me an opportunity to join their team as intern: the leader of Acoustic and Vibrations department Mr. Sylvain Branchereau, Naval Architect Mr. Patrick Chaurand, Structure Engineer Mr. Marc Yu; and especially thanks to Engineer Mr. Clement Lucus. All of them have improved my research from various perspectives by contributing with insightful comments and encouragement.

Moreover, my sincere thanks also go to Prof. Rigo Philippe, Ms. Christine Reynders, and all members who provided me the access to this meaningful and advanced EMSHIP program. Without their valuable support, it would not be possible to conduct this research.

Lastly, I would like to thank my family in Taiwan and Spain for all the support to me and everything to accomplish my thesis.

This thesis was developed in the frame of the European Master Course in “Integrated Advanced Ship Design” named “EMSHIP” for “European Education in Advanced Ship Design”, Ref.:159652-1-2009-1-BE-ERA MUNDUS-EMMC.

Ssu-Chieh Tsai

This page is intentionally left blank.

9. REFERENCE

- Abbot, H. L. (1881). *Report Upon Experiments and Investigations to Develop a System of Submarine Mines for Defending the Harbors of the United States.* USA: US Government Printing Office.
- ANSYS, I. 2. (2009). *ANSYS LS-DYNA User's Guide.* Récupéré sur ANSYS, Inc.: http://orange.engr.ucdavis.edu/Documentation12.1/121/ans_lsd.pdf
- Barras, G. (2012). Numerical simulation of underwater explosions using an ALE method. The pulsating bubble phenomena. *Ocean Engineering, Volume 41*, pp. 56-66. France.
- BRAND, C. L. (1945). *Submarine Report -Depth Charge, Bomb, Mine, Torpedo and Gunfire Damage Including Losses in Action.* Bureau of Ships Navy Department. Hydrographic Office,U.S.: VOLUME II.
- Brett, J. M., & Yiannakopolous, G. (2007, May 3). A study of explosive effects in close proximity to a submerged cylinder. *International Journal of Impact Engineering*, pp. 206-225.
- Cole. (1948). *Underwater Explosions.* Princeton University Press, Princeton.
- Costanzo, F. A. (2010). *Underwater Explosion Phenomena and Shock Physics.* Florida USA, Naval Surface Warfare Center Carderock Division, UERD: Proceedings of the IMAC-XXVIII.
- DeRuntz, J. A. (1989). The underwater shock analysis code and its applications. *60th Shock and Vibration Symposium*.
- Herring, C. (1941). *Theory of the pulsations of the gas bubble produced by an underwater explosion.* USA: United States Office of Scientific Research and Development.
- Hollyer, R. S. (1959). *Direct Shock-Wave Damage to Merchant Ships From Non Contact Underwater Explosions.* Norfolk Naval Shipyard.
- Hunter, K. S., & Geers, T. (2002). An integrated wave-effects model for an underwater explosion bubble. *The Journal of the Acoustical Society of America*, 1584-1601.
- Hunter, K. S., & Geers, T. (2003). Pressure and velocity fields produced by an underwater explosion. *The Journal of the Acoustical Society of America, 115*, 1483-1496.
- Hunter, K. S., & Geers, T. L. (2003). Pressure and velocity fields produced by an underwater explosion. *The Journal of the Acoustical Society of America, 115*.

- Keil, A. (1961). *The response of ships to underwater explosions.* DTIC Document.
- Kelle, J. B., & Kolodner, I. I. (1956). Damping of underwater explosion bubble oscillations. *Journal of applied physics, 27*(10).
- Navarro, M. G. (2015). *Rules and methods for dimensioning embarked materials for surface ships when subjected to UNDEX.* Nantes: Institut Catholique d'Arts et Métiers (ICAM).
- O'Hara, G. J. (1961). Effect upon Shock Spectra of the Dynamic Reaction of Structures. *Journal of the Society for Experimental Stress Analysis, 1*(5), 145-151.
- O'Hara, G. J., & Cunniff, P. F. (1982b). *Efficient Elastic-Plastic Design of Small Foundations.* Washington, D.C.: Naval Research Laboratory Memorandum Report 4918.
- O'Hara, G., & Cunniff, F. P. (1982a). *Efficient Elastic Design of Small Foundations.* Washington, DC: Naval Research Laboratory Memorandum Report 4886.
- Prosperetti, A. (1984). *Bubble phenomena in sound fields: part one.* Ultrasonics.
- Qiankun, Ÿ. J., & Gangyi, D. (2011). A finite element analysis of ship sections subjected to underwater explosion. *International Journal of Impact Engineering*.
- R. S., H. (1959). *Direct Shock-Wave Damage to Merchant Ships From Non Contact Underwater Explosions.* Norfolk Naval Shipyard.
- Rajendran, R., & Narasimhan, K. (2006). Deformation and fracture behavior of specimens subjected to underwater explosion—a review. *International Journal of Impact Engineering*.
- Reid, W. D. (1996). *The response of surface ships to underwater explosions.* Australia: DSTO Aeronautical and Maritime Research Laboratory.
- Remmers, G. M., O'Hara, G. J., & Cunniff, P. F. (1996). Dynamic Design Analysis Method DDAM. *Shock and Vibration, 3*, 461-476.
- Riley, M. (2010). *Analytical Solutions for Predicting Underwater Explosion Gas Bubble Behaviour.* Defence R&D Canada – Atlantic.
- Snay, H. (1956). *Hydrodynamics of underwater explosions.* Washinton D.C.: Symposium on Naval Hydrodynamics.

- Tuitman, J. T. (2010). *Hydro-elastic response of ship structures to slamming induced whipping.* Marine & Transport Technology, Marine & Transport Technology. Institutional Repository.
- Vernon, T. A. (1986). *Whipping response of ship hulls from underwater explosion bubble loading.* DTIC Document.
- Webster, K. G. (2007). Investigation of Close Proximity Underwater Explosion Effects on a Ship-Like Structure Using the Multi-Material Arbitrary Lagrangian Eulerian Finite Element Method.

This page is intentionally left blank.

APPENDIX A1. NODAL DISPLACEMENTS OF CYLINDER MODEL

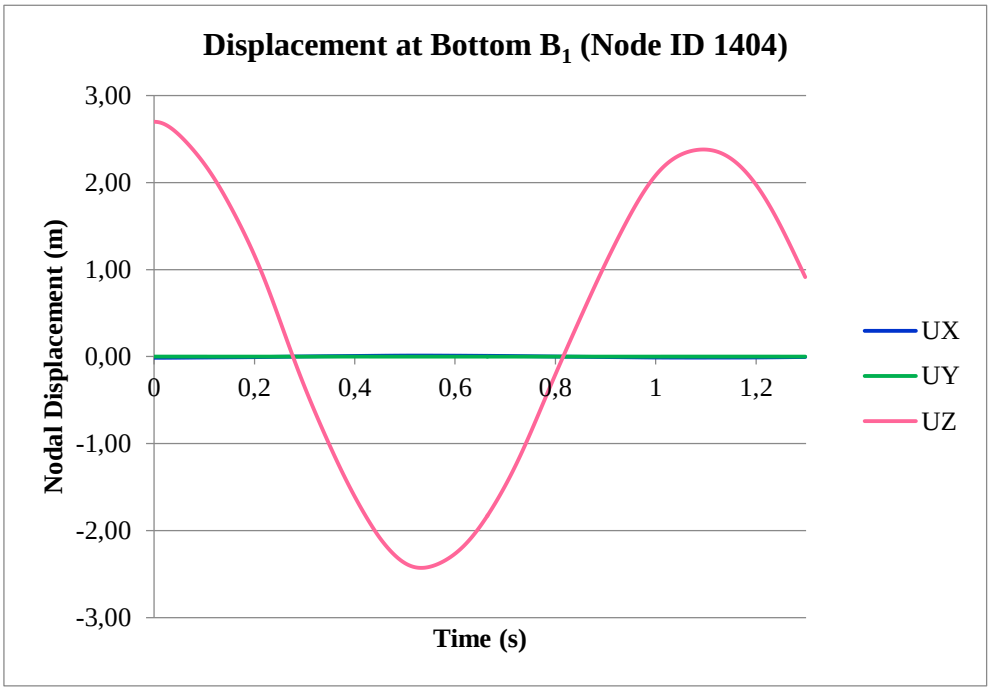

Figure A1.1: Nodal displacements at bottom B_1 of cylinder model (Node ID 1404)

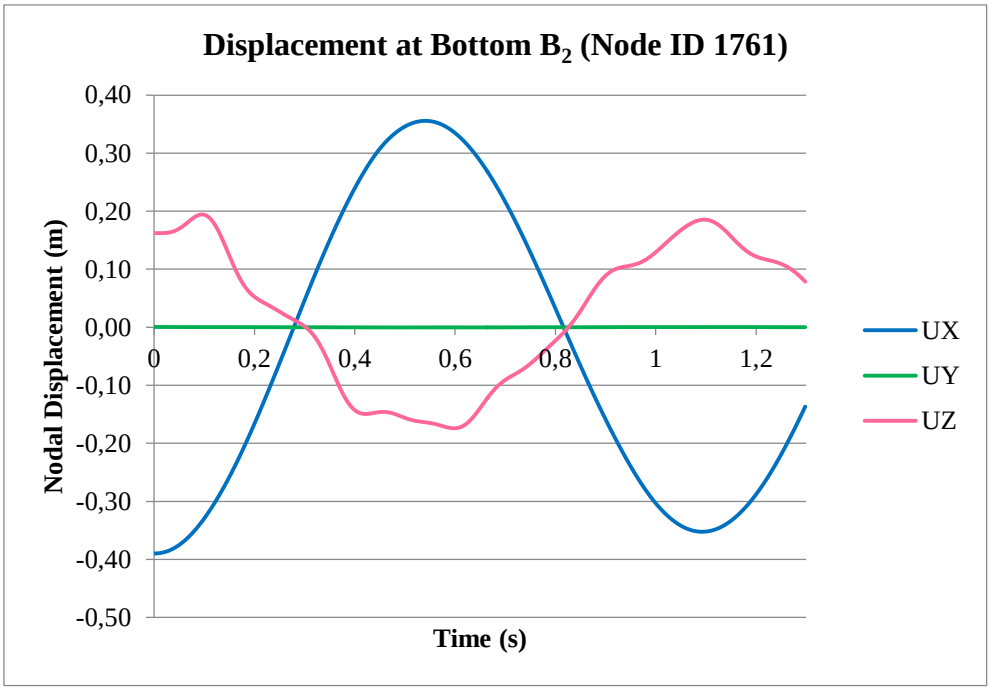

Figure A1.2: Nodal displacements at bottom B_2 of cylinder model (Node ID 1761)

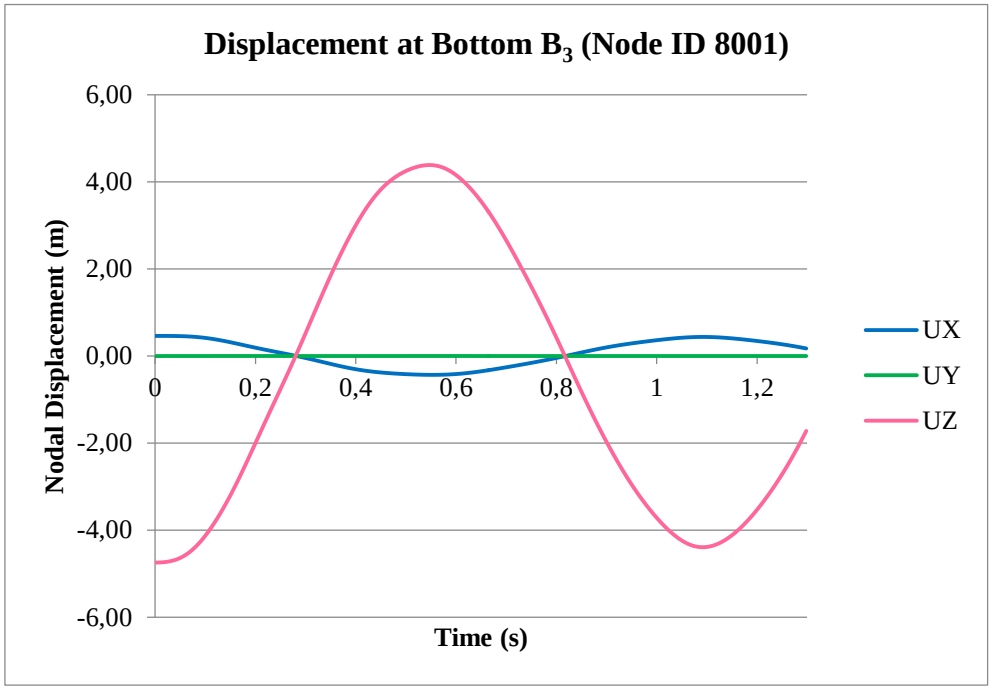

Figure A1.3: Nodal displacements at bottom B_3 of cylinder model (Node ID 8001)

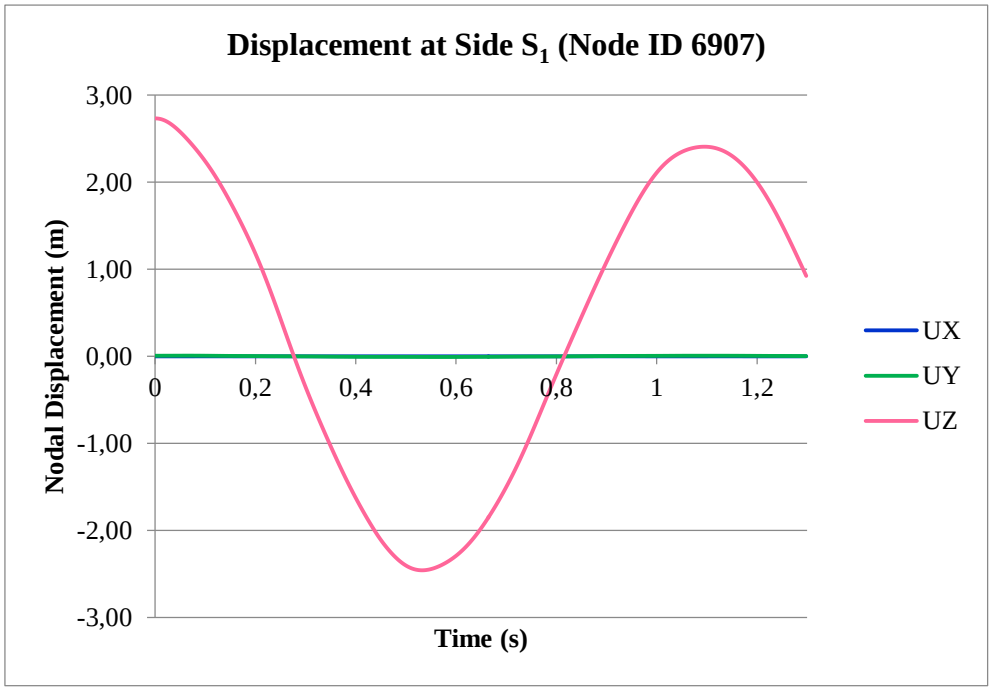

Figure A1.4: Nodal displacements at side S_1 of cylinder model (Node ID 6907)

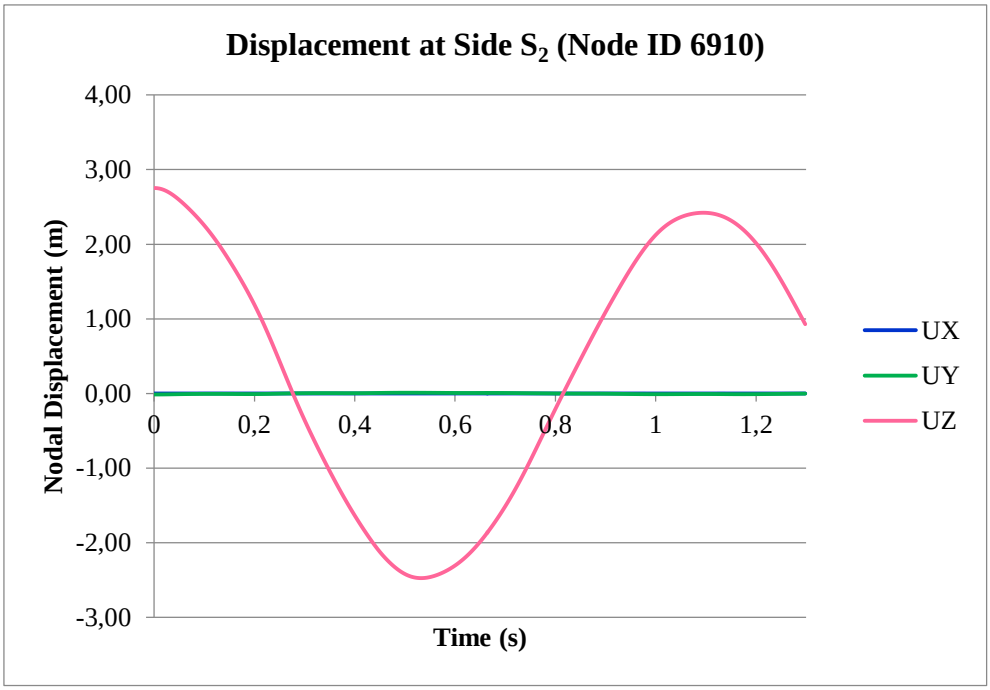

Figure A1.5: Nodal displacements at side S_2 of cylinder model (Node ID 6910)

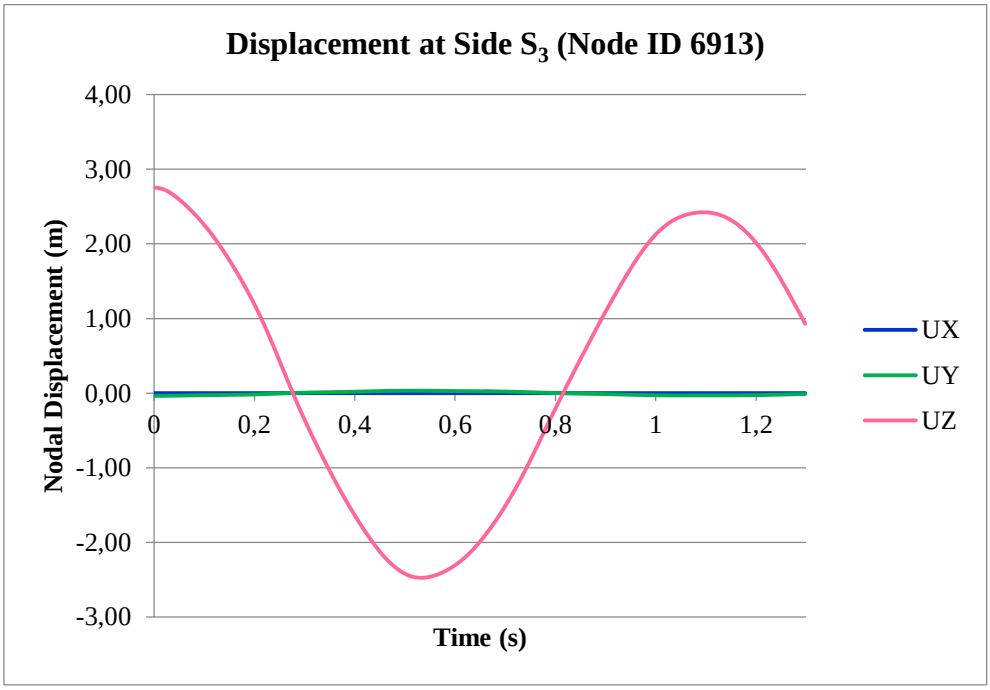

Figure A1.6: Nodal displacements at side S_3 of cylinder model (Node ID 6913)

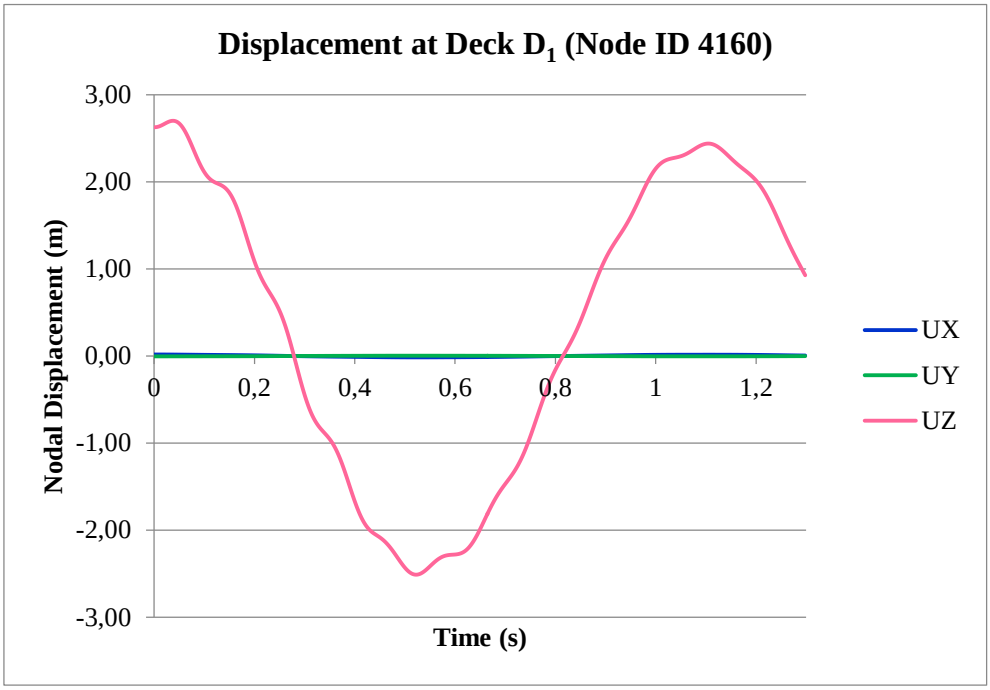

Figure A1.7: Nodal displacements at deck D_1 of cylinder model (Node ID 4160)

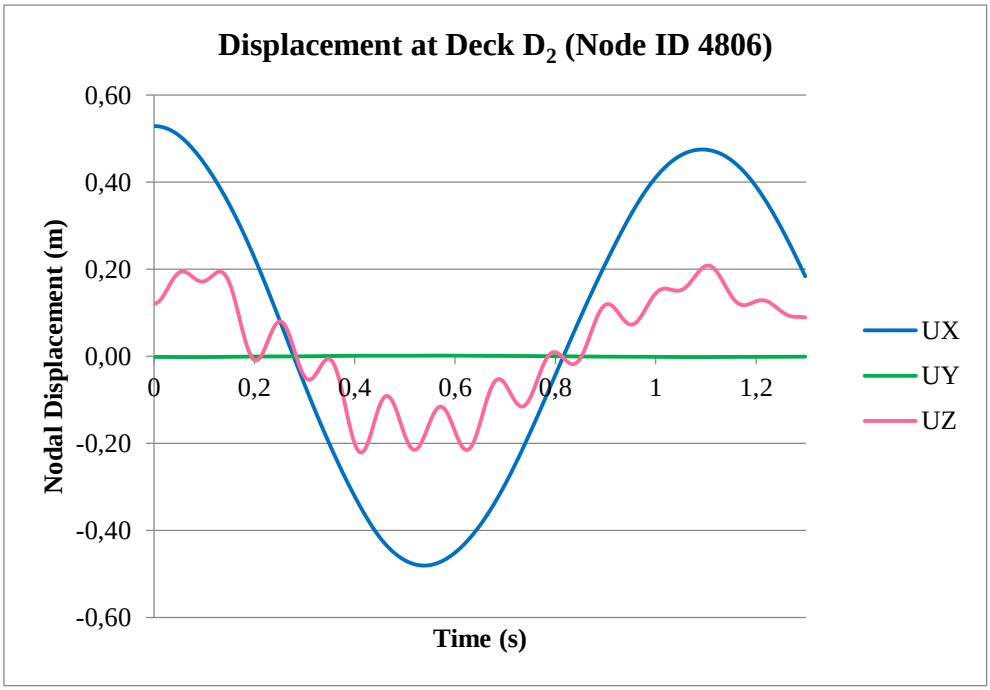

Figure A1.8: Nodal displacements at deck D_2 of cylinder model (Node ID 4806)

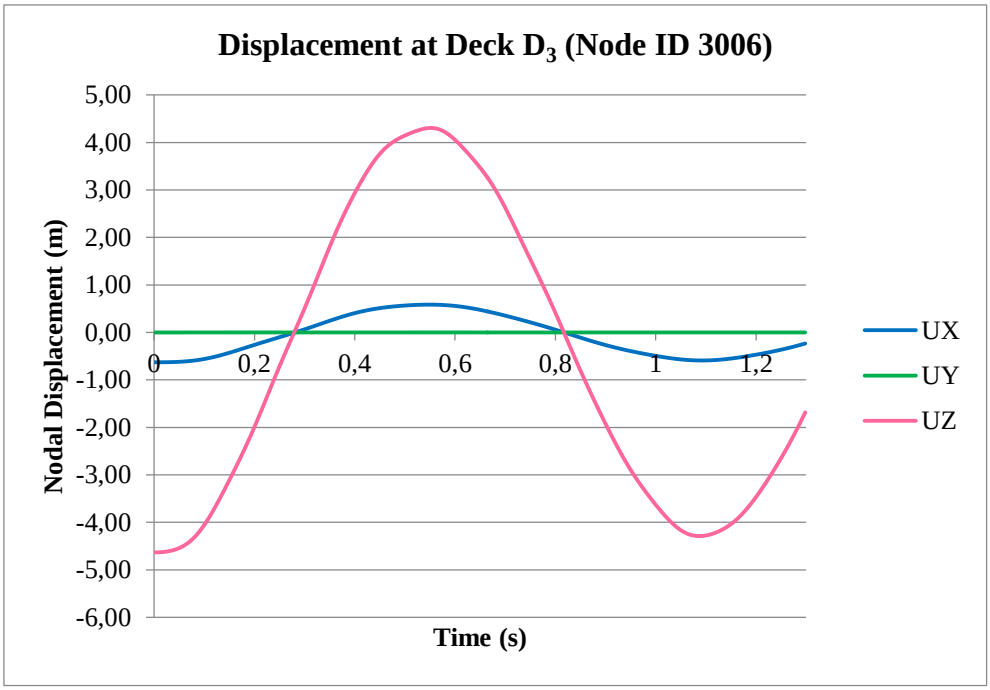

Figure A1.9: Nodal displacements at deck D_3 of cylinder model (Node ID 3006)

This page is intentionally left blank.

APPENDIX A2. NODAL DISPLACEMENTS OF FRIGATE MODEL

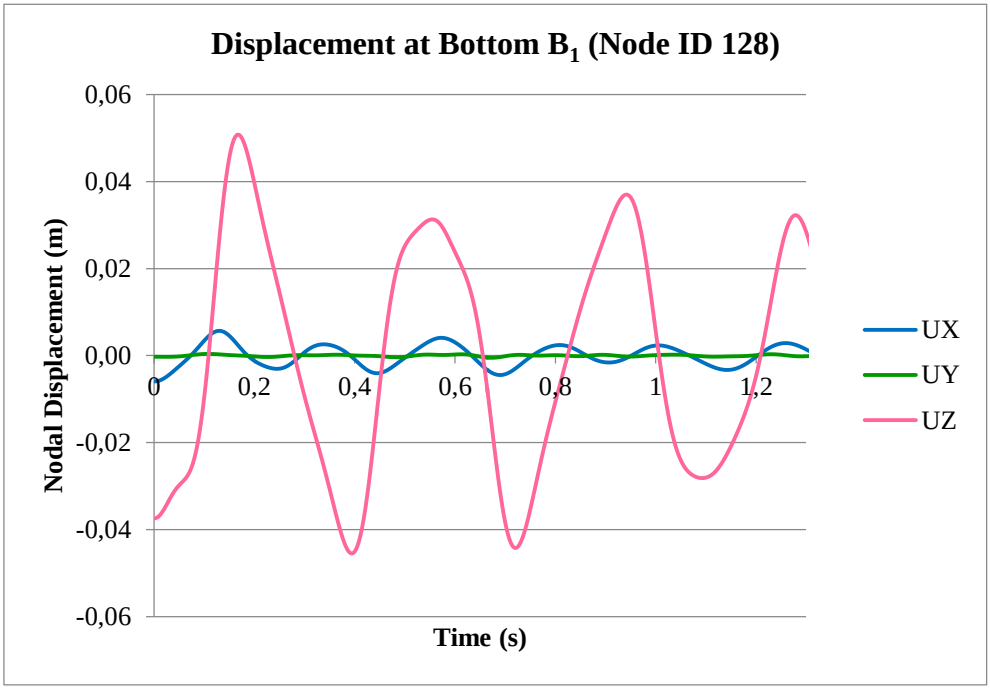

Figure A2.1: Nodal displacements at bottom B_1 of frigate model (Node ID 128)

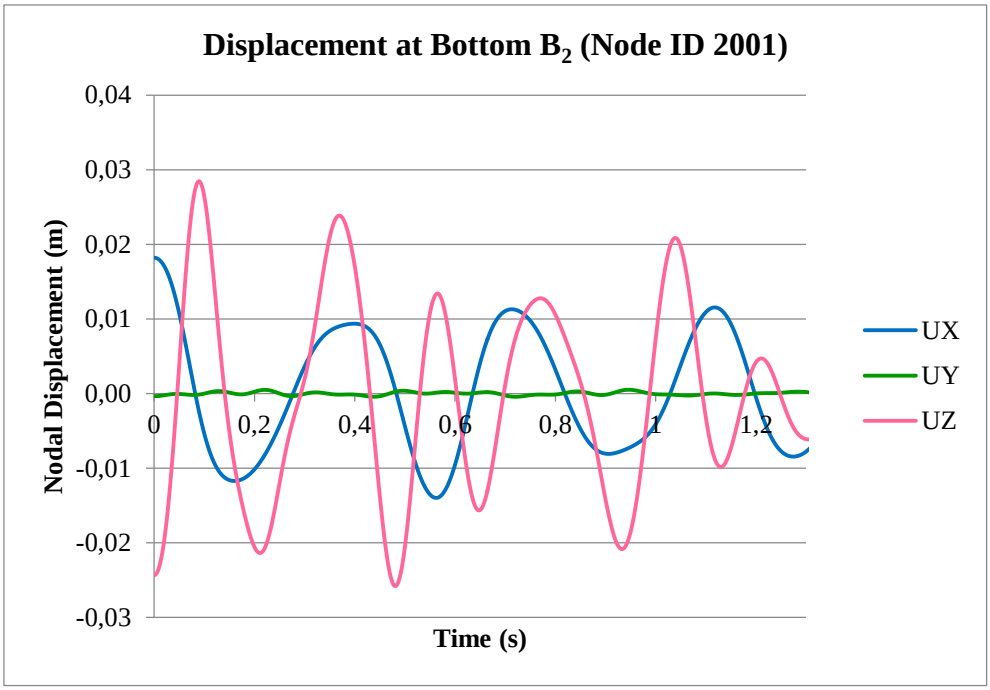

Figure A2.2: Nodal displacements at bottom B_2 of frigate model (Node ID 2001)

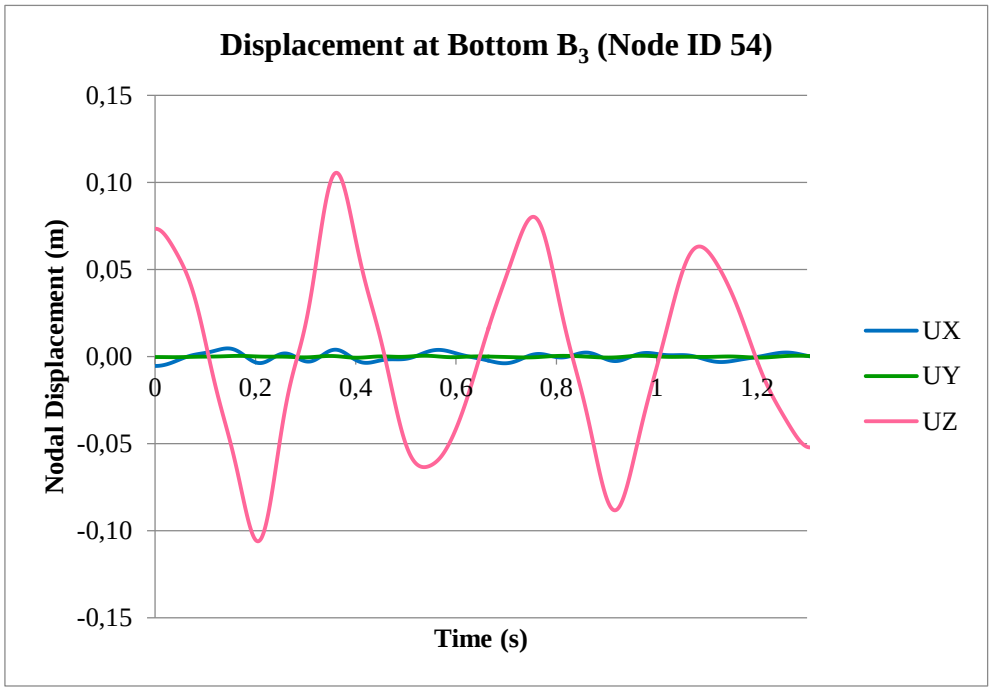

Figure A2.3: Nodal displacements at bottom B_3 of frigate model (Node ID 54)

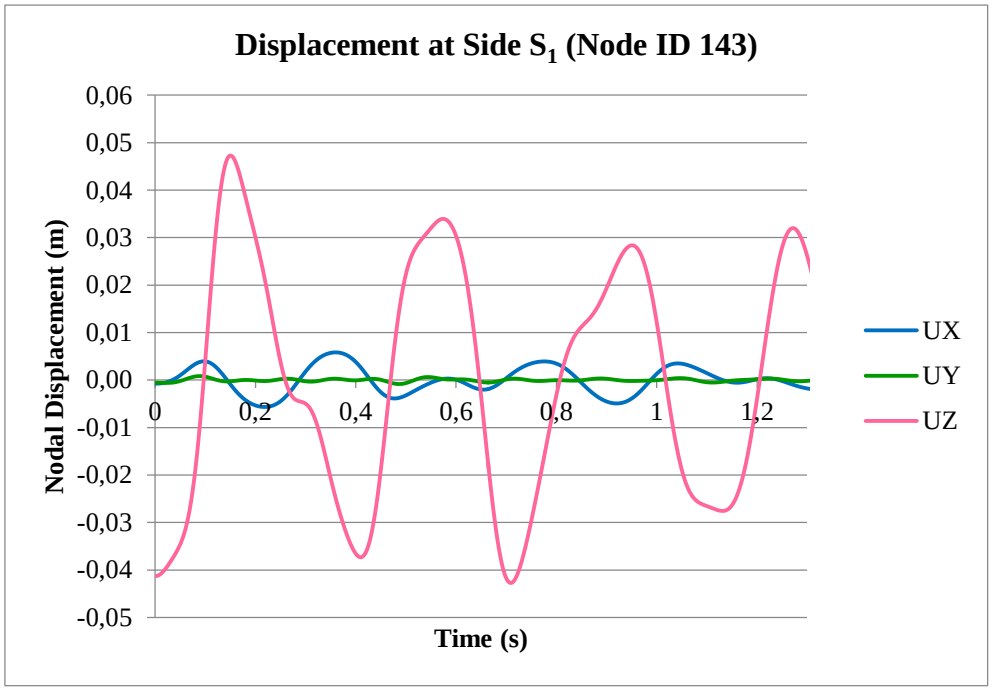

Figure A2.4: Nodal displacements at side S_1 of frigate model (Node ID 143)

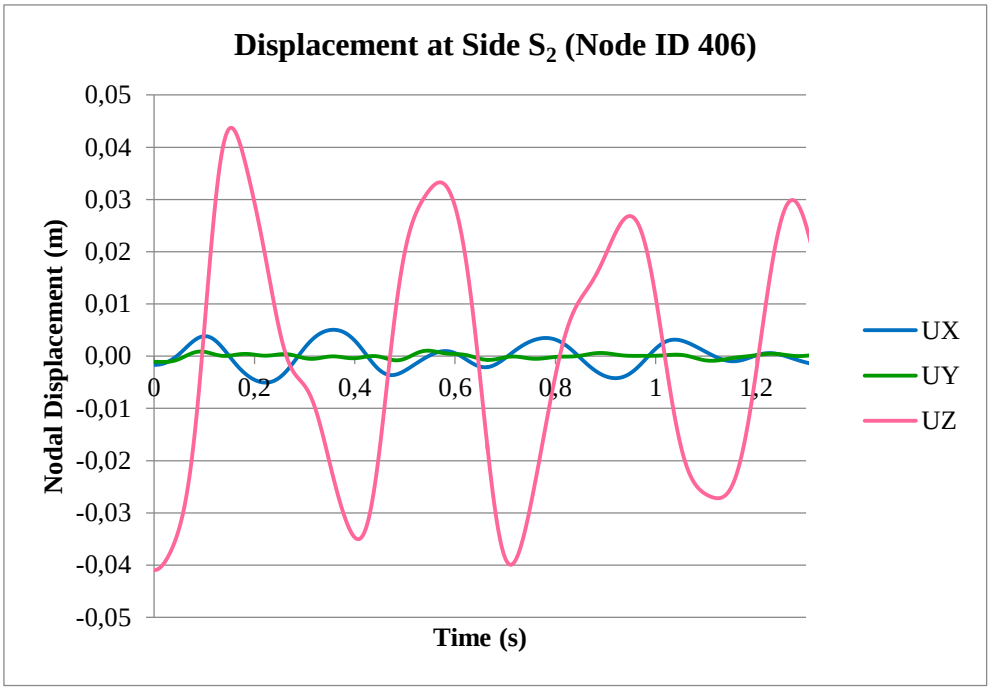

Figure A2.5: Nodal displacements at side S_2 of frigate model (Node ID 406)

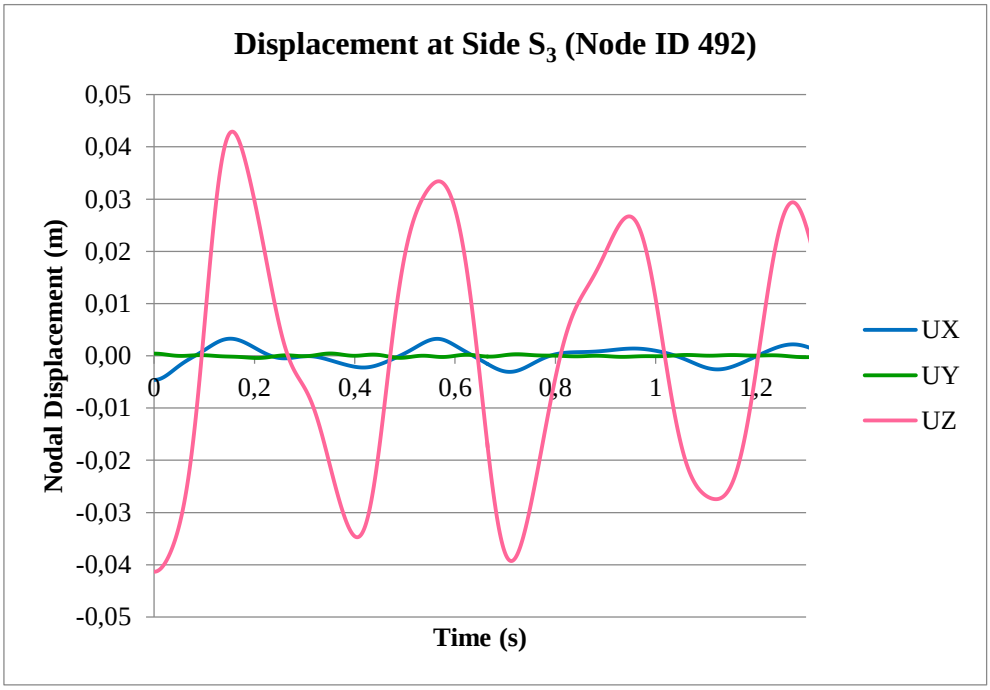

Figure A2.6: Nodal displacements at side S_3 of frigate model (Node ID 492)

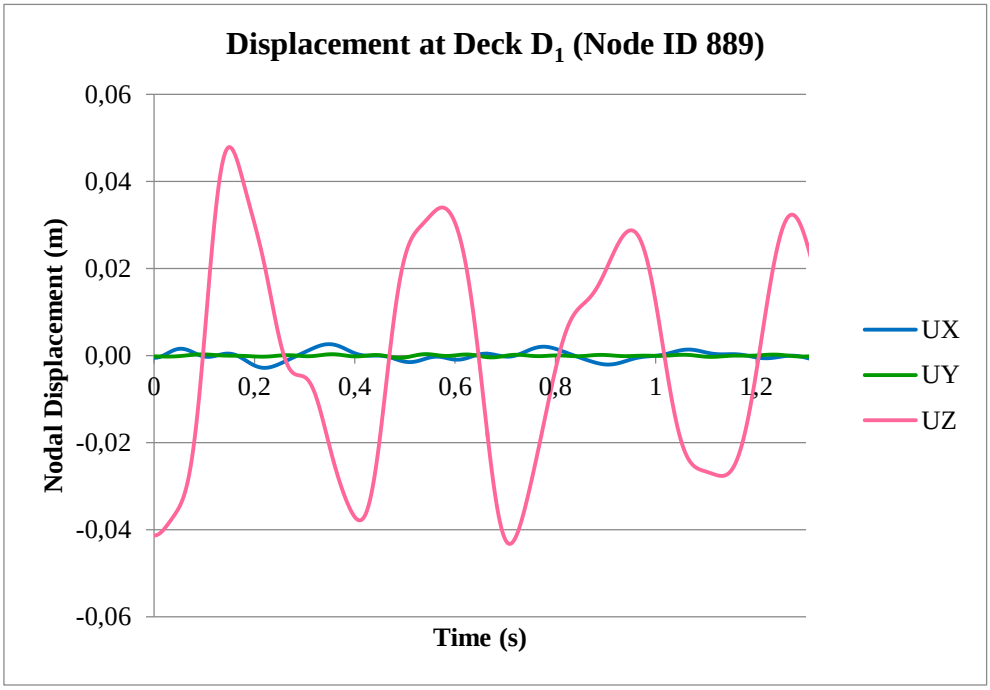

Figure A2.7: Nodal displacements at deck D_1 of frigate model (Node ID 889)

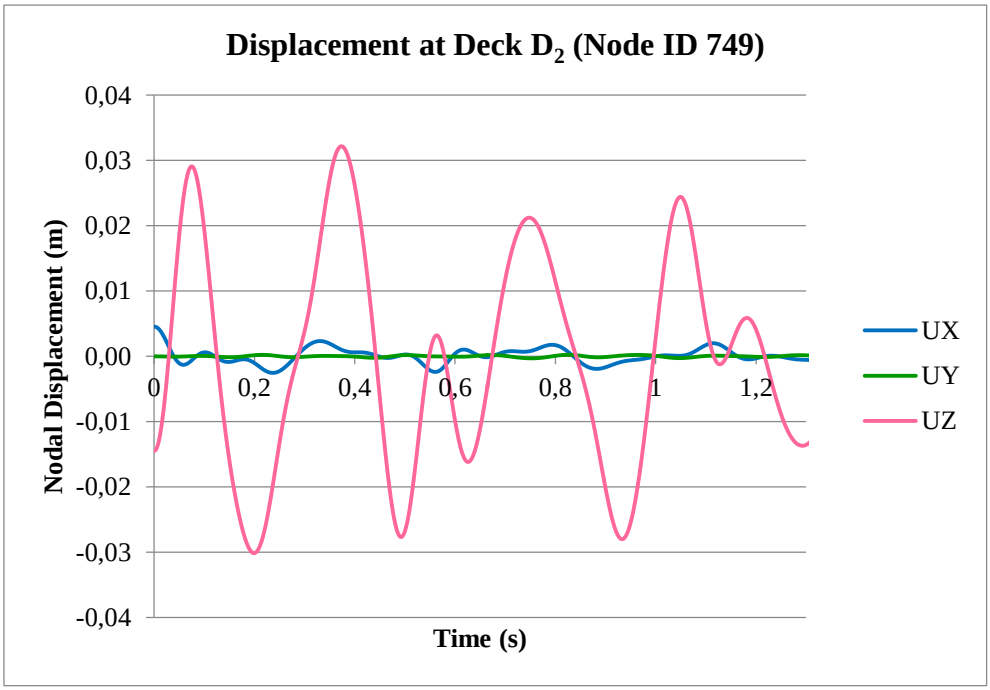

Figure A2.8: Nodal displacements at deck D_2 of frigate model (Node ID 749)

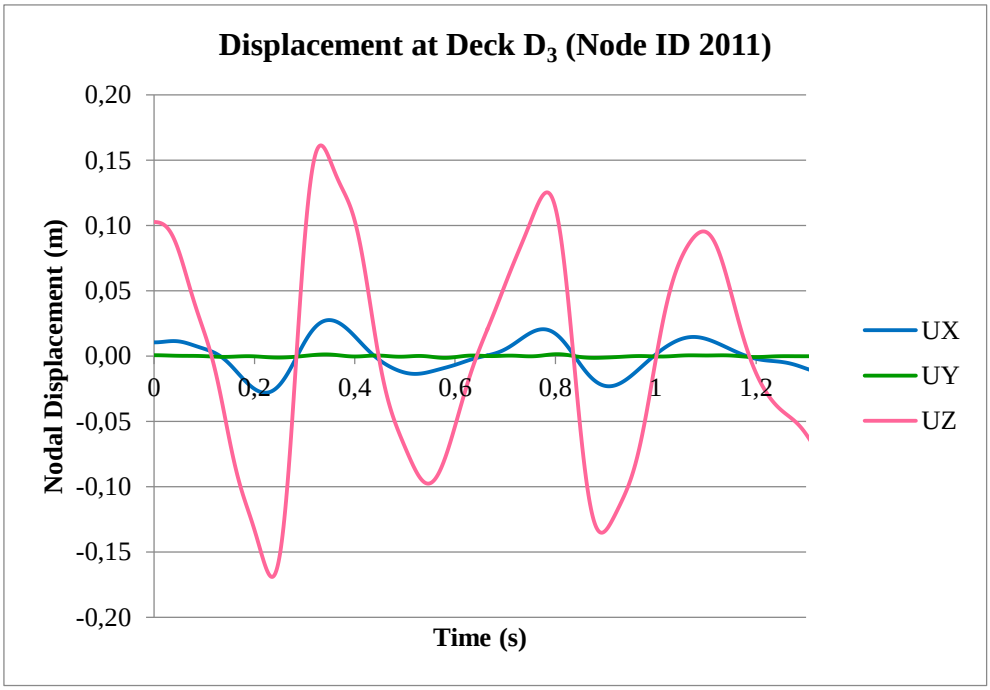

Figure A2.9: Nodal displacements at deck D_3 of frigate model (Node ID 2011)

This page is intentionally left blank.